

PB83-249987

REPORT NO.
UCB/EERC-82/27
NOVEMBER 1982

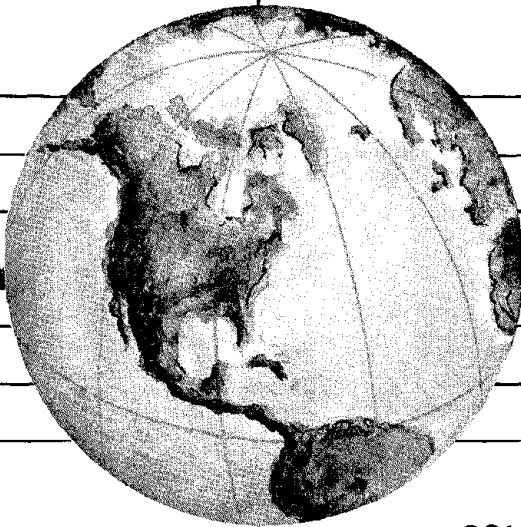
EARTHQUAKE ENGINEERING RESEARCH CENTER

INELASTIC ANALYSIS OF PIPING AND TUBULAR STRUCTURES

by

MANA MAHASUVERACHAI
GRAHAM H. POWELL

Report to Sponsor:
National Science Foundation



COLLEGE OF ENGINEERING

UNIVERSITY OF CALIFORNIA · Berkeley, California

REPRODUCED BY
NATIONAL TECHNICAL
INFORMATION SERVICE
U.S. DEPARTMENT OF COMMERCE
SPRINGFIELD, VA. 22161

For sale by the National Technical Information Service, U.S. Department of Commerce, Springfield, Virginia 22161.

See back of report for up to date listing of EERC reports.

DISCLAIMER

Any opinions, findings, and conclusions or recommendations expressed in this publication are those of the authors and do not necessarily reflect the views of the National Science Foundation or the Earthquake Engineering Research Center, University of California, Berkeley

INELASTIC ANALYSIS OF PIPING AND TUBULAR STRUCTURES

by

Mana Mahasuverachai
Graduate Student

and

Graham H. Powell
Professor of Civil Engineering

Report to
National Science Foundation
under Grant No. CEE 8105790

Report No. UCB/EERC-82/27
Earthquake Engineering Research Center
College of Engineering
University of California
Berkeley, California

November 1982

ABSTRACT

Theories and computational techniques for three inelastic pipe elements are presented. The elements can be used for inelastic stress and deformation analysis of three-dimensional piping systems, pipelines and tubular structures. The "fiber" procedure has been used to model the inelastic behavior of the pipe section in all three cases. The specific elements are as follows.

- (1) A straight pipe element assuming a cubic shape function has been developed and incorporated into the computer programs ANSR and WIPS. This element is suitable for modeling inelastic behavior of straight segments in piping systems, assuming closely-spaced nodes.
- (2) A curved pipe element has been developed and incorporated into the computer programs ANSR and WIPS. This element is based on a combination of beam and shell theories, retaining the essential features of a beam element but introducing aspects of shell behavior to account for cross-section ovaling. This element is suitable for modeling inelastic behavior of curved segments in piping systems, again assuming closely-spaced nodes.
- (3) A straight pipe element which automatically determines an appropriate shape function as the analysis progresses has been developed and incorporated into the computer program ANSR. This is a beam-column element suitable for modeling inelastic straight tubular frame members, not necessarily with closely-spaced nodes.

The elements are all applicable for either small or large displacements analysis. The first two elements also include options for the effects of internal pressure and temperature change.

A number of example structures have been analyzed to test the elements and to assess their acceptability for different applications. These examples include: a pipeline sidebend subjected to internal pressure and temperature changes; a pipe undergoing large displacements following a postulated pipe rupture; and a tubular steel beam-column with development of plastic zones near the member ends.

ACKNOWLEDGEMENTS

The research described in this report was supported in part by the National Science Foundation under Grant No. CEE 8105790 and in part by Lawrence Livermore National Laboratory under Subcontract No. 3371609. The authors wish to express their sincere appreciation for this support.

Sincere appreciation is also expressed to Linda Calvin for preparation of the typescripts and to Gail Feazell and Mary Edmunds-Boyle for preparation of the figures.

TABLE OF CONTENTS

	<u>Page</u>
ABSTRACT	i
ACKNOWLEDGEMENTS	iii
TABLE OF CONTENTS	v
A. OBJECTIVE AND SCOPE	1
A1. INTRODUCTION	3
A1.1 GENERAL	3
A1.2 PIPE ELBOW ELEMENT	3
A1.3 TUBULAR BEAM-COLUMN ELEMENT	4
A1.4 FIBER VERSUS SECTION MODELS	5
A1.5 SCOPE	5
A1.6 REPORT LAYOUT	6
A2. REFERENCES	7
B. PIPE ELEMENT	9
B1. INTRODUCTION	11
B2. ELEMENT PROPERTIES	13
B3. CURVED ELEMENT THEORY	15
B3.1 PROCEDURE AND ASSUMPTIONS	15
B3.2 SLICE STIFFNESS	16
B3.2.1 Deformations and Actions	16
B3.2.2 Subelement Strains due to Owalling	17
B3.2.3 Strain-Deformation Relationships for Slice	18
B3.2.4 Stress-Strain Relationship for Slice Subelements	18
B3.2.5 Stiffness Matrix	19
B3.2.6 Owalling Resistance due to Pipe Wall Bending	20
B3.2.7 Owalling Stiffness due to Internal Pressure	21
B3.2.8 Condensed Slice Stiffness	22
B3.3 ELEMENT STIFFNESS	23

Preceding page blank

Table of Contents (cont'd)

Page

B3.3.1	Choice of Shape Function	23
B3.3.2	Elastic Stiffness	23
B3.3.3	Displacement Transformation	25
B3.3.4	Element Stiffness	25
B3.4	INITIAL STRESS EFFECTS	26
B3.4.1	General	26
B3.4.2	Pressure and Temperature Changes	26
B3.4.3	Strain Rate Effects	27
B3.4.4	Round-Off in Mroz Material Calculations	29
B3.5	CHANGE OF SECTION GEOMETRY DUE TO OVALING	29
B3.6	STATE DETERMINATION	30
B4.	STRAIGHT PIPE THEORY	33
B4.1	PROCEDURE AND ASSUMPTIONS	33
B4.2	SLICE STIFFNESS	34
B4.2.1	Deformations and Actions	34
B4.2.2	Strain-Deformation Relationships for Slice	34
B4.2.3	Stress-Strain Relationships for Slice Subelement	35
B4.2.4	Stiffness Matrix	36
B4.3	ELEMENT STIFFNESS	36
B4.3.1	Deformations and Actions	36
B4.3.2	Choice of Shape Function	37
B4.3.3	Elastic Beam	37
B4.3.4	Inelastic Beam	39
B4.3.5	Internal Degrees of Freedom	39
B4.3.6	Shape Functions	39
B4.3.7	Element Stiffness	41
B4.4	STATE DETERMINATION	42
B5.	REFERENCES	45

Table of Contents

Page

B6.	ANSR-III USER GUIDE	47
C.	MULTI-SLICE TUBE ELEMENT	65
C1.	INTRODUCTION	67
	C1.1 CONCEPT	67
	C1.2 ELEMENT FEATURES	68
C2.	ELEMENT PROPERTIES	69
	C2.1 ELEMENT GEOMETRY	69
	C2.2 SLICE LOCATIONS	69
	C2.2.1 General	69
	C2.2.2 Antisymmetrical Bending	69
	C2.2.3 Other Bending Moment Variations	70
	C2.3 SLICE MODELING	71
	C2.4 COMPUTATIONAL PROCEDURE	71
	C2.4.1 Shape Function	71
	C2.4.2 Overshoot and Unloading Tolerances	72
C3.	THEORY	73
	C3.1 PROCEDURE AND ASSUMPTIONS	73
	C3.2 SLICE STIFFNESS	74
	C3.2.1 Deformations and Actions	74
	C3.2.2 Strain-Deformation Relationships for Slice	74
	C3.2.3 Stress-Strain Relationships for Slice Subelement	75
	C3.2.4 Stiffness Matrix	76
	C3.3 SLICE FLEXIBILITY	76
	C3.4 ELEMENT STIFFNESS	77
	C3.4.1 Deformations and Actions	77
	C3.4.2 Shape Function Calculation	77

Table of Contents	<u>Page</u>
C3.4.3 Stiffness Approach	77
C3.4.4 Weaknesses of Stiffness Approach	79
C3.4.5 Flexibility Approach	79
C3.4.6 Flexibility Calculation	80
C3.4.7 Shape Function	81
C3.4.8 Element Stiffness	81
C3.5 STATE DETERMINATION	82
C3.5.1 Basic Procedure	82
C3.5.2 Linearity in Mroz Material Calculations	83
C3.5.3 Linearity in Use of Shape Function	83
C3.5.4 Prevention Approach	84
C3.5.5 Correction Approach	86
C4. REFERENCES	89
C5. ANSR-III USER GUIDE	91
D. EXAMPLES	101
D1. PIPE WITH AXIAL FORCE AND INTERNAL PRESSURE	103
D1.1 PURPOSE	103
D1.2 CONFIGURATION	103
D1.3 ANSR ANALYSIS MODEL	103
D1.3.1 Assumptions for Analysis	103
D1.3.2 Loadings	103
D1.3.3 ANSR Input	103
D1.4 RESULTS	104
D1.5 CONCLUSION	104
D2. BURIED PIPE BEND WITH TEMPERATURE AND PRESSURE LOADING	105
D2.1 PURPOSE	105
D2.2 CONFIGURATION	105
D2.3 ANSR ANALYSIS MODEL	105

Table of Contents

	<u>Page</u>
D2.3.1 Assumptions of Analysis	105
D2.3.2 Loadings	105
D2.3.3 ANSR Input	106
D2.4 RESULTS	106
D2.5 CONCLUSION	106
D3. PIPE WHIP WITH LARGE DISPLACEMENTS	107
D3.1 PURPOSE	107
D3.2 CONFIGURATION	107
D3.3 ANSR ANALYSIS MODEL	108
D3.3.1 Geometry, Loading, and Pipe Properties .	108
D3.3.2 Analysis Control Parameters	108
D3.3.3 ANSR Input	108
D3.4 RESULTS	109
D4. INELASTIC MULTI-SLICE BEAM COLUMN	111
D4.1 PURPOSE	111
D4.2 CONFIGURATION	111
D4.3 ANSR ANALYSIS MODEL	111
D4.3.1 Assumptions for Analysis	111
D4.3.2 ANSR Input	112
D4.4 RESULTS	112
D4.4.1 Expected Behavior	112
D4.4.2 Load Versus Deflection	112
D4.4.3 Curvature Versus Deflection	113
D4.5 CONCLUSION	114
D5. SUMMARY	115
D5.1 GENERAL	115
D6. REFERENCES	117



A. OBJECTIVE AND SCOPE

This report is divided into four sections (A, B, C, and D). Section A explains the objective and scope of the research and explains the contents of Section B, C, and D.

A1. INTRODUCTION

A1.1 GENERAL

The research described in this report is concerned with the inelastic stress and deformation analysis of piping systems, pipelines and tubular structures. Specific applications which have been considered are as follows.

- (1) Analysis of pipe whip in power piping systems. The structural elements described in this report are applicable to two- or three-dimensional pipe whip analysis, with consideration of pipe yield, ovaling at pipe elbows, and large displacements of the piping system.
- (2) Analysis of pipelines. The structural elements are applicable to both buried and above-ground pipeline systems, accounting for pipe yield, temperature changes, internal pressure, and large displacements.
- (3) Analysis of tubular frame structures, with particular application to steel offshore platforms. Analyses of piping systems and pipelines typically require that the piping be divided into short elements, so that yielding is approximately uniform over any element. Hence, "standard" finite element techniques using predetermined shape functions can be applied to characterize the element behavior. For analysis of tubular frames, however, it is desirable to use longer elements, such that the amount and location of yielding can vary within a single element. In this case, standard finite element techniques may not work well. To account for this problem, a new technique has been developed in which the shape functions are updated as the analysis progresses and the state of the element changes.

A1.2 PIPE ELBOW ELEMENT

In the analysis of piping systems, it is essential to distinguish between straight and curved segments, because a curved pipe is more flexible than a straight pipe of the same cross section. This is due to the fact that the cross section of a curved pipe will deform (oval), which substantially reduces both the stiffness and strength of the pipe. Straight segments of pipe can, in

general, be modeled adequately using straight beam-column elements with circular cross sections. Curved segments are more complicated, however, and require special consideration, especially when inelastic behavior is to be taken into account.

A commonly used procedure for the analysis of pipe bends is to use simple curved beam theory, but with the flexural stiffness scaled by a flexibility factor to account for ovaling [A1]. This is a simple and cheap approach, but it is applicable only for linear analysis. A more accurate procedure would be to use a mesh of shell finite elements to model each pipe bend. However, this approach has the obvious disadvantage that computation costs are likely to be too high for economical analysis of a complete piping system. A compromise procedure is to use elements based on a combination of beam and shell theories, retaining the essential features of a beam element but introducing aspects of shell behavior to account for cross-section ovaling [A2,A3,A4]. Elements of this type can greatly reduce the computation cost compared to the use of shell elements, while still providing good accuracy. A new element based on this approach is described in Section B of this report.

For the special case of a straight element, the theory is substantially simpler. The straight element theory and computational procedure are also described in Section B.

A1.3 TUBULAR BEAM-COLUMN ELEMENT

In the analysis of tubular frame structures, beam-column finite elements based on assumed cubic displaced shapes are commonly used. The use of a cubic shape function implies a linear variation of curvature along the element length. This is correct for a uniform elastic element but may be quite incorrect after yielding occurs. For accurate modeling, therefore, it may be necessary to use short elements in the inelastic regions. It is generally not desirable, however, to divide a beam-column member into short elements, because it increases the numbers of nodes and elements which must be specified. A procedure is described in this report which allows a long, inelastic beam-column member to be modeled accurately using a single element. The procedure is based on varying the element shape function as the state of the element changes, without introducing additional nodes or elements. The details of the

element are presented in Section C.

A1.4 FIBER VERSUS SECTION MODELS

Two basic procedures may be used for modeling the inelastic behavior of a beam-column. In the "section" type of model it is assumed that inelastic behavior is defined for the cross section as a whole, whereas in the "fiber" type of model the member cross section is divided into a number of small areas (fibers). In the section model, stiffness and strength properties are specified for the complete section, and only the stress and strain resultants need to be monitored. In the fiber model, properties are defined for the fibers, and the stresses and strains in each fiber must be monitored. The fiber model thus tends to be more expensive computationally. However, the calculation of cross section properties for the section model may be a difficult task, so that the fiber model tends to be both easier to use and more accurate.

For the pipe elbow element described in Section B, only the fiber type of model is appropriate, whereas the beam-column theory described in Section C is applicable to either the section or fiber type of model. In this report, however, only a fiber model has been developed, for the particular case of a tubular cross section. Other elements could be developed following similar principles.

A1.5 SCOPE

The purpose of the study described in this report has been to explore theoretical and computational techniques for modeling inelastic straight and curved pipe members using the "fiber" type of model. Three separate elements have been developed, as follows.

- (1) A straight pipe element assuming a cubic shape function has been developed and incorporated into the computer programs ANSR-III [A5] and WIPS [A6]. This element is suitable for modeling inelastic behavior of straight segments in piping systems, assuming closely-spaced nodes.

- (2) A curved pipe element has been developed and incorporated into the computer programs ANSR and WIPS. This element is suitable for modeling inelastic behavior of curved segments in piping systems, again assuming closely-spaced nodes.
- (3) A straight pipe element which automatically determines an appropriate shape function as the analysis progresses has been developed and incorporated into the computer program ANSR. This element is suitable for modeling inelastic straight tubular frame members, not necessarily with closely-spaced nodes.

The elements are all applicable for either small or large displacements. The first two elements include options for internal pressure and temperature change effects, making them suitable for inelastic analysis of pipelines and piping systems. The third element has been developed in only a preliminary form. Further work is needed on this element to add practical features.

A1.6 REPORT LAYOUT

Section B presents the theory of the inelastic straight and curved pipe elements. Section C presents the inelastic beam-column element for tubular frames. Both sections have been written as self-contained reports. Examples using all three of the elements are contained in Section D.

A2. REFERENCES

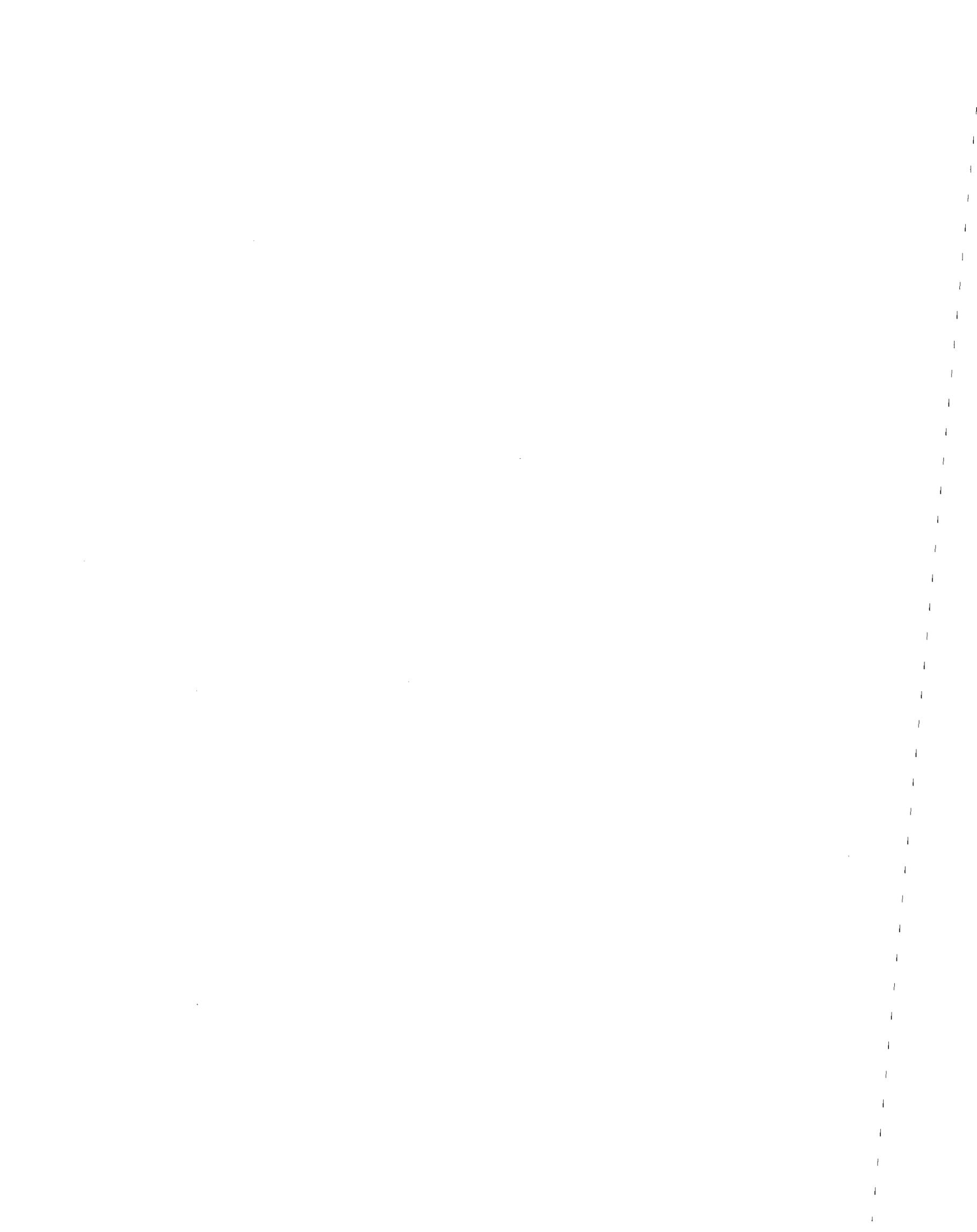
- A1. Dodge, W. G. and Moore, S. E., "Stress Indices and Flexibility Factors for Moment Loadings on Elbows and Curved Pipes," *Welding Research Council Bulletin 179*, December 1972.
- A2. Marcal, P. V., "Elastic-Plastic Behavior of Pipe Bend with In-Plane Bending," *J. Strain Analysis*, Vol. 2, No. 1, pp. 84-96, 1967.
- A3. Hibbitt, H. D., Sorensen, E. P., and Marcal, P. V., "The Elastic-Plastic and Creep Analysis of Pipelines by Finite Elements," in *Pressure Vessel Technology*, Pt. 1, ASME, pp. 239-251, 1973.
- A4. Ohtsubo, H. and Watanabe, O., "Stress Analysis of Pipe Bend by Ring Elements," *Trans. ASME*, Ser. J, Vol. 100, pp. 112-122, 1978.
- A5. Oughourlian, C. V., "General Purpose Computer Program for Nonlinear Structural Analysis," *Ph.D. Thesis*, Department of Civil Engineering, University of California, Berkeley, 1982.
- A6. Powell, G. H., Hollings, J. P., Row, D. G., Chen, P. F-S., Hu, F-C., Mahasuverachai, M., Mosaddad, B., Nicklin, P., Nour-Omid, S., Oughourlian, C. and Riahi, A., "WIPS - Computer Code for Whip and Impact Analysis of Piping Systems," Report to Lawrence Livermore National Laboratory, 1982.



B. PIPE ELEMENT

This section describes the theory of the *straight-curved pipe* element. The basic features of the element are described in Chapters B1 and B2. Details of the theory and computational procedure are described in Chapter B3 for a curved (elbow) element and in Chapter B4 for a straight element. Chapter B5 contains references, and Chapter B6 describes the input data required for the ANSR-III computer code.

Preceding page blank



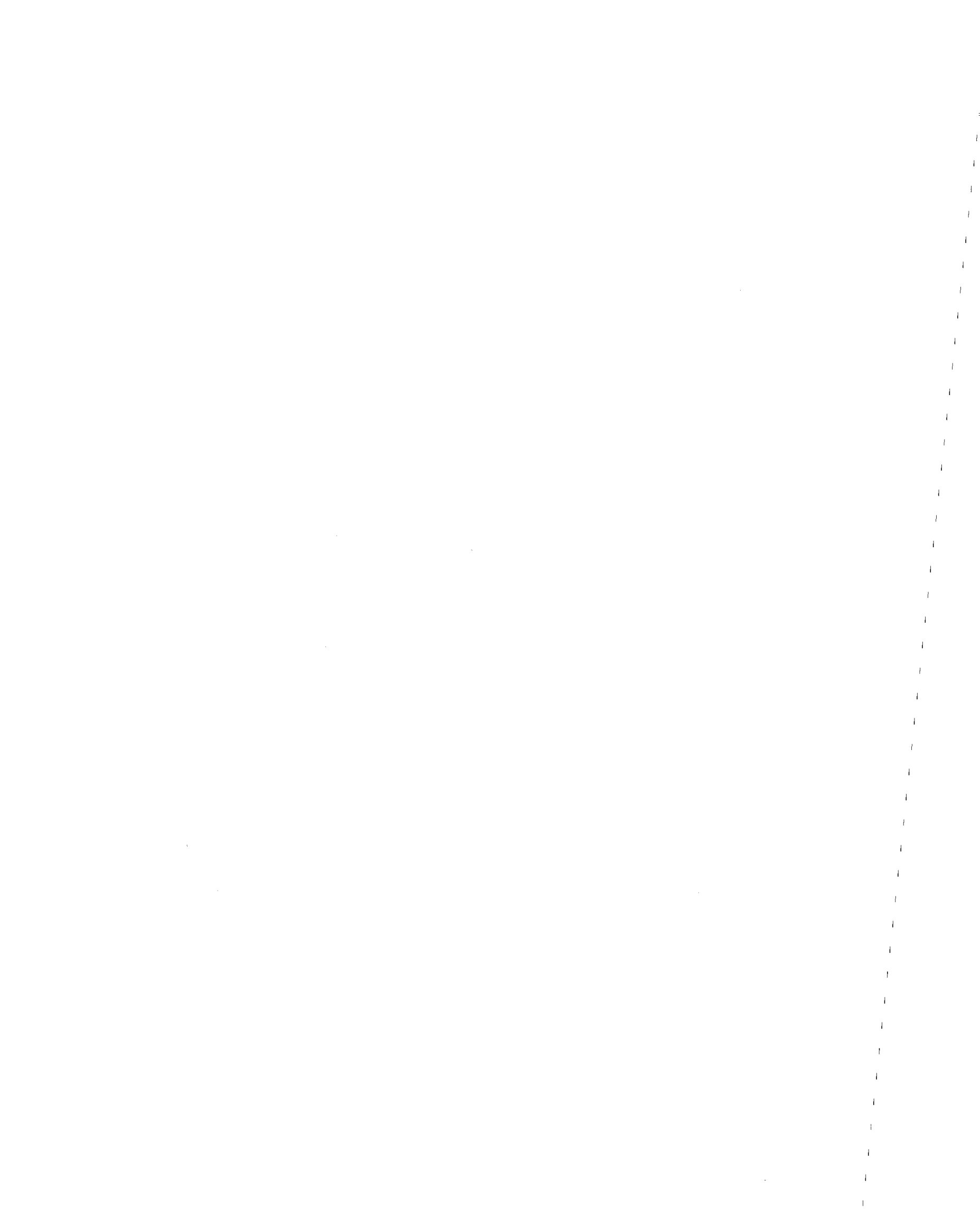
B1. INTRODUCTION

The *pipe* type element has the following features.

- (1) The element may be straight or curved, and arbitrarily oriented in space.
- (2) If the element is straight, it is treated as a three-dimensional beam column. Inelastic behavior is considered by dividing the cross section into subelements (or *fibers*), and monitoring the behavior of each subelement. Longitudinal, circumferential, and torsional stresses are considered.
- (3) If the element is curved, it is similar in many respects to a straight element, but includes additional deformations to account for ovaling. A number of simplifying assumptions are made in developing the ovaling theory.
- (4) The Mroz material model is used, with allowance for strain rate dependence if desired.
- (5) The effects of internal pressure on ovaling stiffness and material yield are considered.
- (6) Large displacement effects may be considered, if desired, using an *engineering* theory (i.e. not a consistent continuum mechanics approach).

A general description of the element properties is presented in Chapter B2. Theoretical details for the curved element are presented in Chapter B3 and for the straight element in Chapter B4.

Preceding page blank



B2. ELEMENT PROPERTIES

Beam-column finite elements based on assumed cubic displaced shapes are commonly used for elastic and inelastic analysis. The straight pipe element is exactly of this type, and the curved pipe element is essentially of this type. However, there are several complicating factors introduced when the element is curved rather than straight. The assumptions and properties are described in physical terms in this chapter. Full theoretical details are presented in Chapters B3 and B4.

The element geometry and coordinate axes are shown in Fig. B2.1. Each element connects two nodes, each with three translational and three rotational degrees of freedom. For a straight element the assumed deformed shape is cubic. For a curved element, however, an assumed cubic shape is inconsistent in a finite element sense. If cubic interpolation along the element axis is assumed, then rigid body motions can be significantly restrained. If cubic interpolation along the element chord is assumed, constant strain states do not exist. For this reason, the deformed shape is assumed to be the exact shape for a curved *elastic* element. This shape can be calculated for any element geometry, as explained in Chapter B3. The element stiffness is formed by numerical integration (Gauss quadrature). The detailed behavior is monitored at two cross sections located at the Gauss points (Fig. B2.1). At each point the pipe cross section is divided into a number of *subelements* (typically 12), as shown. The pipe wall at each subelement is assumed to be subjected to hoop stress (due to pressure), axial stress (due to pressure, bending moment and axial force), and shear stress (due to torsional moment). The inelastic behavior of each subelement is monitored, using the Mroz material theory.

For a curved element a major factor in the behavior is ovaling of the pipe cross section. For in-plane bending, the longitudinal tensions and compressions in the extreme fibers produce opposing forces which compress or extend the pipe section, as shown in Fig. B2.2a. This ovaling can substantially modify the longitudinal stress distribution, so that instead of a linear stress variation over the pipe depth, the variation is strongly nonlinear, as indicated in Fig. B2.2a. This effect can greatly reduce the bending stiffness of the pipe, and because the ovaling

is resisted if internal pressure is present in the pipe, this stiffness depends on the pressure.

Ovalling is also produced by out-of-plane bending of a curved element. However, the ovalling deformation is inclined at 45 degrees to the moment axis, as shown in Fig. B2.2b. This type of ovalling also reduces the bending stiffness and modifies the bending stress distribution.

In an actual curved pipe, the longitudinal, hoop, torsional and ovalling deformations all interact with each other to produce very complex behavior. In the curved element theory, the complexity is reduced by ignoring several of the interaction effects. In particular:

- (1) In-plane and out-of-plane ovalling deformations are assumed to be uncoupled.
- (2) Bending stresses in the pipe wall due to ovalling are assumed not to affect yield of the pipe under the membrane stresses produced by internal pressure, bending and torsion in the pipe (and vice versa).
- (3) Ovalling at any cross section is assumed not to be affected by ovalling at any other cross section. In particular, if a pipe elbow is connected to a straight pipe, the straight pipe is assumed not to restrain the ovalling near the ends of the elbow.

In addition, only two ovalling "modes" are considered, namely, the in-plane and out-of-plane modes shown in Fig. B2.2. Detailed analyses of pipe elbows have shown that it may be necessary to consider higher order ovalling modes to obtain accurate *elastic* stress distributions. It is assumed, in effect, that these higher modes are less important for inelastic behavior.

In spite of the many simplifications which have been made, the curved element has predicted results in close agreement with experiment. The curved element is also, in spite of the simplifications, quite complex theoretically, as shown in Chapter B3. The straight element is less complex, and the theory follows well-established procedures.

B3. CURVED ELEMENT THEORY

B3.1 PROCEDURE AND ASSUMPTIONS

The stiffness and state determination calculations for the element are based on a combination of beam and shell theory.

The element is modelled as shown in Fig. B3.1. At each of the two Gauss integration points a beam *slice* is considered, and each slice is divided into a number of cross-section *subelements*. The subelement stiffnesses are constructed first, allowing for elasto-plastic behavior of the pipe steel. The slice stiffnesses are constructed from the subelement stiffnesses by summation. The complete element stiffness is then constructed from the slice stiffnesses by Gauss quadrature.

The slice deformations consist of six beam-type deformations plus two ovaling deformations. The beam deformations consist of axial deformation, torsional twist, in-plane and out-of-plane curvatures, and in-plane and out-of-plane flexural shear deformations. One ovaling deformation is associated with in-plane bending, and the second with out-of-plane bending (Fig. B3.2).

The beam deformations at each slice are related to the element node displacements by a deformation shape function. The ovaling deformations in any slice are assumed to be independent of the ovaling deformations at other slices. Hence, no shape function is assumed for variation of ovaling along the element length. The ovaling deformations are internal degrees of freedom at each slice and are condensed out before the element stiffness is constructed from the slice stiffnesses.

Each subelement is assumed to be in a state of plane stress, with axial, hoop, and shear stresses. The axial strain in any subelement is affected by axial deformation and curvature of the slice and by the ovaling deformations. The effects of axial deformation and curvature are determined assuming plane (but not necessarily circular) cross sections. The effects of ovaling are determined using the membrane equations for an axisymmetric shell. The shear strain in

any subelement is assumed to be affected by torsional twist only. Flexural shear effects are assumed to be negligible at the subelement level and are ignored (they are introduced at the slice level). The subelement shear strains due to twist are determined assuming plane, circular cross sections.

Hoop strains are not determined from strain-displacement relationships. Rather, the hoop stresses are governed by the equilibrium relationship between internal pressure and hoop stress. The hoop strain in any subelement thus becomes an internal degree of freedom for the subelement and is condensed out before the slice stiffness is constructed.

The hoop stress in equilibrium with the internal pressure is the average value over the pipe wall thickness. In addition, ovaling induces pipe wall bending, and hence stresses which vary through the pipe wall thickness. It is assumed that yielding of slice subelements is not affected by pipe wall bending, and correspondingly that flexural yield of the pipe wall due to ovaling is not affected by subelement yield. That is, it is assumed that membrane and bending effects in the pipe wall are uncoupled.

Although it is not essential to the theory, it is assumed that the centerline radius of the bend is large compared with the pipe radius. This is not generally true for piping elbows. However, in view of the many other assumptions made in developing the theory, this assumption is believed to be reasonable. Ford and Turner [B1] have shown that the assumption produces only small errors.

B3.2 SLICE STIFFNESS

B3.2.1 Deformations and Actions

The slice deformation vector is \underline{y}_s , given by

$$\underline{y}_s^T = \langle \delta \ \psi_n \ \gamma_n \ \psi_r \ \gamma_r \ \phi \ \omega_n \ \omega_r \rangle \quad (B3.1)$$

in which δ = axial strain at pipe axis; ϕ = rate of torsional twist; ψ_n = in-plane bending curvature; ψ_r = out-of-plane bending curvature; γ_n = in-plane flexural shear deformation; γ_r = out-of-plane flexural shear deformation; ω_n = in-plane ovaling (Fig. B3.2); and ω_r = out-of-

plane ovalling.

The corresponding slice action vector is \underline{S}_s , where

$$\underline{S}_s^T = \langle F M_n V_n M_r V_r T \Omega_n \Omega_r \rangle \quad (\text{B3.2})$$

in which F = axial force; T = torsional moment; M_n = in-plane bending moment; M_r = out-of-plane bending moment; V_n = in-plane flexural shear; V_r = out-of-plane flexural shear; Ω_n = generalized force for in-plane ovalling; and Ω_r = generalized force for out-of-plane ovalling. The forces Ω_n and Ω_r are defined only in a virtual work sense.

B3.2.2 Subelement Strains due to Ovalling

The strain-displacement relationships for an axisymmetric membrane (Fig. B3.3) are as follows [B2]:

$$\epsilon_a = \frac{1}{r + a \sin \theta} (v \cos \theta + w \sin \theta) \quad (\text{B3.3a})$$

$$\epsilon_h = \frac{1}{a} \left(\frac{\partial v}{\partial \theta} + w \right) \quad (\text{B3.3b})$$

in which ϵ_a = circumferential strain in membrane (axial strain in pipe) and ϵ_h = meridional strain in membrane (hoop strain in pipe). If it is assumed that the bend radius is large compared with the pipe radius, Eqn. B3.3a can be approximated by

$$\epsilon_a = \frac{1}{r} (v \cos \theta + w \sin \theta) \quad (\text{B3.3c})$$

The two ovalling deformations are shown in Fig. B3.2. These deformations produce both normal (w) and tangential (v) displacements. It is assumed that the hoop strains, ϵ_h , associated with ovalling are zero. The shape functions for membrane displacement are thus chosen as

$$w = \omega_n \cos 2\theta + \omega_r \sin 2\theta \quad (\text{B3.4a})$$

and

$$v = -\frac{1}{2} \omega_n \sin 2\theta + \frac{1}{2} \omega_r \cos 2\theta \quad (\text{B3.4b})$$

Hence, the strain-displacement relationships are

$$\epsilon_a = -\frac{\sin^3\theta}{r} \omega_n + \frac{\cos\theta}{2r} (1 + 2\sin^2\theta) \omega_r \quad (\text{B3.5a})$$

$$\epsilon_h = 0 \quad (\text{B3.5b})$$

B3.2.3 Strain-Deformation Relationships for Slice

Consider slice subelement i , located at angle θ_i (Fig. B3.1). The subelement membrane strains, ϵ_{ai} and $\gamma_{i\theta}$, are related to the slice deformations by

$$d\epsilon_i = \underline{B}_i d\underline{v}_i \quad (\text{B3.6})$$

in which \underline{v}_i is defined by Eqn. B3.1;

$$d\underline{\epsilon}_i^T = \langle d\epsilon_{ai} \ d\gamma_{i\theta} \rangle \quad (\text{B3.7})$$

and

$$\underline{B}_i = \begin{bmatrix} 1 & a\sin\theta_i & 0 & -a\cos\theta_i & 0 & 0 & \frac{-\sin^3\theta_i}{r} & \frac{\cos\theta_i(1+2\sin^2\theta_i)}{2r} \\ 0 & 0 & 0 & 0 & 0 & a & 0 & 0 \end{bmatrix} \quad (\text{B3.8})$$

This transformation assumes that plane sections remain plane, that the change in cross section shape due to ovaling is negligible, and that the ratio of cross section radius to bend radius (a/r) is small. A modification of the transformation to allow for significant change of cross section shape is considered later.

Note that the shear deformations, γ_n and γ_r , are assumed not to influence the subelement strains. The effects of these deformations are considered separately.

B3.2.4 Stress-Strain Relationship for Slice Subelements

Each subelement is assumed to be in a state of membrane stress and strain (plane stress). The hoop stress is controlled by the internal pressure, according to the well-known equation

$$\sigma_h = P \frac{(a-0.5t)}{t} = \frac{Pa'}{t} \quad (\text{B3.9})$$

in which P = internal pressure; a = radius to pipe wall mid-thickness; t = wall thickness; and $a' = a - 0.5t$.

The Mroz plasticity theory is used. The details of the procedures used to implement this theory are described in reference [B3]. For any given state of subelement i , an elasto-plastic stress-strain relationship is determined as

$$d\underline{\sigma}_i = \underline{D}_i d\underline{\epsilon}_i \quad (\text{B3.10})$$

in which

$$d\underline{\sigma}_i^T = \langle d\sigma_{ai} \ d\tau_i \ d\sigma_{hi} \rangle \quad (\text{B3.11})$$

$$d\underline{\epsilon}_i^T = \langle d\epsilon_{ai} \ d\gamma_i \ d\epsilon_{hi} \rangle \quad (\text{B3.12})$$

and in which $\underline{D}_i = 3 \times 3$ elasto-plastic constitutive matrix and the stresses and strains are membrane values. From Eqns. B3.10 and B3.9 it follows that

$$[\underline{D}_i] \begin{Bmatrix} d\epsilon_{ai} \\ d\gamma_i \\ d\epsilon_{hi} \end{Bmatrix} = \begin{Bmatrix} d\sigma_{ai} \\ d\tau_i \\ a' dP/t \end{Bmatrix} \quad (\text{B3.13})$$

in which dP is known. Hence, \underline{D}_i can be reduced, by static condensation, to a 2×2 matrix, \underline{D}_{ri} , in terms of axial and shear stresses only. If $dP = 0$, the result can be written as:

$$[\underline{D}_{ri}] \begin{Bmatrix} d\epsilon_{ai} \\ d\gamma_i \end{Bmatrix} = \begin{Bmatrix} d\sigma_{ai} \\ d\tau_i \end{Bmatrix} \quad (\text{B3.14})$$

If dP is not zero, an initial stress effect must be included, as described later.

B3.2.5 Stiffness Matrix

The transformation matrix \underline{B} (Eqn. B3.8) considers the effects of axial deformation, bending, and torsion, and the axial membrane strains due to ovaling. A *partial* tangent stiffness matrix for the slice, \underline{k}_{sp} , which considers only these effects, is thus given by

$$\underline{k}_{sp} = 2\pi \frac{at}{N} \sum_{i=1}^N \underline{B}_i^T \underline{D}_{ri} \underline{B}_i \quad (\text{B3.15})$$

in which N = number of slice subelements around pipe circumference.

The matrix \underline{k}_{sp} has zero values in the rows and columns corresponding to the shear defor-

mations γ_r and γ_n , because the transformation \underline{B} does not consider flexural shear effects. It is assumed that the flexural shear stiffness is not affected by yielding of the pipe wall, and hence, that the elastic shear stiffness can be used. For an effective shear area equal to one-half of the cross section area, the shear stiffnesses are defined by

$$dV_r = G\pi at \cdot d\gamma_r = k_\gamma \cdot d\gamma_r \quad (\text{B3.16a})$$

and

$$dV_n = G\pi at \cdot d\gamma_n = k_\gamma \cdot d\gamma_n \quad (\text{B3.16b})$$

in which G = elastic shear modulus. The stiffness coefficients $k_{sp}(3,3)$ and $k_{sp}(5,5)$ are set equal to k_γ .

The slice stiffness matrix, \underline{k}_{sp} , now includes the influence of ovaling on axial strains but does not consider bending of the pipe wall due to ovaling. The matrix also does not consider the effect of internal pressure on ovaling stiffness. These effects are included as follows.

B3.2.6 Ovaling Resistance due to Pipe Wall Bending

Consider the ovaling deformation associated with in-plane bending (Fig. B3.2a). The radial and tangential displacements, from Eqns. B3.4 are

$$w = \omega_n \cos 2\theta \quad (\text{B3.17a})$$

and

$$v = -\frac{1}{2} \omega_n \sin 2\theta \quad (\text{B3.17b})$$

From the strain-displacement relationships for an axisymmetric shell, the pipe wall curvature in the hoop direction, ψ_w , is

$$\psi_w = \frac{1}{a^2} \left(\frac{\partial v}{\partial \theta} - \frac{\partial^2 w}{\partial \theta^2} \right) \quad (\text{B3.18})$$

Hence, from Eqns. B3.17,

$$\psi_w = \frac{3}{a^2} \cos 2\theta \omega_n \quad (\text{B3.19})$$

It is assumed that the bending strength of the pipe wall is not affected by the presence of axial

and hoop membrane stresses. Hence, for any given steel stress-strain relationship, a moment-curvature relationship can be determined for the pipe wall. For a given state of strain at location θ on the pipe wall, let the moment-curvature relationship be

$$dm_w = j_w d\psi_w \quad (\text{B3.20})$$

Hence, from Eqns. B3.19 and B3.20, a generalized ovaling stiffness can be defined by

$$d\Omega_{hn} = \frac{9}{a^4} \int_0^{2\pi} \cos^2 2\theta \cdot j_w \cdot a d\theta \cdot d\omega_n \quad (\text{B3.21a})$$

or

$$d\Omega_{hn} = k_{wh} d\omega_n \quad (\text{B3.21b})$$

By integrating around the pipe circumference, the relationship between Ω_{hn} and ω_n can be determined. When normalized to $\Omega/\Omega_y = 1$ and $\omega/\omega_y = 1$, where Ω_y and $\omega_y =$ values at first yield, the relationship depends on the steel stress-strain curve but is independent of the ratio of pipe radius to wall thickness.

The normalized $\Omega-\omega$ relationships have been calculated for three different stress-strain curves, as shown in Fig. B3.4. It can be seen that the shapes of the curves do not vary greatly. Hence, for any given stress-strain curve, the $\Omega-\omega$ relationship can be estimated from Fig. B3.4 without evaluating Eqn. B3.21.

For analysis, a trilinear relationship is assumed, as shown in Fig. B3.5. The same trilinear relationship is used for both in-plane and out-of-plane ovaling, and it is further assumed that the ovaling deformations ω_n and ω_r are uncoupled. Hence, the ovaling stiffness, k_{wh} , is added to the diagonal terms $k_{sp}(7,7)$ and $k_{sp}(8,8)$ of the slice stiffness matrix.

B3.2.7 Ovaling Stiffness due to Internal Pressure

The equilibrium relationship between internal pressure and hoop stress is given by Eqn. B3.9. This assumes that the pipe radius, a , remains constant. As the cross section ovals, however, the pipe radius changes, with the result that for constant hoop stress an equilibrium error develops. This error can be regarded as an unbalanced internal pressure, which tends to resist

ovalling.

Consider in-plane ovoiding, ω_n (Fig. B3.2a). From Eqn. B3.19, the change in hoop curvature at location θ in the pipe wall is

$$\psi_w = \frac{3}{a^2} \cos 2\theta \omega_n \quad (\text{B3.22})$$

Hence, the unbalanced pressure, P_u , is given by

$$P_u = \sigma_n t \psi_w = P(a - 0.5t) \psi_w \quad (\text{B3.23})$$

in which P = internal pressure. Assuming t/a is small, it follows from Eqns. B3.23 and B3.22 that

$$P_u = \frac{3P}{a} \cos 2\theta \omega_n \quad (\text{B3.24})$$

Hence, the generalized force associated with P_u is given by

$$\Omega_{pn} = \frac{3P}{a} \int_0^{2\pi} \cos^2 2\theta \cdot a d\theta \cdot \omega_n \quad (\text{B3.25a})$$

or

$$\Omega_{pn} = 3P\pi\omega_n = k_{wp}\omega_n \quad (\text{B3.25b})$$

It is assumed that the same stiffness applies for both in-plane and out-of-plane ovoiding and that the stiffnesses are uncoupled. Hence, the stiffness k_{wp} is added to the diagonal terms $k_{sp}(7,7)$ and $k_{sp}(8,8)$ of the slice stiffness.

B3.2.8 Condensed Slice Stiffness

After addition of the ovoiding stiffnesses, the partial slice stiffness, \underline{k}_{sp} , becomes the slice stiffness, \underline{k}_s . The ovoiding deformations are assumed to be internal degrees of freedom for the slice. Hence, the 8 x 8 matrix can be condensed to a 6 x 6 matrix, \underline{k}_{sr} , in terms of the stress resultants on the pipe cross section.

and β (positive or negative) defines the slice location (Fig. B3.7).

The elastic slice flexibility is defined by

$$\underline{v}_{sr} = \underline{f}_s \underline{s}_{sr} \quad (\text{B3.30})$$

in which

$$\underline{v}_{sr}^T = \langle \delta \psi_n \gamma_n \psi_r \gamma_r \phi \rangle \quad (\text{B3.31})$$

and

$$\underline{f}_s = \text{diag} \left[\frac{1}{EA} \quad \frac{1}{\alpha EI} \quad \frac{2}{GA} \quad \frac{1}{\alpha EI} \quad \frac{2}{GA} \quad \frac{1}{2GI} \right] \quad (\text{B3.32})$$

in which E = Young's modulus; G = shear modulus; A = cross section area; I = cross section moment of inertia; and α = flexibility factor to account for ovaling. The flexibility factor follows from the ovaling theory described in the preceding sections (from the reduced slice stiffness, \underline{k}_{sr} , for the elastic case, determine the effective EI value). The result is

$$\alpha = 1 - \frac{9}{10 + \frac{12}{1-\nu^2} \left(\frac{tr}{a^2} \right)^2 + \frac{48Pr^2}{Eat}} \quad (\text{B3.33})$$

in which ν = Poisson's ratio. The flexibility factor given by the well-known von Karman theory [B4] is (for $P=0$)

$$\alpha = 1 - \frac{9}{10 + 12 \left(\frac{tr}{a^2} \right)^2} \quad (\text{B3.34})$$

which is essentially identical to Eqn. B3.33.

From Eqns. B3.26 and B3.30, the element 6×6 flexibility matrix, \underline{F}_N , in symmetric-antisymmetric coordinates follows as

$$\underline{F}_N = \int_{-\phi}^{+\phi} \underline{b}_N^T \underline{f}_s \underline{b}_N r d\beta \quad (\text{B3.35})$$

in which r and β are defined in Fig. B3.7. The flexibility coefficients can be obtained by closed form integration. The matrix \underline{F}_N uncouples into two 2×2 plus two 1×1 submatrices, so that only 8 coefficients need to be evaluated.

The element stiffness, \underline{K}_N , in symmetric-antisymmetric coordinates is easily obtained by inverting \underline{F}_N .

B3.3.3 Displacement Transformation

The deformations at a slice, \underline{v}_{sr} , can be obtained as follows.

From Eqns. B3.30 and B3.26

$$\underline{v}_{sr} = \int_s \underline{b}_N \underline{N} \quad (\text{B3.36})$$

Hence,

$$\underline{v}_{sr} = \int_s \underline{b}_N \underline{K}_N \underline{n} = \underline{a}_n \underline{n} \quad (\text{B3.37})$$

in which \underline{n} contains displacements corresponding to \underline{N} . A transformation between the symmetric-antisymmetric deformations and the 12 local displacements (Fig. B3.6a) can easily be constructed. This can then be combined with the well-known coordinate rotation transformation from local to global displacements, \underline{r} , (Fig. B3.6b). A combined transformation between symmetric-antisymmetric deformations and global displacements follows in the form

$$\underline{n} = \underline{a}_r \underline{r} \quad (\text{B3.38})$$

Hence, from Eqn. B3.37,

$$\underline{v}_{sr} = \int_s \underline{b}_N \underline{K}_N \underline{a}_r \underline{r} = \underline{a}_{sr} \underline{r} \quad (\text{B3.39})$$

Matrix \underline{a}_{sr} is the required transformation between nodal displacements and slice deformations.

B3.3.4 Element Stiffness

The transformation matrix, \underline{a}_{sr} , is formed for each slice (Gauss point) in the element. The element stiffness then follows as

$$\underline{K} = \sum_i w_i \underline{a}_{sr}^T \underline{k}_{sr} \underline{a}_{sr} \quad (\text{B3.40})$$

in which w_i = Gauss quadrature weighting function and \underline{k}_{sr} is the 6 x 6 slice stiffness.

B3.4 INITIAL STRESS EFFECTS

B3.4.1 General

The effects of loads which originate at the element level are treated as initial stress effects. Pipe elements can, in general, be subjected to initial stresses due to changes in temperature, changes in internal pressure, and creep. Loads which originate at the element level are also introduced when rate-dependent plasticity is considered. Temperature, pressure, and creep produce real initial stresses, with physical meanings. The initial stresses caused by strain rate effects exist only in a mathematical sense.

Initial stresses affect the analysis in two ways. First, they contribute to the load vector; and, second, they influence the state determination calculation. Initial stresses do not affect the stiffness calculation.

B3.4.2 Pressure and Temperature Changes

At a slice subelement, i , the tangent stress-strain relationship, including initial stress effects, is

$$\begin{Bmatrix} d\sigma_{ai} \\ d\tau_i \\ a' dP/dt \end{Bmatrix} = [D_i] \begin{Bmatrix} d\epsilon_{ai} - \alpha dT \\ d\gamma_i \\ d\epsilon_{hi} - \alpha dT \end{Bmatrix} \quad (B3.41)$$

in which dP = pressure increment, dT = temperature increment, and α = coefficient of thermal expansion. Eqn. B3.41 can be condensed to the form

$$\begin{Bmatrix} d\sigma_{ai} \\ d\tau_i \end{Bmatrix} = [D_{ri}] \begin{Bmatrix} d\epsilon_{ai} \\ d\gamma_i \end{Bmatrix} + \begin{Bmatrix} d\sigma_{a0i} \\ d\tau_{0i} \end{Bmatrix} \quad (B3.42)$$

or

$$d\underline{\sigma}_{ri} = \underline{D}_{ri} d\underline{\epsilon}_i + d\underline{\sigma}_{0ri} \quad (B3.43)$$

Application of the procedures of Section B3.2 produces the slice stiffness relationship

$$d\underline{S}_s = \underline{k}_s d\underline{v}_s + d\underline{S}_{s0} \quad (B3.44)$$

in which \underline{k}_s is as defined in Section B3.2.8, and

$$d\underline{S}_{s0} = \frac{2\pi at}{N} \sum_{i=1}^N \underline{B}_i^T d\underline{\sigma}_{0ri} + \begin{Bmatrix} \pi a^2 dP \\ 0 \\ 0 \\ 0 \\ 0 \\ 0 \\ 0 \\ 0 \end{Bmatrix} \quad (B3.45)$$

is the initial slice force. The last term in this equation is the axial force in the contained fluid (pipe inside area times fluid pressure). Because the increment of slice ovaling forces is zero, Eqn. B3.44 can be condensed to the form:

$$\underline{dS}_{sr} = \underline{k}_{sr} \underline{dv}_{sr} + \underline{dS}_{sor} \quad (\text{B3.46})$$

By the procedure of Section B3.3, this relationship can be transformed to the following relationship in symmetric-antisymmetric coordinates:

$$\underline{dN} = \underline{K}_N \underline{dn} + \underline{dN}_o \quad (\text{B3.47})$$

in which $\underline{N}, \underline{n}$ and \underline{K}_N are as defined in Section B3.3.3, and

$$\underline{dN}_o = \sum_i w_i \underline{a}_{ni}^T \underline{dS}_{sori} \quad (\text{B3.48})$$

in which w_i = Gauss weighting factor at slice i and the transformation \underline{a}_n is defined by Eqn. B3.37. Finally, \underline{dN}_o is transformed to global coordinates using the transformation of Eqn. B3.38.

B3.4.3 Strain Rate Effects

The general theory for material strain rate dependence has been presented by Mosaddad [B3]. Certain additional assumptions have been made in applying this theory to the pipe element. A summary of the assumptions is as follows.

- (a) It is assumed that strain rate effects influence only the membrane stresses. The bending stiffness of the pipe wall is assumed to be rate independent.
- (b) Strain increments are divided into elastic and plastic components:

$$\underline{d\epsilon} = \underline{d\epsilon}_e + \underline{d\epsilon}_p \quad (\text{B3.49})$$

- (c) Stress increments are divided into plastic and damping components:

$$\underline{d\sigma} = \underline{d\sigma}_p + \underline{d\sigma}_d \quad (\text{B3.50})$$

- (d) Total stress increments and elastic strain increments are related by Hooke's law:

$$\underline{d\sigma} = \underline{D}_e \underline{d\epsilon}_e \quad (\text{B3.51})$$

- (e) Mroz effective plastic stress increments are related to effective plastic strain increments by the rate-independent Mroz model:

$$d\sigma_p^* = \underline{n}_\sigma^T d\underline{\sigma}_p = K d\underline{\epsilon}_p^* \quad (\text{B3.52})$$

in which $d\sigma_p^*$ = effective plastic stress increment; $d\underline{\epsilon}_p^*$ = effective plastic strain increment; \underline{n}_σ^T = unit vector normal to the yield surface; and K = tangent plastic modulus.

- (f) The damping stress increment is defined by:

$$d\underline{\sigma}_d = C \left(\frac{1}{dt} d\underline{\epsilon}_p - \dot{\underline{\epsilon}}_p \right) \quad (\text{B3.53})$$

in which C = damping coefficient, dt = time step, and $\dot{\underline{\epsilon}}_p$ is the plastic strain rate. This equation assumes that the backward difference integration scheme is used.

- (g) The flow rule is defined by:

$$d\underline{\epsilon}_p = \underline{n}_\sigma d\underline{\epsilon}_p^* \quad (\text{B3.54})$$

With these assumptions, the governing equations are obtained as follows. Premultiply Eqn. B3.50 by \underline{n}_σ^T and substitute Eqns. B3.52 - B3.54 into Eqn. B3.50 to get the effective plastic strain increment as:

$$d\underline{\epsilon}_p^* = \frac{\underline{n}_\sigma^T d\underline{\sigma} + C \underline{n}_\sigma^T \dot{\underline{\epsilon}}_p}{K + C/dt} \quad (\text{B3.55})$$

By virtue of Eqns. B3.51, B3.54, and B3.55, Eqn. B3.49 can be written as:

$$d\underline{\epsilon} = \left[\underline{D}_e^{-1} + \frac{\underline{n}_\sigma \underline{n}_\sigma^T}{K + C/dt} \right] d\underline{\sigma} + \frac{C \underline{n}_\sigma^T \dot{\underline{\epsilon}}_p}{K + C/dt} \underline{n}_\sigma \quad (\text{B3.56})$$

Inversion of Eqn. B3.56 by the Sherman-Morrison formula results in:

$$d\underline{\sigma} = \underline{D} d\underline{\epsilon} + d\underline{\sigma}_{or} \quad (\text{B3.57})$$

in which

$$\underline{D} = \underline{D}_e - C_1 (\underline{D}_e \underline{n}_\sigma) (\underline{D}_e \underline{n}_\sigma)^T \quad (\text{B3.58})$$

$$d\underline{\sigma}_{or} = -C_1 \underline{C} \underline{n}_\sigma^T \dot{\underline{\epsilon}}_p \cdot \underline{D}_e \underline{n}_\sigma \quad (\text{B3.59})$$

and

$$C_1 = \left(\underline{n}_\sigma^T \underline{D}_e \underline{n}_\sigma + K + \frac{C}{dt} \right)^{-1} \quad (\text{B3.60})$$

For a finite time step, dt is replaced by Δt . The last term in Eqn. B3.57, $d\sigma_{or}$, is then treated as an initial stress. In each time step, the initial stresses, $d\sigma_{or}$, are transformed to initial element forces and assembled into the effective load vector for the step.

B3.4.4 Round-Off in Mroz Material Calculations

In the state determination calculation for the Mroz material, the stresses calculated assuming linear behavior are scaled so that the stress point lies exactly on the yield surface. This means that the calculated hoop stress in any slice subelement may not exactly satisfy Eqn. B3.9. If this error is not corrected, it may accumulate over a number of load increments and reach a significant magnitude.

The error is corrected by determining, for each subelement, the internal pressure corresponding to the calculated hoop stress. The difference between this pressure and the actual pressure is then a pressure error. At each iteration, this value is added to dP in Eqn. B3.41 and treated as an initial stress effect. This prevents accumulation of error.

B3.5 CHANGE OF SECTION GEOMETRY DUE TO OVALLING

Ovalling may produce significant changes in cross section geometry. One result of this is that an elbow is stronger for in-plane bending which increases the bend angle (and thus stretches the cross section) than for bending which decreases the bend angle (and thus collapses the section). This effect is taken into account as follows.

At each stiffness reformulation, a deformed slice geometry is determined, taking into account the total ovalling deformation. Modified strain-deformation relationships for the slice element (Eqn. B3.6) are then written as

$$\begin{Bmatrix} d\epsilon_{a1} \\ dy_1 \end{Bmatrix} = \begin{bmatrix} 1 & (x_{o1} + \Delta x_1) & 0 & -(y_{o1} + \Delta y_1) & 0 & 0 & \frac{-\sin^2 \theta_1}{r} & \frac{\cos \theta_1 (2\sin^2 \theta_1 + 1)}{2r} \\ 0 & 0 & 0 & 0 & 0 & a & 0 & 0 \end{bmatrix} \begin{Bmatrix} dv \\ -a \end{Bmatrix} \quad (B3.61)$$

in which

$$\begin{aligned}x_{oi} &= a \cos \theta_i \\ \Delta x_i &= (\omega_n \cos 2\theta_i) \cos \theta_i - \frac{1}{2} (\omega_n \sin 2\theta_i) \sin \theta_i \\ y_{oi} &= a \sin \theta_i \\ \Delta y_i &= (\omega_n \cos 2\theta_i) \sin \theta_i - \frac{1}{2} (\omega_n \sin 2\theta_i) \cos \theta_i\end{aligned}$$

and ω_n is the total in-plane ovaling deformation. The slice stiffness is then formed using the same procedures as before.

B3.6 STATE DETERMINATION

When an increment of global displacement, $\Delta \underline{r}$, has been determined, the state determination proceeds as follows.

- (1) Calculate element deformation increment:

$$\Delta \underline{n} = \underline{a}_r \Delta \underline{r} \quad (\text{B3.62})$$

- (2) Calculate the beam-type deformation increments for each slice:

$$\Delta \underline{y}_{sr} = \underline{a}_n \Delta \underline{n} \quad (\text{B3.63})$$

- (3) Calculate the ovaling deformation increments:

$$\begin{pmatrix} \Delta \omega_n \\ \Delta \omega_r \end{pmatrix} = \underline{T}_i \Delta \underline{y}_{sr} + \underline{K}_\omega^{-1} (\Delta \underline{\Omega}_e - \Delta \underline{\Omega}_o) \quad (\text{B3.64})$$

in which \underline{T}_i is the transformation matrix obtained during condensation of the slice stiffness from 8 x 8 to 6 x 6; \underline{K}_ω is the slice stiffness associated with ovaling deformations; $\Delta \underline{\Omega}_e$ is the error in generalized ovaling force due to nonlinearity in the preceding state determination; and $\Delta \underline{\Omega}_o$ are generalized initial forces from terms $S_{so}(7)$ and $S_{so}(8)$ in Eqn. B3.45.

- (4) Calculate the generalized ovaling forces, $\underline{\Omega}_h$, associated with bending of the pipe wall. Update the ovaling stiffness, if necessary.
- (5) Calculate axial and shear strain increments using Eqn. B3.6 or Eqn. B3.61 if change of cross section due to ovaling is considered.

- (6) Calculate hoop strain increments from the axial and shear strain increments, taking into account any unbalanced hoop stresses due to either internal pressure change or errors from scaling the stresses to the yield surface. The hoop stress error can be obtained from:

$$\Delta\sigma_{hei} = \frac{Pa'}{t} - \sigma_{hi} \quad (B3.65)$$

in which P = current internal pressure and σ_{hi} = current hoop stress. Hence,

$$\Delta\epsilon_{hi} = \left(\Delta\sigma_{hei} - D_{31} \Delta\epsilon_{ai} - D_{32} \Delta\gamma_i \right) / D_{33} \quad (B3.66)$$

in which D_{ij} = term in the constitutive matrix \underline{D}_i .

- (7) Obtain subelement stresses by Mroz material state determination.
- (8) Obtain slice forces by summing the stresses over the cross section. Add the axial force in the fluid column. Calculate the generalized ovalling forces as

$$\underline{\Omega} = \underline{\Omega}_a + \underline{\Omega}_h + \underline{\Omega}_p \quad (B3.67)$$

in which $\underline{\Omega}_a$, $\underline{\Omega}_h$, and $\underline{\Omega}_p$ are ovalling forces associated with axial strain, pipe wall bending, and internal pressure, respectively. The force $\underline{\Omega}_h$ is obtained at Step (4). The forces $\underline{\Omega}_a$ and $\underline{\Omega}_p$ are obtained from

$$\underline{\Omega}_a = \frac{2\pi at}{Nr} \sum_{i=1}^N \sigma_{ai} \left\{ \begin{array}{c} -\sin^3\theta_i \\ 0.5\cos\theta_i (2\sin^2\theta_i + 1) \end{array} \right\} \quad (B3.68)$$

and

$$\underline{\Omega}_p = 3p\pi \left\{ \begin{array}{c} \omega_n \\ \omega_r \end{array} \right\} \quad (B3.69)$$

Because the generalized ovalling forces are assigned zero values, it follows that

$$\underline{\Omega}_e = -\underline{\Omega} \quad (B3.70)$$

- (9) Calculate the element resisting forces in symmetric-antisymmetric modes:

$$\underline{N} = \sum_i w_i \underline{a}_{ni}^T \underline{S}_{sri} \quad (B3.71)$$

- (10) Transform to global coordinates to obtain the element resisting force as

$$\underline{R}' = \underline{a}_r^T \underline{N} \quad (B3.72)$$



B4. STRAIGHT PIPE THEORY

B4.1 PROCEDURE AND ASSUMPTIONS

The stiffness and state determination calculations for the element are based essentially on beam theory.

The element can be modeled as either a "Gauss slice" model (Fig. B4.1a) or as an "end slice" model (Fig. B4.1b). For WIPS, the default option is the Gauss model. At each of the two integration points, a beam *slice* is considered, and each slice is divided into a number of cross section *subelements*. The subelement stiffnesses are constructed first, allowing for elasto-plastic behavior of the pipe steel. The slice stiffnesses are constructed from the subelement stiffnesses by summation. The complete element stiffness is then constructed from the slice stiffnesses by either Gauss quadrature (for the Gauss model) or by closed form integration (for the end slice model).

The slice deformations consist of six beam type deformations, namely axial deformation, torsional twist, in-plane and out-of-plane curvatures, and in-plane and out-of-plane flexural shear deformations.

The complete element has six nodal degrees of freedom at each end (Fig. B4.2), which provide six rigid body modes plus six element deformations. In addition, two internal degrees of freedom are considered to allow linear variation of axial strain and torsional twist along the element length. These degrees of freedom are added to avoid excessive constraint by allowing linear strain variation along the element axis. A typical beam formulation allows only constant strain, which is reasonable if the element axis is also the centroidal axis of the beam. In an inelastic element, however, the effective centroidal axis will shift as the cross section yields.

The slice deformations are related to the element deformations by shape functions which include the effects of shear deformation. Each subelement of a slice is assumed to be in a state of plane stress, with axial, hoop, and shear stresses. The effects of axial deformation and curvature on axial strains are determined assuming plane, circular cross sections. The shear strain

is assumed to be affected by torsional twist only. Flexural shear effects are assumed to be negligible at the subelement level and are ignored (they are introduced at the slice level). The subelement shear strains due to twist are determined assuming plane, circular cross sections.

Hoop strains are not determined from strain-displacement relationships. Rather the hoop stresses are governed by the equilibrium relationship between internal pressure and hoop stress. The hoop strain in any subelement thus becomes an internal degree of freedom for the subelement and is condensed out before the slice stiffness is constructed.

B4.2 SLICE STIFFNESS

B4.2.1 Deformations and Actions

The slice deformation vector, \underline{y}_s , is given by:

$$\underline{y}_s^T = \langle \delta \ \psi_z \ \psi_y \ \phi \ \gamma_{xy} \ \gamma_{xz} \rangle \quad (\text{B4.1})$$

in which δ = axial strain at pipe axis; ψ_z = bending curvature about element z axis; ψ_y = bending curvature about y axis; ϕ = rate of torsional twist; γ_{xy} = flexural shear deformation in x-y plane; and γ_{xz} = flexural shear deformation in x-z plane.

The corresponding slice action vector is \underline{S}_s , where

$$\underline{S}_s^T = \langle F \ M_z \ M_y \ T \ V_{xy} \ V_{xz} \rangle \quad (\text{B4.2})$$

in which F = axial force; M_z and M_y = bending moments; T = torsional moment; and V_{xy} and V_{xz} = flexural shear forces.

B4.2.2 Strain-Deformation Relationships for Slice

Consider slice subelement i, located at angle θ_i (as for a curved element, Fig. B3.1). The subelement membrane strains, ϵ_{ai} and γ_{i} , are related to the slice deformations by:

$$d\epsilon_{ai} = \underline{B}_i d\underline{y}_s \quad (\text{B4.3})$$

in which \underline{y}_s is defined by Eqn. B4.1;

$$d\epsilon_i^T = \langle d\epsilon_{ai} \ d\gamma_i \rangle \quad (\text{B4.4})$$

and

$$\underline{B}_i = \begin{bmatrix} 1 & a \sin \theta_i & -a \cos \theta_i & 0 & 0 & 0 \\ 0 & 0 & 0 & a & 0 & 0 \end{bmatrix} \quad (\text{B4.5})$$

This transformation assumes that plane sections remain plane and circular. It is also implied that the pipe thickness is small compared to the pipe diameter.

Note that the slice shear deformations, γ_{xy} and γ_{xz} , are assumed not to influence the subelement strains. The effects of these deformations are considered separately.

B4.2.3 Stress-Strain Relationships for Slice Subelement

Each subelement is assumed to be in a state of membrane stress and strain (plane stress). The hoop stress is controlled by the internal pressure, according to the well-known equation

$$\sigma_h = P \frac{(a - 0.5t)}{t} = \frac{Pa'}{t} \quad (\text{B4.6})$$

in which P = internal pressure; a = radius to pipe wall mid-thickness; t = wall thickness; and $a' = a - 0.5t$.

The Mroz plasticity theory is used. The details of the procedures used to implement this theory have been described by Mosaddad [B3] and are not repeated here. For any given state of subelement i , an elasto-plastic stress-strain relationship is determined as

$$d\underline{\sigma}_i = \underline{D}_i d\underline{\epsilon}_i \quad (\text{B4.7})$$

in which

$$d\underline{\sigma}_i^T = \langle d\sigma_{ai} \quad d\tau_i \quad d\sigma_{hi} \rangle \quad (\text{B4.8})$$

$$d\underline{\epsilon}_i^T = \langle d\epsilon_{ai} \quad d\gamma_i \quad d\epsilon_{hi} \rangle \quad (\text{B4.9})$$

and in which $\underline{D}_i = 3 \times 3$ elasto-plastic constitutive matrix and the stresses and strains are membrane values. From Eqns. B4.7 and B4.6 it follows that

$$\underline{D}_i = \begin{bmatrix} d\epsilon_{ai} \\ d\gamma_i \\ d\epsilon_{hi} \end{bmatrix} = \begin{bmatrix} d\sigma_{ai} \\ d\tau_i \\ a'dP/t \end{bmatrix} \quad (\text{B4.10})$$

in which dP is known. Hence, \underline{D}_i can be reduced, by static condensation, to a 2×2 matrix,

\underline{D}_{ri} in terms of axial and shear stresses only. If $dP = 0$, the result can be written as:

$$[\underline{D}_{ri}] \begin{Bmatrix} d\epsilon_{ai} \\ d\gamma_i \end{Bmatrix} = \begin{Bmatrix} d\sigma_{ai} \\ d\tau_i \end{Bmatrix} \quad (\text{B4.11})$$

If dP is not zero, an initial stress effect must be included, as described later.

B4.2.4 Stiffness Matrix

The transformation matrix \underline{B} (Eqn. B4.5) considers the effects of axial deformation, bending, and torsion. A tangent stiffness matrix for the slice, \underline{k}_s , which considers only these effects, is thus given by:

$$\underline{k}_s = 2\pi \frac{at}{N} \sum_{i=1}^N \underline{B}_i^T \underline{D}_{ri} \underline{B}_i \quad (\text{B4.12})$$

in which N = number of slice subelements around pipe circumference.

The matrix \underline{k}_s has zero rows and columns corresponding to the shear deformations γ_{xy} and γ_{xz} , because the transformation \underline{B} does not consider flexural shear effects. It is assumed that the flexural shear stiffness is not affected by yielding of the pipe wall, and hence, that the elastic shear stiffness can be used. For an effective shear area equal to one-half of the cross section area, the shear stiffnesses are defined by:

$$dV_{xy} = G\pi at \cdot d\gamma_{xy} = k_y \cdot d\gamma_{xy} \quad (\text{B4.13a})$$

and

$$dV_{xz} = G\pi at \cdot d\gamma_{xz} = k_y \cdot d\gamma_{xz} \quad (\text{B4.13b})$$

in which G = elastic shear modulus. The stiffness coefficients $k_s(5,5)$ and $k_s(6,6)$ are set equal to k_y .

B4.3 ELEMENT STIFFNESS

B4.3.1 Deformations and Actions

The element degrees of freedom, after deletion of the six rigid body modes, are given by:

$$\underline{y}_m^T = \langle u_x \theta_{zi} \theta_{zj} \theta_x \theta_{yi} \theta_{yj} u_{xm} \theta_{xm} \rangle \quad (\text{B4.14})$$

in which u_x = axial extension; θ_{zi} = z-axis rotation at element end i; θ_{zj} = z-axis rotation at end j; θ_x = torsional twist; θ_{yi} = y-axis rotation at end i; θ_{yj} = y-axis rotation at end j; u_{xm} = additional axial degree of freedom at element midpoint (displacement relative to the element ends); and θ_{xm} = additional torsional deformation at element midpoint (twist relative to element ends).

The corresponding element action vector is \underline{S}_m , where

$$\underline{S}_m^T = \langle F_x \ M_{zi} \ M_{zj} \ T_x \ M_{yi} \ M_{yj} \ F_{xm} \ T_{xm} \rangle \quad (\text{B4.15})$$

The forces F_{xm} and T_{xm} are defined only in a virtual work sense and are assigned zero values.

B4.3.2 Choice of Shape Function

For straight beam elements, it is common to use a cubic hermitian polynomial shape function, which is exact for a uniform elastic beam. If shear deformations are included, the shape can no longer be obtained from kinematic considerations only. Rather the equilibrium relationship between moments and shears must be considered, with the result that the shape function depends on the ratio of the flexural and shear stiffnesses. If a shape function is determined using the *elastic* stiffness values, then when the beam becomes inelastic it is implied that the ratio between the flexural and shear stiffnesses remains constant. This is unlikely to be correct. A more reasonable assumption, in general, is that the flexural stiffness changes whereas the shear stiffness remains constant. This assumption is made for the formulation of the slice stiffness and must be retained at the element level to avoid inconsistencies. For this reason, the shape function is continually updated as the analysis proceeds, using a strain energy minimization procedure as follows.

B4.3.3 Elastic Beam

A shape function is "exact" if it satisfies both the homogeneous governing equation for the element and the displacement boundary conditions at the element ends. An important property of an exact shape function is that it corresponds to a strain energy which is an "absolute" minimum.

For a uniform elastic beam element loaded only at its ends, the governing equation is a homogeneous fourth order differential equation, and the exact displaced shape is at most cubic. If shear deformations are ignored, the exact shape is the well-known cubic hermitian polynomial. If shear deformations are considered, the exact shape can be obtained by solving the differential equation directly, or alternatively by using a linear combination of polynomials up to cubic and choosing the combination factors to minimize the strain energy.

For a finite element formulation, the alternative method is preferable. Consider a uniform beam in which both flexural and shear deformations are present. Impose a unit rotation at the end $x = 0$, with the end $x = L$ fixed (Fig. B4.3a). The beam will have bending deformation plus a constant shear deformation, γ . If $v(x)$ defines the transverse displacement of the beam axis, the boundary conditions are:

$$\begin{aligned}v(0) &= 0 \\v'(0) &= 1 - \gamma \\v(L) &= 0 \\v'(L) &= -\gamma\end{aligned}$$

A combination of cubic and quadratic polynomials which satisfies these boundary conditions is:

$$v(x) = c \left(x - \frac{2x^2}{L} + \frac{x^3}{L^2} \right) + \frac{1-c}{2} \left(x - \frac{x^2}{L} \right) \quad (\text{B4.16})$$

in which

$$c = 1 - 2\gamma \quad (\text{B4.17})$$

The strain energy of the beam is:

$$U = \frac{1}{2} \int_0^L EI (v''(x))^2 dx + \frac{1}{2} GA' L (\gamma_{xy})^2 \quad (\text{B4.18})$$

Substitution of Eqns. B4.16 and B4.17 into Eqn. B4.18, and minimization with respect to c results in:

$$c = \frac{1 + \alpha_z}{1 + \beta_z} \quad (\text{B4.19})$$

in which

$$\alpha_z = \frac{4}{GA'L^2} \int_0^L EI \left(\frac{6x}{L^2} - \frac{3}{L} \right) dx = 0 \quad (\text{B4.20})$$

and

$$\beta_z = \frac{4}{GA'L^2} \int_0^L EI \left(\frac{6x}{L^2} - \frac{3}{L} \right)^2 dx = \frac{12EI}{GA'L^2} \quad (\text{B4.21})$$

These equations define the shape function.

B4.3.4 Inelastic Beam

For an inelastic beam, the stiffness along the element length can vary, and hence, the governing differential equation is generally not known. Thus, it is not generally possible to obtain the shape function by a closed form solution. A simple and effective procedure is to apply strain energy minimization with certain assumptions. In Eqn. B4.16, the shape function depends on the ratio of flexural stiffness to shear stiffness. As an approximation, the diagonal terms of the slice stiffness matrix are assumed to define effective flexural stiffnesses, and the slice shear stiffnesses are assumed to remain constant. The shape function is then obtained, as described in Section B4.3.6.

B4.3.5 Internal Degrees of Freedom

The two internal degrees of freedom, u_{xm} and θ_{xm} , are included to allow for linear variation of axial and torsional deformations along the element axis. The shape functions associated with these degrees of freedom do not involve flexural or shear deformations. No strain energy is associated with these deformations because the corresponding generalized forces are assigned zero values.

B4.3.6 Shape Functions

Displacement shape functions relating element deformations to the longitudinal, transverse, and twisting displacements along the element are obtained by strain energy minimization. They can be expressed as:

$$\begin{pmatrix} du(x) \\ dv(x) \\ dw(x) \\ d\phi(x) \end{pmatrix} = \underline{N}(x) d\underline{v}_m \quad (\text{B4.22})$$

in which u = longitudinal displacement; v and w = transverse displacements in the y and z directions, respectively; ϕ = twist; and \underline{N} is given by:

$$\underline{N}(x) = \begin{bmatrix} x/L & 0 & 0 & 0 & 0 & 0 & N_{17} & 0 \\ 0 & N_{22} & N_{23} & 0 & 0 & 0 & 0 & 0 \\ 0 & 0 & 0 & 0 & N_{35} & N_{36} & 0 & 0 \\ 0 & 0 & 0 & x/L & 0 & 0 & 0 & N_{48} \end{bmatrix} \quad (\text{B4.23})$$

in which

$$\begin{aligned} N_{17} &= N_{48} = \frac{-4x^2}{L} + 4x \\ N_{22} &= \frac{1+\alpha_z}{1+\beta_z} \left[x - \frac{2x^2}{L} + \frac{x^3}{L^2} \right] + \frac{\beta_z - \alpha_z}{2(1+\beta_z)} \left[x - \frac{x^2}{L} \right] \\ N_{23} &= \frac{1-\alpha_z}{1+\beta_z} \left[\frac{x^3}{L^2} - \frac{x^2}{L} \right] + \frac{\beta_z + \alpha_z}{2(1+\beta_z)} \left[\frac{x^2}{L} - x \right] \\ N_{35} &= \frac{1+\alpha_y}{1+\beta_y} \left[x - \frac{2x^2}{L} + \frac{x^3}{L^2} \right] + \frac{\beta_y - \alpha_y}{2(1+\beta_y)} \left[x - \frac{x^2}{L} \right] \\ N_{36} &= \frac{1-\alpha_y}{1+\beta_y} \left[\frac{x^3}{L^2} - \frac{x^2}{L} \right] + \frac{\beta_y + \alpha_y}{2(1+\beta_y)} \left[\frac{x^2}{L} - x \right] \end{aligned}$$

The shape functions relating the element degrees of freedom to the slice deformations are obtained by differentiating the displacement shape functions. They can be expressed as:

$$d\underline{v}_s = \underline{a} d\underline{v}_m \quad (\text{B4.24})$$

in which $d\underline{v}_s$ and $d\underline{v}_m$ are defined by Eqns. B4.1 and B4.14, and

$$\underline{a} = \begin{bmatrix} 1/L & 0 & 0 & 0 & 0 & 0 & -8q & 0 \\ 0 & a_{22} & a_{23} & 0 & 0 & 0 & 0 & 0 \\ 0 & 0 & 0 & 0 & a_{35} & a_{36} & 0 & 0 \\ 0 & 0 & 0 & 1/L & 0 & 0 & 0 & -8q \\ 0 & a_{52} & a_{53} & 0 & 0 & 0 & 0 & 0 \\ 0 & 0 & 0 & 0 & a_{65} & a_{66} & 0 & 0 \end{bmatrix} \quad (\text{B4.25})$$

in which the transformation \underline{a} is defined in terms of dimensionless coordinates q (Fig. B4.3b)

as:

$$\begin{aligned}
a_{22} &= \frac{-6(1+\alpha_z)}{(1+\beta_z)} q + 1; \\
a_{23} &= \frac{-6(1-\alpha_z)}{(1+\beta_z)} q - 1; \\
a_{35} &= \frac{-6(1+\alpha_y)}{(1+\beta_y)} q + 1; \\
a_{36} &= \frac{-6(1-\alpha_y)}{(1+\beta_y)} q - 1; \\
a_{52} &= \frac{(\beta_z - \alpha_z)}{2(1+\beta_z)} L; \\
a_{53} &= \frac{(\beta_z + \alpha_z)}{2(1+\beta_z)} L; \\
a_{65} &= \frac{(\beta_y - \alpha_y)}{2(1+\beta_y)} L; \\
a_{66} &= \frac{(\beta_y + \alpha_y)}{2(1+\beta_y)} L; \\
\alpha_z &= \frac{24}{GA'L^2} \int_{-1/2}^{1/2} k_s(2,2) q \, dq \\
\beta_z &= \frac{144}{GA'L^2} \int_{-1/2}^{1/2} k_s(2,2) q^2 \, dq \\
\alpha_y &= \frac{24}{GA'L^2} \int_{-1/2}^{1/2} k_s(3,3) q \, dq \\
\beta_y &= \frac{144}{GA'L^2} \int_{-1/2}^{1/2} k_s(3,3) q^2 \, dq
\end{aligned}$$

For the Gauss model, the integrals are obtained by Gauss quadrature. For the end slice model, the integrals are evaluated in closed form, assuming that $k_s(2,2)$ and $k_s(3,3)$ vary linearly along the element length.

The shape function is updated at each element stiffness reformulation. If shear deformations are ignored, reformulation is not necessary.

B4.3.7 Element Stiffness

For the Gauss model, the shape function, \underline{a} , is formed at each slice (Gauss point) in the element. The element stiffness then follows as:

$$\underline{K} = \sum_i w_i \underline{a}_i^T \underline{k}_{si} \underline{a}_i \quad (\text{B4.26})$$

in which w_i = Gauss quadrature weighting function at slice i , and \underline{k}_{si} is the 6 x 6 stiffness at

slice i .

For the end slice model, the element stiffness is calculated assuming that the slice stiffness, \underline{k}_s , varies linearly along the element length. Hence, the element stiffness can be obtained by closed form integration as:

$$\underline{K} = L \int_{-1/2}^{1/2} \underline{a}^T \underline{k}_s \underline{a} \, dq \quad (\text{B4.27})$$

The additional axial and torsional degrees of freedom at the element midpoint are internal degrees of freedom for the element. The 8×8 element stiffness, \underline{K} , is thus condensed to a 6×6 matrix in terms of element actions at pipe ends. This stiffness is expanded to include element rigid body displacements and then transformed to a 12×12 global stiffness. The transformations are well known and are not repeated here.

B4.4 STATE DETERMINATION

When an increment of global displacement, $\underline{\Delta}_r$, has been determined, the state determination proceeds as follows.

- (1) Calculate element deformation increment:

$$\underline{\Delta}_{vmr} = \underline{a}_r \underline{\Delta}_r \quad (\text{B4.28})$$

- (2) Calculate axial and torsional deformation increments at element midpoint:

$$\begin{Bmatrix} \Delta U_{xm} \\ \Delta \theta_{xm} \end{Bmatrix} = \underline{T} \underline{\Delta}_{vmr} + \underline{K}_{ii}^{-1} \left\{ \underline{S}_{mi} - \underline{S}_{oi} \right\} \quad (\text{B4.29})$$

in which \underline{T} is the transformation matrix obtained during condensation of the element stiffness from 8×8 to 6×6 ; \underline{K}_{ii} is the element stiffness associated with axial and torsional deformation at the element midpoint; \underline{S}_{mi} is the equilibrium error in the generalized axial force and torsional moment at the element midpoint due to nonlinearities in the preceding state determination; and \underline{S}_{oi} is the equilibrium error in the generalized force and moment due to initial stress effects.

- (3) Calculate the slice deformation increment using Eqn. B4.24.
- (4) Calculate axial and shear strain increments using Eqn. B4.3.
- (5) Calculate hoop strain increments from the axial and shear strain increments, taking into account any unbalanced hoop stresses due to either internal pressure change or errors from scaling the hoop stresses to the yield surface. Use Eqns. C1.3.65 and C1.3.66.
- (6) Obtain subelement stresses following the state determination procedure for the Mroz material.
- (7) Obtain the slice forces, \underline{S}_s , by summing the stresses over the cross section. The slice axial force due to internal pressure is also added.
- (8) Calculate the element resisting forces:

$$\underline{S}_m = L \int_{-1/2}^{1/2} \underline{a}^T \underline{S}_s dq \quad (\text{B4.30})$$

For the Gauss slice model, the integral of Eqn. B4.25 is carried out using Gauss quadrature and, for the end slice model, it is obtained in closed form assuming linear variations of slice actions along the element length.

Because the generalized axial force and torsional moment at the element midpoint are assigned zero values, it follows that:

$$\underline{S}_{me} = - \begin{Bmatrix} F_{xm} \\ T_{xm} \end{Bmatrix} = - \begin{Bmatrix} S_m(7) \\ S_m(8) \end{Bmatrix} \quad (\text{B4.31})$$

- (9) Transform the resisting forces at the pipe ends to global coordinates;

$$\underline{R}^i = \underline{a}_r^T \underline{S}_{mr} \quad (\text{B4.32})$$

B5. REFERENCES

- B1. Turner and Ford, "Examination of the Theories for Calculating the Stresses in Pipe Bends Subjected to In-Plane Bending," *Proc. Inst. Mech. Engrs.*, Vol. 171, pp. 513-525, 1957.
- B2. Timoshenko, S. P. and Woinowsky, S., **Theory of Plates and Shells**, McGraw-Hill, 1959.
- B3. Mosaddad, B., "Computational Models for Cyclic Plasticity, Rate Dependence and Creep," *Ph.D. Thesis*, Civil Engineering Department, University of California, Berkeley, June 1982.
- B4. Von Karman, T., "Uber die Formaunderung Dunnwandiger Rohre," *Innsbeson Ingenieure*, Vol. 55, pp. 1889-1895, 1911.

Preceding page blank

B6. ANSR-III USER GUIDE

INPUT DATA

INELASTIC STRAIGHT-CURVED PIPE ELEMENT

1. GROUP DATA CONTROL INFORMATION

Columns	Note	Name	Data
1 - 5(I)			Element type number. Input 4.
6 - 10(I)			Number of elements in group.
11 - 15(I)		MFST	Element number of first element in group. Default = 1.
16 - 25(F)			Initial stiffness damping factor, β_0 .
26 - 35(F)			Current stiffness damping factor, β_T .
36 - 40			Not used.
41 - 80(A)		GRHED	Optional group heading.

2. CROSS SECTION AND MATERIAL CONTROL INFORMATION

Columns	Note	Name	Data
1 - 5(I)		NOMAT	Number of different materials.
6 - 10(I)		NOSEC	Number of different cross sections.

3. MATERIAL PROPERTIES

NOMAT sets of cards, two cards per set.

3(a) FIRST CARD

Columns	Note	Name	Data
1 - 5(I)			Material number.
6 - 10(I)	(1)	NPT	Number of linear segments in stress-strain curve (max. 3).
11 - 20(F)			Poisson's ratio in elastic range.
21 - 30(F)	(2)		Yield overshoot tolerance. Default = .02.

Preceding page blank

Columns	Note	Name	Data
31 - 40(F)	(3)		Angle tolerance for stiffness reformulation. Default = 0.1 radian.
41 - 80(F)			Coefficient of thermal expansion.

3(b) SECOND CARD

Columns	Note	Name	Data
1 - 10(F)			Modulus (in uniaxial tension or compression).
11 - 20(F)	(1)		Stress at which modulus changes.
21 - 60(F)			Etc., repeat for NPT segments.

4. CROSS SECTION PROPERTIES

NOSEC sets of cards, two cards per set.

4(a) FIRST CARD

Columns	Note	Name	Data
1 - 5(I)	(4)		Number of subelements in cross section (max. 12). Default = 12.
6 - 10(I)	(5)		Type of model: (a) 0 = End slice model (straight pipe only). (b) 2 = Gauss model with 2 Gauss slices.
11 - 15(I)			Flexural shear deformation code: (a) 0 = shear deformations included. (b) 1 = shear deformations ignored.
16 - 25(F)			Outside diameter.
26 - 35(F)			Wall thickness.

4(b) SECOND CARD - BLANK IF STRAIGHT PIPE

Columns	Note	Name	Data
1 - 5(I)	(6)		Large Owalling Code: (a) 0 = small ovaling. (b) 1 = large ovaling.
6 - 15			Not used.

Columns	Note	Name	Data
16 - 20(I)	(7)		Number of linear segments in generalized force-ovalling curve (max. 3).
21 - 30(F)	(8)		Factor for ovalling stiffness (to account for stiffening effect of adjacent straight pipe). Default = 1.0.
31 - 40(F)	(9)		Factor for ovalling yield. Default = 1.0.
41 - 60(F)	(9)		Strain hardening ratios for inelastic ovalling (NNC values, in ten-column fields).

5. ELEMENT SPECIFICATION

As many cards as needed to specify all elements.

Columns	Note	Name	Data
1 - 5(I)			Element number, or number of first element in a series.
6 - 10(I)			Node I.
11 - 15(I)		INODJ	Node J.
16 - 20(I)	(10)		Node K. Default for straight element = automatic assignment. Must be bend center for a curved element.
21 - 25(I)			Node number increment for generation. Default = 1.
26 - 30(I)			Number of elements to be generated in this series. Default = 1.
31 - 35(I)			Material number. Default = 1.
36 - 40(I)			Output code: (a) 1 = output actions at nodes only. (b) 2 = also output actions and deformations at slices. (c) 3 = also output stresses and strains at slices. Default = 2.
41 - 45(I)			Cross section number. Default = 1.

Columns	Note	Name	Data
46 - 50(I)	(11)		Large displacement code: (a) 0 = small displacements. (b) 1 = large displacement analysis ignoring change in bend radius. (c) 2 = large displacement analysis accounting for change in bend radius.
51 - 55(I)			Curved element code: (a) 0 = straight. (b) 1 = curved.
56 - 60(I)	(12)		Symmetry code: (a) 0 = full 3D motion. (b) 1 = motion in element xy-plane only.

NOTES: INELASTIC STRAIGHT-CURVED PIPE ELEMENT

- (1) The actual stress-strain curve must be approximated by a number of linear segments. A maximum of 3 segments (trilinear curve) is allowed. The maximum stress in the last segment must be set very high. (The default value in the computer code is 10^{20}).
- (2) In the event-to-event procedure, if zero tolerance were used, a new step would be required each time an element yielded, and the number of steps could be excessive. A degree of overshoot of the nominal yield value is permitted. At the end of any substep, all elements which are between their nominal yield stresses and the permissible overshoot values are assumed to yield simultaneously.
- (3) When the element yields, the tangent stress-strain relationship can, in general, change continuously, and hence, the structure stiffness should strictly be modified in every load step. In many cases, however, the stiffness change from one step to the next may be small, and it may be reasonable to retain the same stiffness for several steps. This tolerance enables the user to control the frequency of stiffness reformulation.
- (4) The number of subelements in a cross section must be an even number, so that the cross section has symmetry about the two principal axes. If symmetry (motion in element xy-plane) is specified, the maximum number of subelements in the cross section is 24 (i.e. 12 in half section).
- (5) The pipe element may be straight or curved. If the element is straight, the slice locations may be at the element ends (end slice model) or at the two Gauss points inside the element (Gauss slice model). If the element is curved, the Gauss slice model must be specified.
- (6) For curved elements, ovaling may produce significant changes in cross section geometry. If large ovaling is specified, a deformed slice geometry is determined, taking into account the total ovaling deformation. Thus, a curved pipe is stronger for in-plane bending which increases the bend angle than for bending which decreases the bend angle.
- (7) A normalized force-ovaling relationship for pipe wall bending is developed based on the trilinear stress-strain curve. The approximation of the actual curve is done by approximating the normalized curve by a number of linear segments. A maximum of three segments (trilinear curve) is allowed.
- (8) The theory assumes that ovaling at any cross section is unrestrained. When an elbow is connected to straight pipes, there may be substantial restraint of ovaling, especially if the elbow is short. The ovaling stiffness factor allows the user to correct approximately for the restraint by increasing the ovaling stiffness. The nominal ovaling stiffness (the hoop bending part excluding the effect of internal pressure) is multiplied by the specified factor.

NOTES: INELASTIC STRAIGHT-CURVED PIPE ELEMENT (Continued)

- (9) First yield in ovaling is assumed to occur when the maximum bending strain due to ovaling reaches the steel yield strain. The subsequent shape of the curve relating ovaling deformation to ovaling force is shown in Fig. 4, and the trilinear approximation used for analysis is shown in Fig. 2. The first stiffness change in the trilinear curve typically occurs at about 1.3 times the ovaling at first yield, and this factor is used to predict the first yield in ovaling. The ovaling yield factor allows the user to adjust this first yield value. The second stiffness change is always assumed to occur at twice the deformation for the first yield.
- (10) If element generation is used, this node is the same for all elements in the series.
- (11) The effect of in-plane element curvature in the element geometry can be considered. If this option is selected, the bend radius and bend angle of curved pipe are updated as the analysis proceeds.
- (12) In many cases, the structure is symmetrical and motion occurs only in the element xy-plane. In such cases, only one half of the element cross section needs to be considered, and out-of-plane motions can be ignored. The computational effort at the element level is thus substantially reduced. If symmetry is specified, only **one half** of the element is considered. Structure loads and masses must be specified taking this into account.

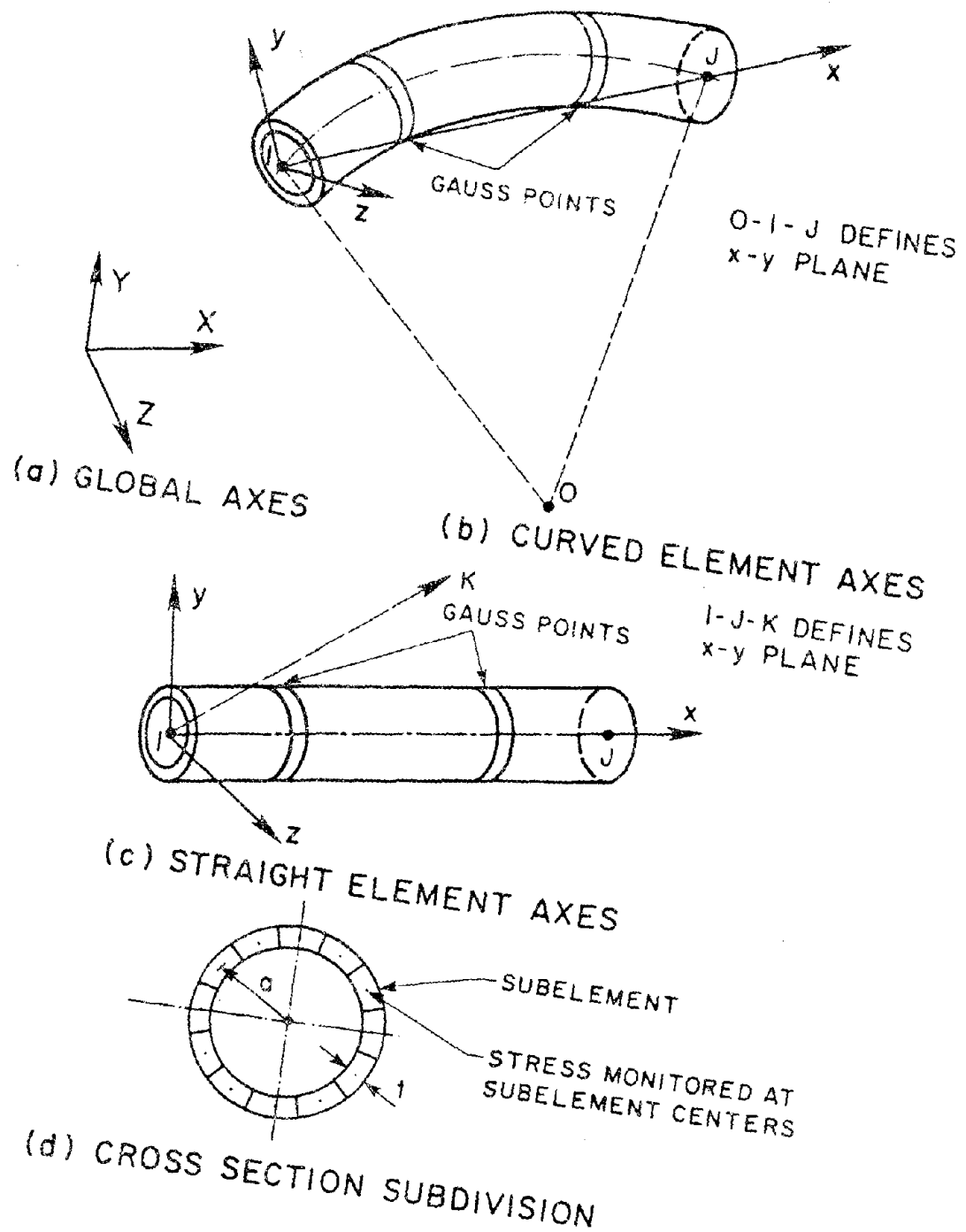
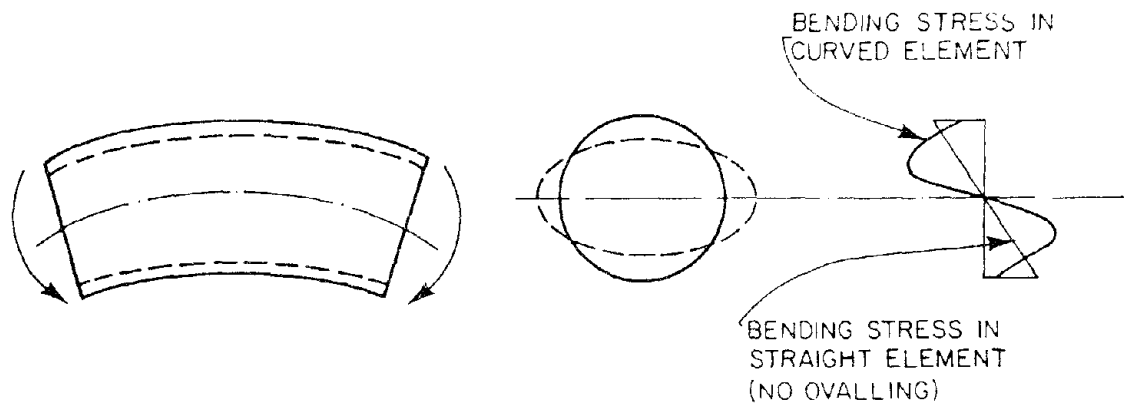
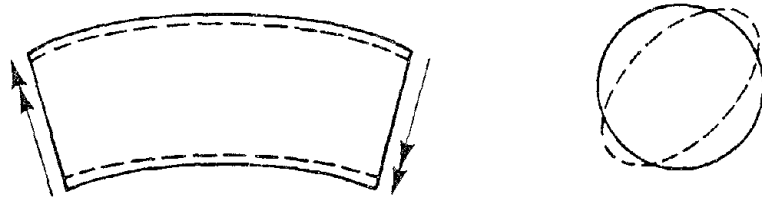


FIG. B2.1 CURVED AND STRAIGHT ELEMENTS



(a) IN-PLANE BENDING



(b) OUT-OF-PLANE BENDING

FIG. B2.2 OVALLING IN A CURVED ELEMENT

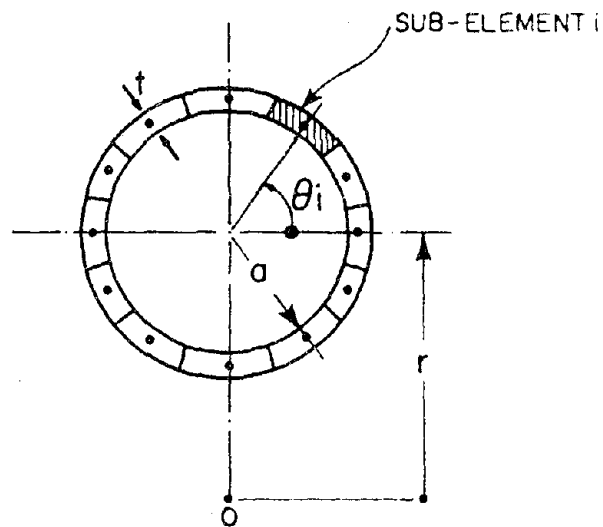
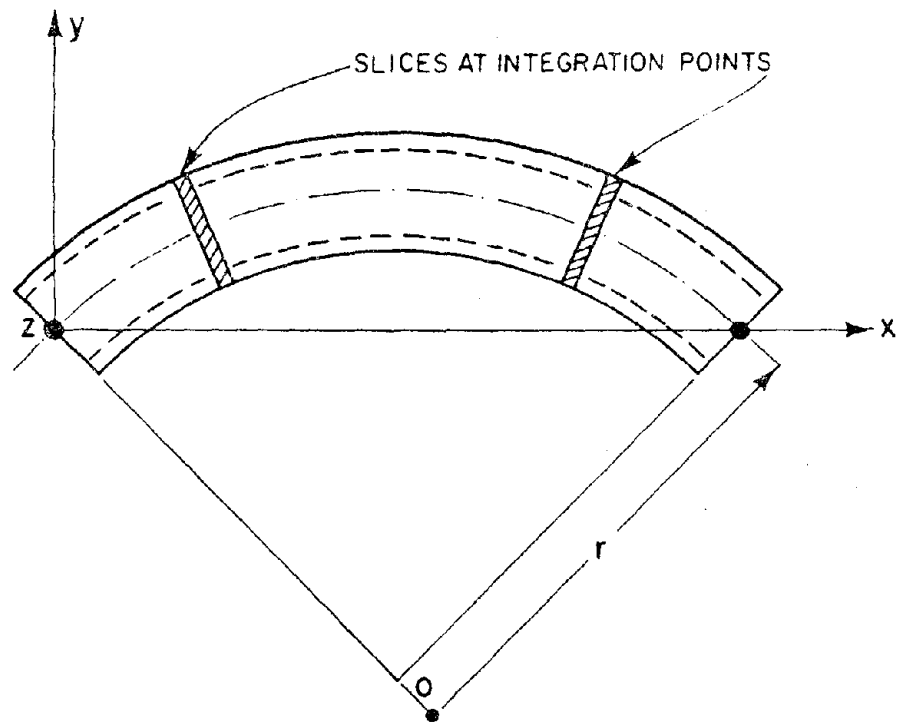
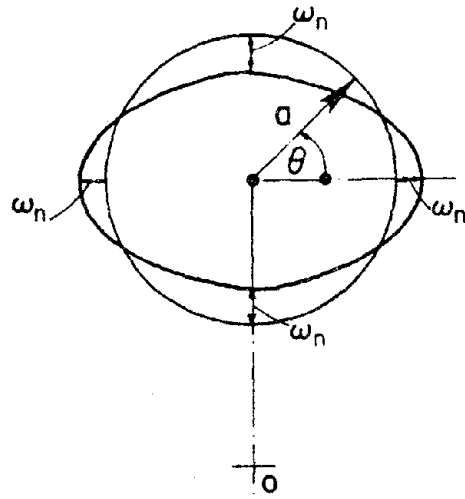
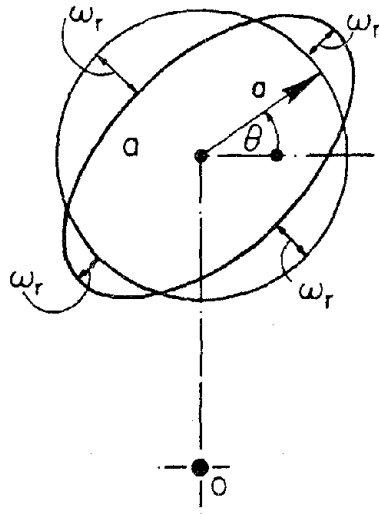


FIG. B3.1 CURVED PIPE ELEMENT



(a) IN-PLANE OVALLING



(b) OUT-OF-PLANE OVALLING

FIG. B3.2 OVALLING DEFORMATIONS

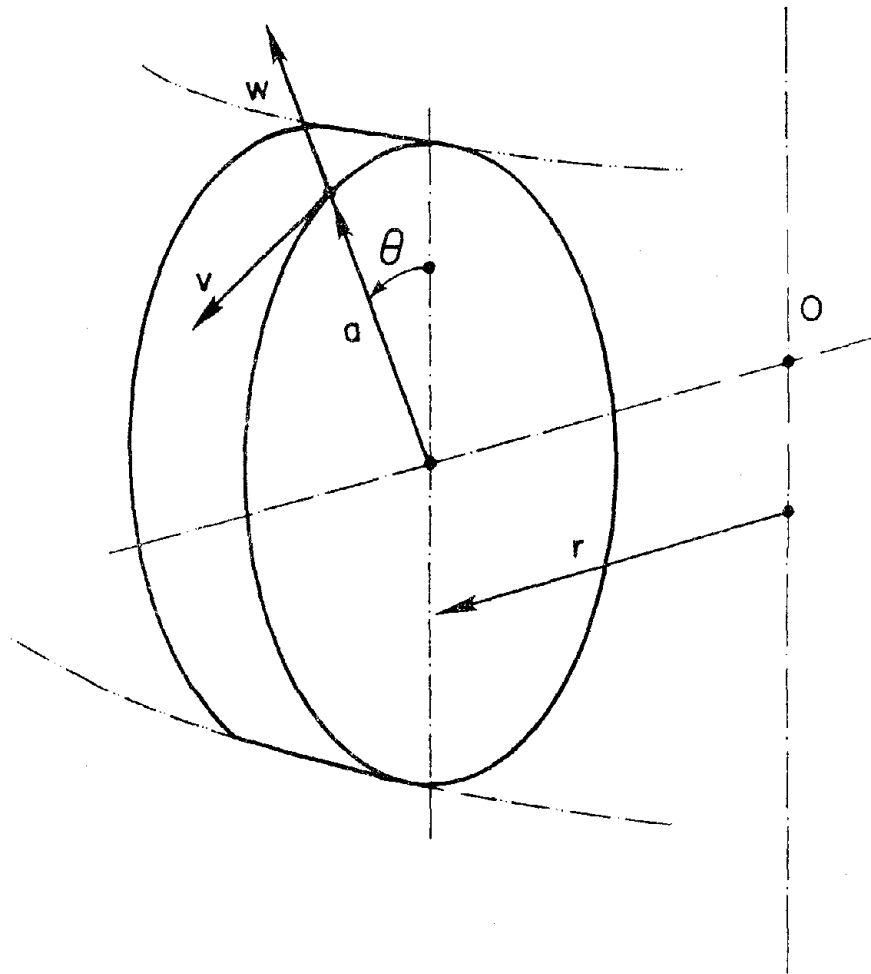
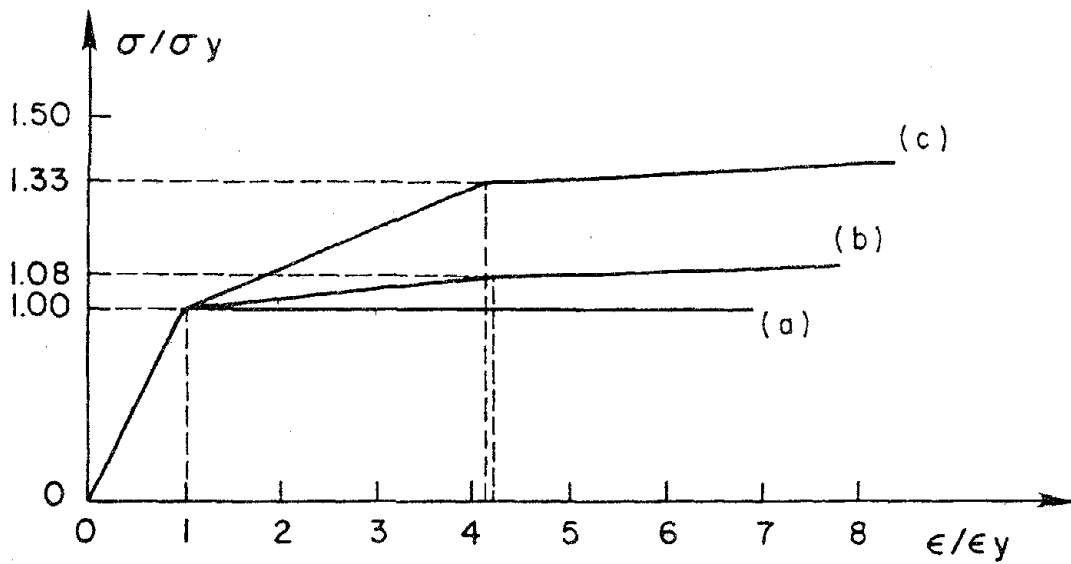
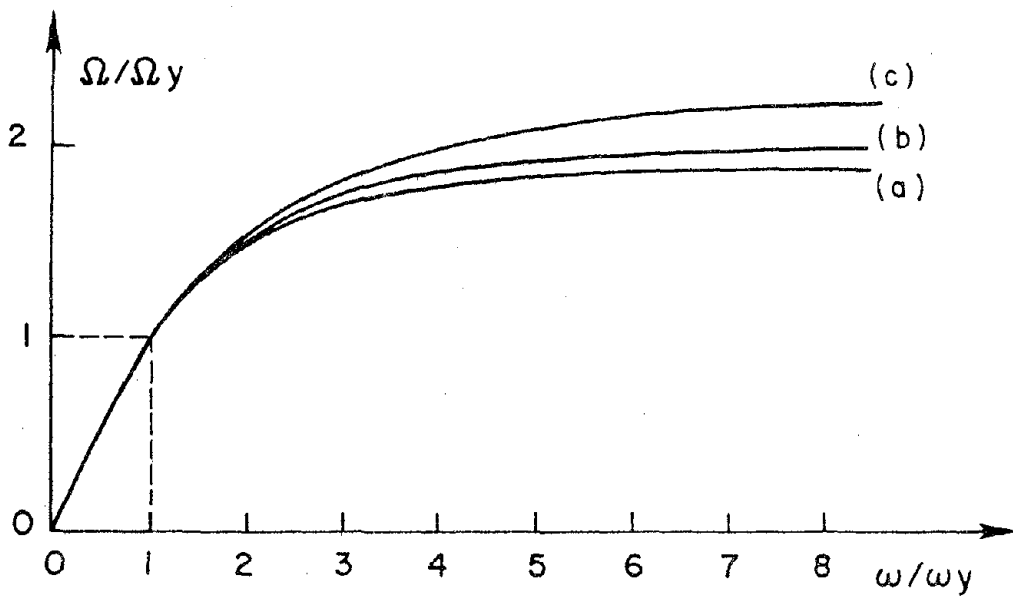


FIG. B3.3 AXISYMMETRIC SHELL (TORUS)



(a) NORMALIZED STRESS-STRAIN CURVES



(b) CORRESPONDING NORMALIZED FORCE-OVALLING CURVES

FIG. B3.4 FORCE-OVALLING RELATIONSHIPS DUE TO PIPE WALL BENDING

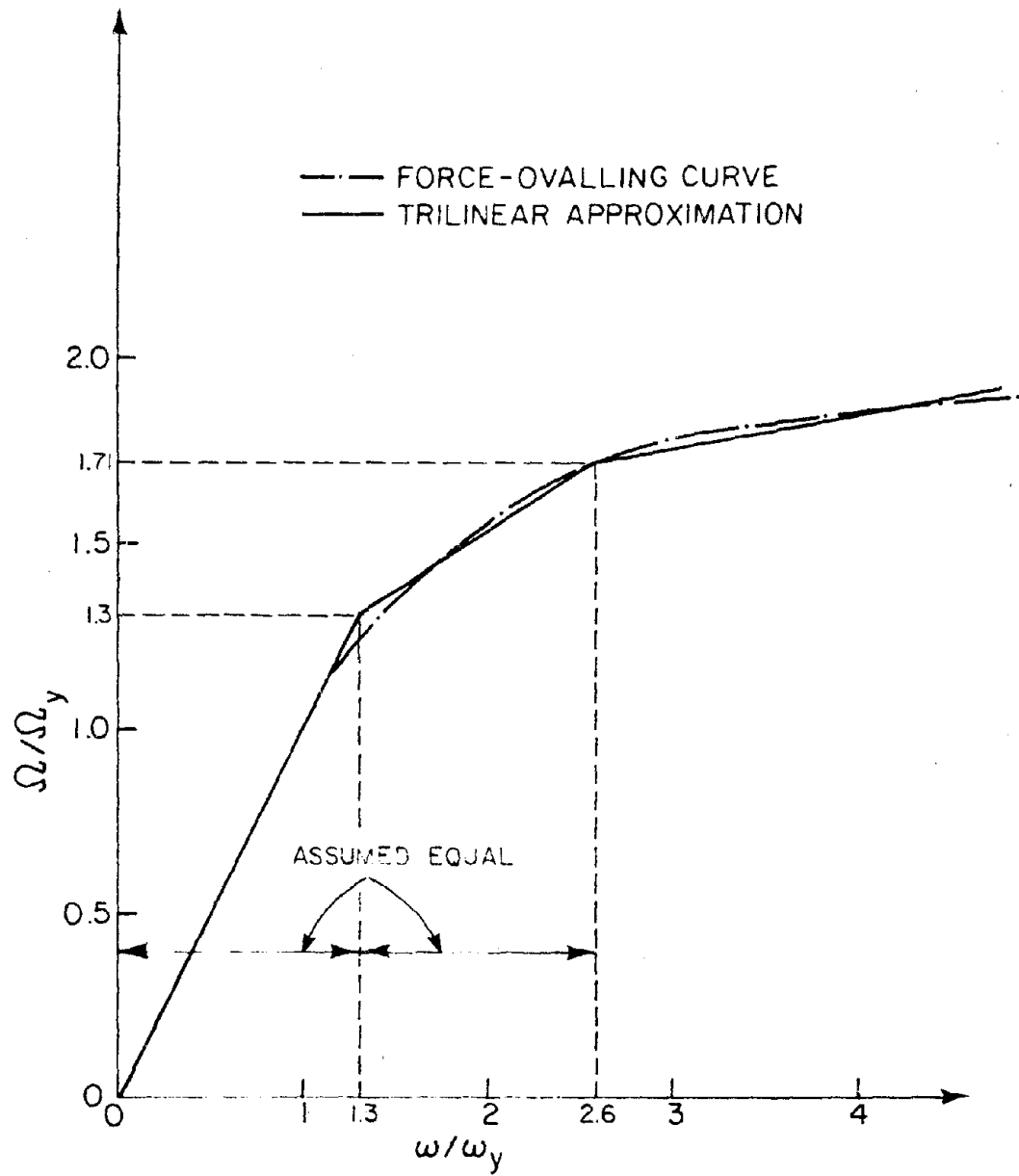
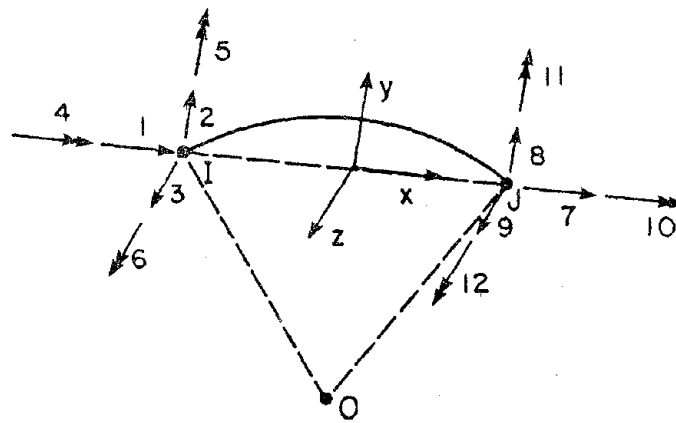
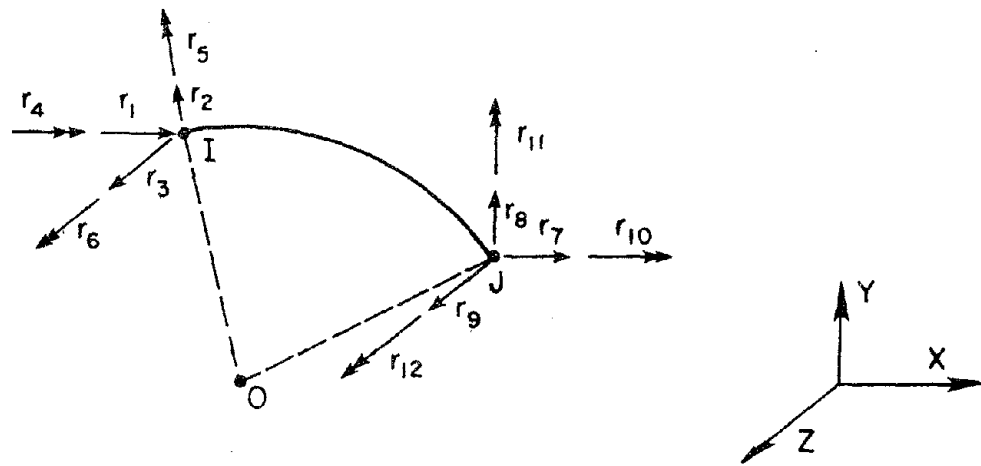


FIG. B3.5 TRILINEAR FORCE-OVALLING APPROXIMATION



(a) LOCAL DISPLACEMENTS



(b) GLOBAL DISPLACEMENTS

FIG. B3.6 ELEMENT DEGREES OF FREEDOM

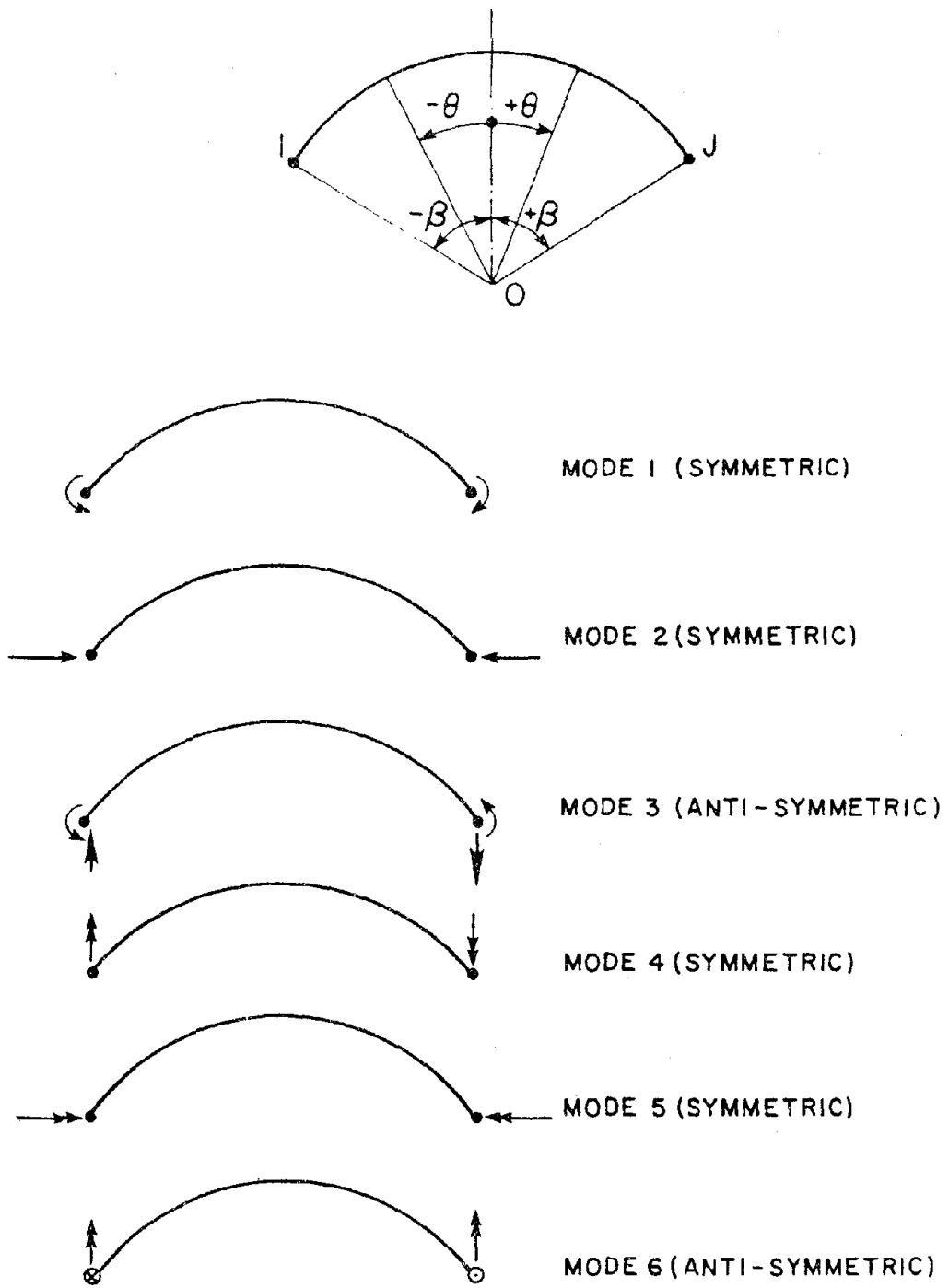
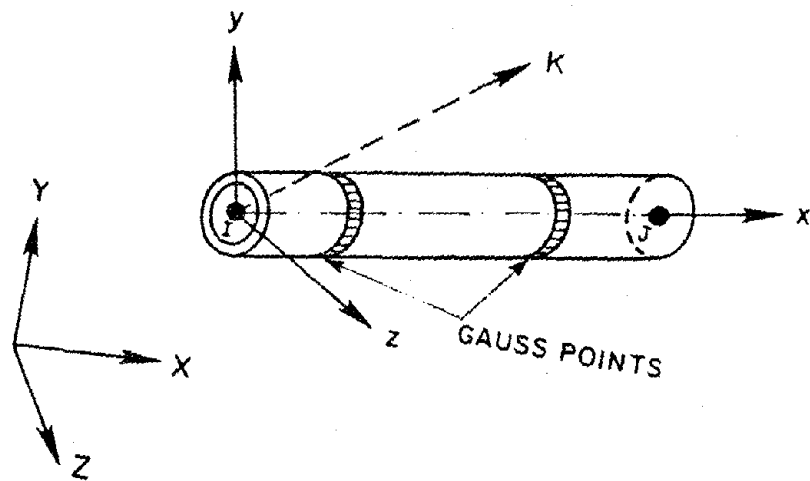
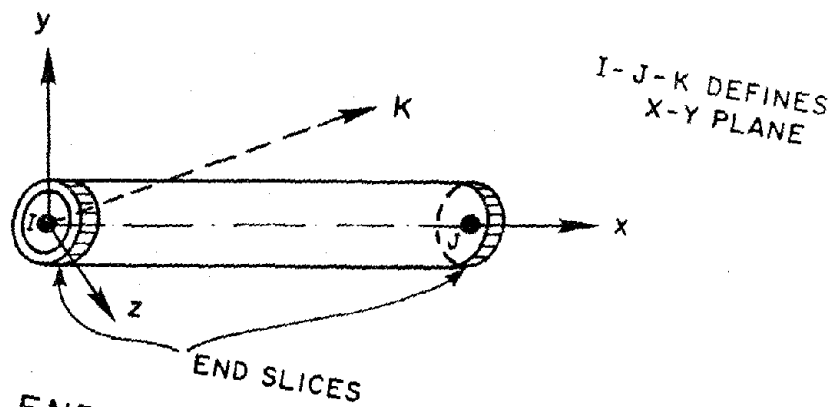


FIG. B3.7 SYMMETRIC-ANTISYMMETRIC MODES

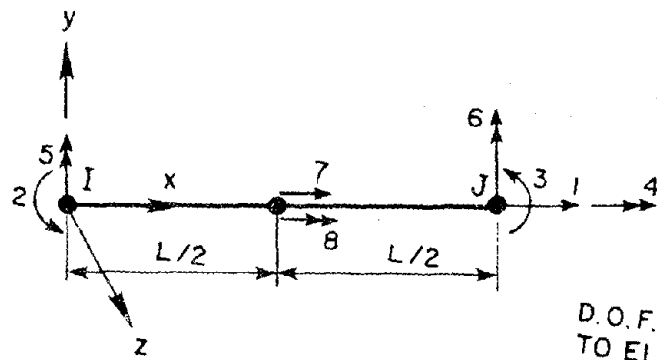


(a) GAUSS SLICE MODEL



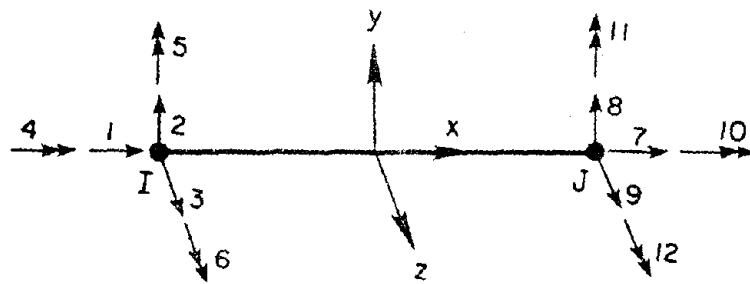
(b) END SLICE MODEL

FIG. B4.1 STRAIGHT PIPE ELEMENT

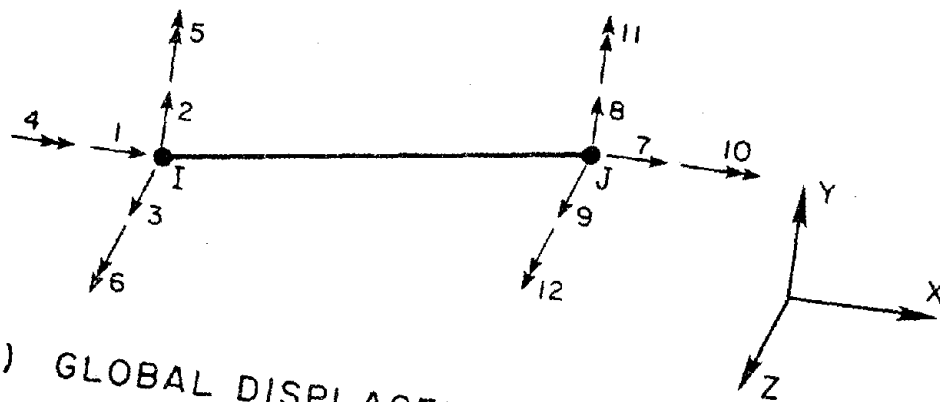


D.O.F. 7 & 8 RELATIVE TO ELEMENT ENDS

(a) DEFORMATION DEGREES OF FREEDOM

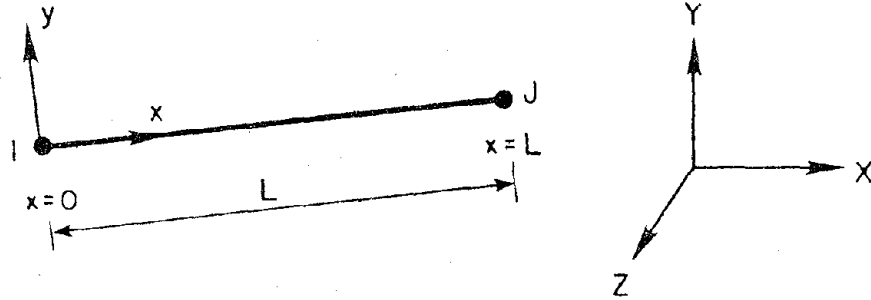


(b) LOCAL DISPLACEMENTS

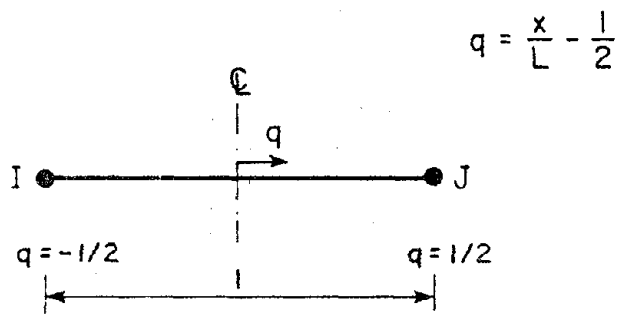


(c) GLOBAL DISPLACEMENTS

FIG. B4.2 ELEMENT DEGREES OF FREEDOM



(a) LOCAL COORDINATES



(b) DIMENSIONLESS COORDINATES

FIG. B4.3 COORDINATE SYSTEMS

C. MULTI-SLICE TUBE ELEMENT

This section describes the theory of the "multi-slice" tube element. The basic features of the element are described in Chapters C1 and C2. Details of the theory and computational procedure are described in Chapter C3. Chapter C4 contains references, and Chapter C5 describes the input data required for the ANSR-III computer code.



C1. INTRODUCTION

C1.1 CONCEPT

For finite element analysis of beam-columns, the use of a cubic polynomial shape function implies a linear variation of curvature along the element length. This is correct for a uniform elastic beam. If the beam becomes inelastic, however, the assumption of linear curvature variation is no longer correct.

Linear curvature variation within a single element may be reasonable if a complete beam is subdivided into short elements. However, this is usually not desirable because it increases the numbers of nodes and elements which must be specified. A compromise is to divide a complete beam into short subelements and treat the beam as a substructure. This also introduces complications, however, one of which is that unbalanced forces will generally be associated with the internal degrees of freedom of the substructure. The need to eliminate these unbalances adds to the complexity of the analysis.

An alternative approach is to treat a complete beam as a single element and to vary the shape function as the state of the element changes. Pecknold et al [C1] have used this approach for reinforced concrete columns, varying the shape function according to predetermined rules as the element yields. Their procedure is applicable, however, only for special cases in which the deformation modes of the element are known fairly accurately in advance. For the general case it is not possible to establish predetermined rules for variation of the shape function.

A new procedure has been explored for the "multi-slice" element described herein. With this procedure, it is not necessary to establish predetermined rules for varying the shape function. Instead, the procedure automatically determines appropriate functions as the analysis progresses and the state of the element changes.

Preceding page blank

C1.2 ELEMENT FEATURES

The basic features of the multi-slice element are as follows. A more detailed qualitative description is presented in Chapter C2. The theory is presented in Chapter C3.

- (1) The element must be straight but may be arbitrarily oriented in space.
- (2) Only small element deformations are considered (i.e. the element is assumed to remain essentially straight). However, large rigid body motions are permitted.
- (3) The element behavior is monitored at a number of *slices*, one at each end and up to seven within the element length. The internal slice locations must be specified by the analyst. These locations must be selected so that spread of plasticity along the element length is modeled accurately.
- (4) Only a pipe cross section is currently permitted. The cross section is subdivided into a number of subelements (fibers) at each slice. The inelastic behavior at each subelement is monitored using the Mroz material theory.

C2. ELEMENT PROPERTIES

C2.1 ELEMENT GEOMETRY

The element geometry and coordinate axes are shown in Fig. C2.1. Each element connects two nodes, each with three translational and three rotational degrees of freedom. The element does *not* have any internal degrees of freedom (that is, the theory is not based on substructuring concepts).

C2.2 SLICE LOCATIONS

C2.2.1 General

Yielding of the element is monitored at up to 9 *slices* along the element length, one slice at each end and up to 7 internal slices. The number of internal slices and their locations must be specified by the analyst.

Inelastic behavior of a complete element is modeled by monitoring the inelastic behavior of each slice and assuming linear variation of the inelastic properties between slices (the details are presented in Chapter C3). The slices must be located in such a way that this linear variation provides a close approximation of the true properties.

C2.2.2 Antisymmetrical Bending

Consider, as an example, an element subjected to equal and opposite end rotations (and hence end moments), as shown in Fig. C2.2a. For a rotation value below that causing first yield, the variations of both bending moment and curvature along the element are linear (Fig. C2.2b). The governing inelastic property in this example is the EI value, relating moment to curvature, which for loading below yield is constant along the element length. Hence, the exact result can be obtained with only two slices (one at each end), and internal slices are not needed.

If the element end rotations exceed the yield values, the moment variation along the length is still linear (because it is governed by equilibrium), but the curvature variation

becomes nonlinear (Fig. C2.2c). In this case, if only two slices are assumed, the curvature variation in the mathematical model is still linear, and the relationship between the actual and calculated curvatures would be as indicated in Fig. C2.2 d. The maximum curvature would thus be grossly underestimated.

If, however, four slices are assumed, the curvature variation can be multilinear, for example, as shown in Fig. C2.2e. A much better approximation of the true curvature variation can thus be obtained, and the maximum curvature can be predicted more accurately. It may be noted that the theory actually assumes a linear variation of slice *flexibility*, represented in this case by the value $1/EI$. When this is combined with the linear moment variation, a *quadratic* curvature variation can result. This permits a closer approximation of the true curvature than the multilinear variation shown in Fig. C2.2e.

As the number of slices is increased, the element becomes progressively more accurate. This is the case, however, only if the additional slices are placed in the part of the element which yields. Consider the same antisymmetric loading, and assume an elastic-perfectly-plastic material. For this material, the bending shape factor for a pipe cross section is 1.28. Hence, the maximum end moment is $1.28 M_y$, where M_y = moment at first yield, and the maximum extent of yield in the element is as shown in Fig. C2.3a. In this case, the best results would be obtained by placing a slice at each end, a slice at the end of each region of potential yield, and additional slices within the regions of potential yield (Fig. C2.3b). It must be noted, however, that for materials which are not elastic-perfectly-plastic, the regions of potential yield will be longer. The situation is also more complex if the bending moment variation is not known, as considered in the following section.

C2.2.3 Other Bending Moment Variations

Antisymmetrical (or essentially antisymmetrical) moment loads, as considered in the preceding section, are commonly imposed on the members of flexural frames. If it is known in advance that the element loading will be of antisymmetrical type, slice locations can be selected as indicated in the preceding section. In general, however, the bending moment variation will

not be known in advance. In addition, (1) the moment variation may change progressively; (2) loading, unloading, and reloading will occur for dynamic or cyclic static loading; and (3) an element will generally not be subjected to simple uniaxial bending, but to biaxial bending combined with axial force, possibly with substantial torsional moments also present. Because of these factors, the variations of curvature (and other slice deformations) along the element length may change greatly as a structure is loaded. The problem is more serious if a single element is used to model a long structural member, and less serious if long members are subdivided into several short elements.

At the time of writing, very little experience has been obtained with the multi-slice element, and resources are not sufficient to perform extensive studies. Hence, no recommendations can be made on the number of slices required for specific cases, nor on their locations. The examples in Section D can provide some guidance.

C2.3 SLICE MODELING

For each slice, the pipe cross section is divided into a number of *subelements* (typically 12), as shown in Fig. C2.1. The pipe wall at each subelement is assumed to be subjected to hoop stress (due to pressure), axial stress (due to pressure, bending moment and axial force), and shear stress (due to torsional moment). The inelastic behavior at the center of each subelement is monitored using the Mroz material theory. Owalling of cross sections is *not* considered.

C2.4 COMPUTATIONAL PROCEDURE

C2.4.1 Shape Function

The computational procedure is described in detail in Chapter C3. The procedure is essentially as follows.

At any time, the states of stress and strain at all subelements at all slices are known. A tangent flexibility matrix (4 x 4) is constructed for each slice. For all other cross sections, the

flexibility is assumed to vary linearly between the flexibilities of the two adjacent slices. From the slice flexibilities, a flexibility matrix for the element as a whole is formed (by closed form integration). From this flexibility matrix, a shape function is constructed, which relates the deformations at the slices to the displacements of the nodes at the element ends. This shape function can be used to construct the element tangent stiffness matrix (which turns out, not surprisingly, to be the inverse of the element flexibility matrix). More importantly, the shape function is used to determine slice deformation increments in the state determination phase.

C2.4.2 Overshoot and Unloading Tolerances

Each time a cross section subelement yields or unloads, the element flexibility changes. Hence, the element shape function also changes. For an exact result, the bending moments must vary linearly along the element, and the axial force and torsional moment must be constant. An exact result will be obtained in the state determination phase only if the shape function is recalculated each time a change occurs in the properties of a cross section subelement.

To avoid the computational cost associated with recalculating the shape function each time a subelement changes its state, some yield overshoot is allowed at the subelement level. The amount of overshoot is specified by the analyst (typically 2%-10% of the material yield strength). The shape function is recalculated only when the stress in any subelement overshoots the yield value by the specified overshoot. Several subelements may then have changed state, and the number of shape function recalculations is reduced.

A similar stress tolerance is used for subelement unloading. In addition, it is possible for the stress at a subelement to move around the Mroz yield surface so that the direction of plastic flow changes. Such a change in direction changes the tangent stress-strain relationship, and hence, also the slice and element stiffnesses. To avoid recalculation of the shape function each time a flow direction changes slightly, the analyst is required to specify an angle tolerance (typically about 0.1 radians). The shape function is recalculated only if the flow direction at any subelement changes by more than this tolerance.

C3. THEORY

C3.1 PROCEDURE AND ASSUMPTIONS

The stiffness and state determination calculations for the element are based essentially on beam theory. The theory is presented herein for a pipe element with a thin-walled circular cross section. The theory can be modified for other cross section shapes.

The element is modeled as shown in Fig. C3.1. One beam slice is located at each element end, and a maximum of seven additional slices may be specified at arbitrary locations along the element length. Each slice is divided into a number of cross section subelements. The subelement stiffnesses are constructed first, allowing for elasto-plastic behavior of the pipe steel. The slice stiffnesses are constructed from the subelement stiffnesses by summation. The slice flexibilities are obtained by inverting the slice stiffnesses, and a complete element flexibility is constructed from the slice flexibilities by closed-form integration. The element stiffness is then obtained by inverting the element flexibility.

The deformations at any slice consist of six beam-type deformations, namely axial deformation, torsional twist, major plane and minor plane curvatures, and major plane and minor plane flexural shear deformations. The major plane is assumed to be the local xy plane. Cross-section warping is not considered in the theory presented herein.

The complete element has six nodal degrees of freedom at each end, which provide six rigid body modes plus six element deformations. The slice deformations are related to the element deformations by shape functions, which are progressively updated as the element yields.

Each subelement is assumed to be in a state of plane stress, with axial, hoop, and shear stresses. The effects of axial deformation and curvature on the axial strains are determined assuming a plane, circular cross section. The shear strain is assumed to be affected by torsional twist only. Flexural shear effects are assumed to be negligible at the subelement level and are ignored (they are introduced at the slice level). The subelement shear strains due to twist are determined assuming plane, circular cross sections.

Hoop strains are not determined from strain-displacement relationships. Rather, the hoop stresses are governed by the equilibrium relationship between internal pressure and hoop stress. The hoop strain in any subelement thus becomes an internal degree of freedom for the subelement and is condensed out before the slice stiffness is calculated.

C3.2 SLICE STIFFNESS

C3.2.1 Deformations and Actions

The slice deformation vector, \underline{v}_s , is given by:

$$\underline{v}_s^T = \langle \delta \ \psi_z \ \psi_y \ \phi \ \gamma_{xy} \ \gamma_{xz} \rangle \quad (C3.1)$$

in which δ = axial strain at pipe axis; ψ_z = bending curvature about element z axis; ψ_y = bending curvature about y axis; ϕ = rate of torsional twist; γ_{xy} = flexural shear deformation in x-y plane; and γ_{xz} = flexural shear deformation in x-z plane.

The corresponding slice action vector is \underline{S}_s , where

$$\underline{S}_s^T = \langle F \ M_z \ M_y \ T \ V_{xy} \ V_{xz} \rangle \quad (C3.2)$$

in which F = axial force; M_z and M_y = bending moments; T = torsional moment; and V_{xy} and V_{xz} = flexural shear forces.

C3.2.2 Strain-Deformation Relationships for Slice

Consider slice subelement i , located at angle θ_i (Fig. C2.1(b)). The subelement membrane strains, ϵ_{ai} and γ_i , are related to the slice deformations by:

$$d\epsilon_i = \underline{B}_i d\underline{v}_s \quad (C3.3)$$

in which

$$d\epsilon_i^T = \langle d\epsilon_{ai} \ d\gamma_i \rangle \quad (C3.4)$$

ϵ_{ai} = axial strain in subelement i ; γ_i = torsional shear strain; \underline{v}_s is defined by Eqn. C3.1; and

$$\underline{B}_i = \begin{bmatrix} 1 & a \sin \theta_i & -a \cos \theta_i & 0 & 0 & 0 \\ 0 & 0 & 0 & a & 0 & 0 \end{bmatrix} \quad (C3.5)$$

This transformation assumes that plane sections remain plane and circular. It is also implied

that the pipe thickness is small compared to the pipe diameter.

Note that the slice shear deformations, γ_{xy} and γ_{xz} , are assumed not to influence the subelement strains. The effects of these deformations are considered separately.

C3.2.3 Stress-Strain Relationships for Slice Subelement

Each subelement is assumed to be in a state of membrane stress and strain (plane stress). The hoop stress is controlled by the internal pressure, according to the well-known equation

$$\sigma_h = P \frac{(a - 0.5t)}{t} = \frac{Pa'}{t} \quad (C3.6)$$

in which P = internal pressure; a = radius to pipe wall mid-thickness; t = wall thickness; and $a' = a - 0.5t$.

The Mroz plasticity theory is used to model subelement yield. The details of the procedures used to implement this theory have been described in detail by Mosaddad [C. 2] and are not repeated here. For any given state of subelement i , an elasto-plastic stress-strain relationship is determined as

$$d\underline{\sigma}_i = \underline{D}_i d\underline{\epsilon}_i \quad (C3.7)$$

in which

$$d\underline{\sigma}_i^T = \langle d\sigma_{ai} \ d\tau_i \ d\sigma_{hi} \rangle \quad (C3.8)$$

$$d\underline{\epsilon}_i^T = \langle d\epsilon_{ai} \ d\gamma_i \ d\epsilon_{hi} \rangle \quad (C3.9)$$

where σ_{hi} = hoop stress in subelement i (the same in all subelements); ϵ_{hi} = hoop strain in subelement i ; and \underline{D}_i = 3 x 3 elasto-plastic constitutive matrix. From Eqns. C3.7 and C3.6 it follows that

$$\underline{D}_i \cdot \begin{Bmatrix} d\epsilon_{ai} \\ d\gamma_i \\ d\epsilon_{hi} \end{Bmatrix} = \begin{Bmatrix} d\sigma_{ai} \\ d\tau_i \\ a'dP/t \end{Bmatrix} \quad (C3.10)$$

in which dP is known. Hence, \underline{D}_i can be reduced, by static condensation, to a 2 x 2 matrix, \underline{D}_{ri} , in terms of axial and shear stresses only. If $dP = 0$, the result can be written as:

$$[\underline{D}_{ri}] \begin{Bmatrix} d\epsilon_{ai} \\ d\gamma_i \end{Bmatrix} = \begin{Bmatrix} d\sigma_{ai} \\ d\tau_i \end{Bmatrix} \quad (C3.11)$$

If dP is not zero, an initial stress effect must be included.

C3.2.4 Stiffness Matrix

The transformation matrix \underline{B} (Eqn. C3.5) considers the effects of axial deformation, bending, and torsion. A tangent stiffness matrix for the slice, \underline{k}_s , which considers only these effects, is thus given by:

$$\underline{k}_s = 2\pi \frac{at}{N} \sum_{i=1}^N \underline{B}_i^T \underline{D}_{ii} \underline{B}_i \quad (C3.12)$$

in which N = number of slice subelements around pipe circumference.

The matrix \underline{k}_s has zero rows and columns corresponding to the shear deformations γ_{xy} and γ_{xz} , because the transformation \underline{B} does not consider flexural shear effects. It is assumed that the flexural shear stiffness is not affected by yielding of the element, and hence, that the elastic shear stiffness can be used. For an effective shear area equal to one-half of the cross section area, the shear stiffnesses are defined by:

$$dV_{xy} = G\pi at \cdot d\gamma_{xy} = k_\gamma \cdot d\gamma_{xy} \quad (C3.13a)$$

and

$$dV_{xz} = G\pi at \cdot d\gamma_{xz} = k_\gamma \cdot d\gamma_{xz} \quad (C3.13b)$$

in which G = elastic shear modulus. The slice stiffness coefficients $k_s(5,5)$ and $k_s(6,6)$ are set equal to k_γ .

C3.3 SLICE FLEXIBILITY

The slice flexibility, \underline{f}_s , is obtained by inverting the slice stiffness. That is,

$$\underline{f}_s = \underline{k}_s^{-1} \quad (C3.14)$$

In the computer coding, the 4 x 4 slice stiffness without the shear stiffness is first inverted, and the flexibility coefficients $f_s(5,5)$ and $f_s(6,6)$ are set equal to $1/k_\gamma$.

C3.4 ELEMENT STIFFNESS

C3.4.1 Deformations and Actions

The element deformations and displacements are shown in Fig. C3.2. The element degrees of freedom, after deletion of the six rigid body modes, are defined by the vector \underline{v}_m , where:

$$\underline{v}_m^T = \langle u_x \theta_{zi} \theta_{zj} \theta_x \theta_{yi} \theta_{yj} \rangle \quad (C3.15)$$

where u_x = axial extension; θ_{zi} = z-axis rotation at element end i; θ_{zj} = z-axis rotation at end j; θ_x = torsional twist; θ_{yi} = y-axis rotation at end i; and θ_{yj} = y-axis rotation at end j.

The corresponding element action vector is \underline{S}_m , where:

$$\underline{S}_m^T = \langle F_x M_{zi} M_{zj} T_x M_{yi} M_{yj} \rangle \quad (C3.16)$$

C3.4.2 Shape Function Calculation

For finite element analysis of straight beams, it is common to use a cubic Hermitian polynomial shape function. This permits a linear curvature variation and is exact for a uniform elastic beam loaded only at its ends. If the beam becomes inelastic, however, the assumption of linear curvature variation is no longer correct and equilibrium within the element is violated. This can lead to serious errors. For the multi-slice element, however, it is possible to calculate, for any state of the element, an "exact" shape function. This shape function is calculated by the computer program and is progressively updated as the state of the element changes.

A multi-slice shape function can be calculated using either a stiffness or a flexibility approach. Both approaches have been explored and that based on flexibility has been found to be superior. For completeness, the steps for both approaches are considered in the following sections.

C3.4.3 Stiffness Approach

The stiffness approach is based on substructuring theory, in which a complete element is regarded as a substructure divided at the internal slices into a number of substructure elements

(Fig. C3.3). The steps in the computation are as follows.

- (1) For each slice, form the current tangent stiffness, \underline{k}_s , using Eqn. C3.12.
- (2) Place "external" nodes at the two end slices and an "internal" node at each internal slice, dividing the substructure into several elements. Each node has three translational and three rotational degrees of freedom. The properties of each substructure element are determined by the properties of the two slices which the element joins.
- (3) For each substructure element assume a cubic shape function, and assume that the stiffness varies linearly along the element length (i.e., interpolate between the slice stiffnesses, \underline{k}_s , for the slices which the element joins). With this assumption a stiffness matrix can be calculated in closed form for each substructure element.
- (4) Assemble the element stiffnesses to obtain a complete substructure stiffness, in terms of 6 displacements at each internal node and a total of 6 displacements at the two external nodes. The external node displacements are conveniently chosen as those shown in Fig. C3.3.
- (5) Select one of the 6 external node displacements. Impose a unit value of this displacement, with the remaining 5 external displacements constrained to be zero and all internal displacements unrestrained. Solve for the internal displacements.
- (6) Using the displacements from Step (5) and the cubic shape functions for the substructure elements, calculate the slice deformations at the two ends of each element. Two slice deformation vectors will be calculated for each internal slice, and these will not necessarily be equal. Average the two vectors to obtain the slice deformations.
- (7) The slice deformations from Step (6) define one column of the shape function for the complete element (i.e. the deformations at all slices for a unit value of one external displacement). Repeat Steps (5) and (6) for each external displacement in turn to obtain a complete displacement transformation matrix.

C3.4.4 Weaknesses of Stiffness Approach

The procedure described in the preceding section has been explored and found to have a number of weaknesses when compared with the flexibility approach. These weaknesses are as follows.

- (1) The calculated slice deformations are discontinuous at the internal nodes, and average values are used to obtain the shape functions. This averaging is not necessary in the flexibility approach.
- (2) The calculated element stiffness is only approximate, whereas that obtained by the flexibility approach is "exact".
- (3) The computational cost is higher than for the flexibility approach.

C3.4.5 Flexibility Approach

The flexibility approach also considers a complete element as a substructure consisting of a number of substructure elements. However, the substructure flexibility properties are determined, rather than its stiffness properties. The flexibility properties are then used to determine both the stiffness matrix for the complete element and the element shape function. The procedure is as follows.

- (1) For each slice, form the current tangent flexibility, f_s , using Eqn. C3.14.
- (2) Select the displacements shown in Fig. C3.4 as the substructure deformations, and the corresponding forces as the substructure actions. The substructure is thus statically determinate.
- (3) From equilibrium (linear variation of slice actions along the substructure length), express the actions at each slice in terms of the substructure end actions. This defines a force transformation matrix.
- (4) Assume that the slice flexibility varies linearly between each pair of slices. Hence, using the force transformation from Step (3), determine the substructure flexibility matrix.

- (5) Obtain the shape function using the substructure flexibility from Step (4), the slice flexibilities from Step (1), and the force transformation from Step (3). The theory is presented in the next section. Also obtain the substructure (i.e. complete element) stiffness as the inverse of the substructure flexibility.

C3.4.6 Flexibility Calculation

An element flexibility in terms of the element degrees of freedom after deletion of the six rigid body modes is first obtained. This flexibility is then used to obtain the shape functions.

The element actions correspond to the six deformations shown in Fig. C3.4. The equilibrium relationship between the slice actions and the element actions is:

$$\underline{S}_s = \underline{b} \underline{S}_m \quad (C3.17)$$

in which \underline{S}_s and \underline{S}_m are defined by Eqns. (C3.2) and (C3.16), respectively, and

$$\underline{b} = \begin{bmatrix} 1 & 0 & 0 & 0 & 0 & 0 \\ 0 & 1-x/L & -x/L & 0 & 0 & 0 \\ 0 & 0 & 0 & 0 & 1-x/L & -x/L \\ 0 & 0 & 0 & 1 & 0 & 0 \\ 0 & 1/L & 1/L & 0 & 0 & 0 \\ 0 & 0 & 0 & 0 & -1/L & -1/L \end{bmatrix} \quad (C3.18)$$

A slice flexibility relationship can be written as:

$$d\underline{v}_s = \underline{f}_s \underline{S}_s \quad (C3.19)$$

in which \underline{f}_s is the inverse of the slice stiffness, \underline{k}_s , developed in Section C3.2.

Equations C3.17 and C3.19, plus a standard application of the virtual forces principle, lead to the element flexibility relationship:

$$d\underline{v}_m = \underline{f}_m d\underline{S}_m \quad (C3.20)$$

in which

$$\underline{f}_m = \int_0^L \underline{b}^T \underline{f}_s \underline{b} dx \quad (C3.21)$$

After transformation to dimensionless coordinates, q , as shown in Fig. C3.5, Eqn. C3.21 becomes:

$$\underline{f}_m = \sum_{i=1}^n L_i \int_{-1/2}^{1/2} \underline{b}_i^T \underline{f}_{si} \underline{b}_i dq \quad (C3.22)$$

in which n = number of substructure elements (equal to the number of slices minus one); and L_i = length of element i . The integration in Eqn. C3.22 can be carried out in closed form if it is assumed that the slice flexibility, f_s , varies linearly between slices.

C3.4.7 Shape Function

The deformation increments at any slice, $d\underline{v}_s$, can be obtained in terms of the element deformations (Fig. C3.4), as follows.

From Eqns. C3.17 and C3.19:

$$d\underline{v}_s = \underline{f}_s \underline{b} d\underline{S}_m \quad (C3.23)$$

Hence, from Eqn. C3.20:

$$d\underline{v}_s = \underline{f}_s \underline{b} \underline{f}_m^{-1} d\underline{v}_m \quad (C3.24)$$

The shape functions relating increments of slice deformation to increments of element deformation can thus be expressed as:

$$\underline{a} = \underline{f}_s \underline{b} \underline{f}_m^{-1} \quad (C3.25)$$

C3.4.8 Element Stiffness

From the slice stiffness relationship of Eqn. C3.12, the transformation relating slice deformations and element deformations (Eqn. C3.25) and standard application of the virtual displacements principle, the complete element stiffness can be obtained as:

$$\underline{K} = \int_0^L \underline{a}^T \underline{k}_s \underline{a} dx \quad (C3.26)$$

Hence, substitute \underline{a} from Eqn. C3.25 into Eqn. C3.26, and note that $\underline{f}_s = \underline{k}_s^{-1}$, to get:

$$\begin{aligned} \underline{K} &= \int_0^L \underline{f}_m^{-1} \underline{b}^T \underline{f}_s \underline{k}_s \underline{f}_s \underline{b} \underline{f}_m^{-1} dx \\ &= \underline{f}_m^{-1} \int_0^L \underline{b}^T \underline{f}_s \underline{b} dx \cdot \underline{f}_m^{-1} \\ &= \underline{f}_m^{-1} \end{aligned} \quad (C3.27)$$

That is, the element stiffness matrix obtained using the shape function is the same as that obtained by inverting the element flexibility. Computationally, the element stiffness is obtained

from Eqn. C3.27 and the shape function is thus used only in the state determination phase. The stiffness \underline{K} is in terms of element deformations only. It is expanded to include the element rigid body displacements, and then transformed to the 12 x 12 global stiffness. The transformations are well known and are not repeated here.

C3.5 STATE DETERMINATION

C3.5.1 Basic Procedure

The shape function, \underline{a} , defined by Eqn. C3.25 is exact for an infinitesimally small displacement increment. For such an increment, the slice deformation increment is obtained using the shape function as:

$$\underline{dv}_s = \underline{a} \underline{dv}_m \quad (C3.28)$$

Hence, the slice action increment is:

$$\begin{aligned} \underline{dS}_s &= \underline{k}_s \underline{dv}_s \\ &= \underline{k}_s \underline{a} \underline{dv}_m \end{aligned} \quad (C3.29)$$

From Eqns. C3.25 and C3.27, this is the same as:

$$\begin{aligned} \underline{dS}_s &= \underline{k}_s \underline{f}_s \underline{b} \underline{K} \underline{dv}_m \\ &= \underline{b} \underline{K} \underline{dv}_m \end{aligned} \quad (C3.30)$$

Alternatively, the slice action increment can be obtained directly from the equilibrium relationship as:

$$\begin{aligned} \underline{dS}_s &= \underline{b} \underline{dS}_m \\ &= \underline{b} \underline{K} \underline{dv}_m \end{aligned} \quad (C3.31)$$

These two approaches thus given the same result, which reflects the fact that the shape function is "exact" for infinitesimal element deformations. In an actual state determination, however, the element deformation will be finite. This introduces two complications, one associated with the material calculations, and a more important one associated with change in the shape function. These complications are considered in the following sections.

C3.5.2 Linearity in Mroz Material Calculations

In the state determination calculation for the Mroz material, the stresses are calculated assuming linear behavior. They are then scaled so that the stress point lies exactly on the yield surface. This means that the calculated hoop stress in any slice subelement may not exactly satisfy Eqn. C3.6. If this error is not corrected, it may accumulate over a number of load increments and introduce significant inaccuracy in the solution.

The error is corrected by determining, for each slice subelement, the internal pressure corresponding to the calculated hoop stress. The difference between this pressure and the actual pressure is then a "pressure error." At each iteration, this pressure error is added to dP in Eqn. C3.10 and treated as an initial stress effect.

C3.5.3 Linearity in Use of Shape Function

If the shape function is assumed not to change for a finite deformation increment of the element, the slice deformation increments are given by Eqn. C3.28. The strains in the slice, and hence the subelement stresses and slice actions, then follow. However, if the slice deformation increments are sufficiently large that additional yielding (or unloading) occurs, the shape function will change, and hence the calculated slice actions will not satisfy the equilibrium requirement (Eqn. C3.17). If equilibrium errors develop and are not corrected, they can accumulate over a number of load increments and reach a significant magnitude.

Internal equilibrium errors may be avoided by either a "prevention" or a "correction" approach. In the prevention approach, the state determination calculation is divided into small steps so that no significant equilibrium errors develop. In the correction approach, large steps are allowed and equilibrium errors are permitted to develop. These errors are then eliminated by applying corrections in subsequent state determinations. Both approaches have been explored, and that based on prevention has been found to be more stable. For completeness the procedures for both approaches are described in the following sections.

C3.5.4 Prevention Approach

The prevention approach seeks to prevent significant internal equilibrium errors from developing by adjusting the shape function, \underline{g} , each time a significant change (an "event") occurs in the element state. An event occurs if significant yielding or unloading occurs in any slice subelement. The definition of "significant" is controlled by means of an overshoot tolerance, which allows subelements to go somewhat beyond new yield or unloading before an event is detected.

When an increment of global displacement, $\Delta \underline{r}$, has been determined, the state determination proceeds as follows.

- (1) Calculate the element deformation increment:

$$\Delta \underline{v}_m = \underline{a}_r \Delta \underline{r} \quad (C3.32)$$

in which \underline{a}_r is a well known displacement transformation matrix.

- (2) Calculate the slice deformation increments:

$$\Delta \underline{v}_s = \underline{g} \Delta \underline{v}_m \quad (C3.33)$$

using the current shape function, \underline{g} .

- (3) Calculate the subelement axial and shear strain increments from Eqn. C3.3.
- (4) Calculate the subelement hoop strain increments from:

$$\Delta \epsilon_h = (\Delta \sigma_{h_e} - D_{31} \Delta \epsilon_a - D_{32} \Delta \gamma) / D_{22} \quad (C3.34)$$

in which D_{ij} = term in the constitutive matrix, \underline{D} , and the hoop stress error is obtained from:

$$\Delta \sigma_{h_e} = \frac{p a'}{t} - \sigma_h \quad (C3.35)$$

- (5) Calculate, for each subelement, an event factor, allowing for overshoot of yield or unloading.
- (6) Use the minimum event factor from Step (5) to scale the subelement strain and element deformation increments. Using the scaled strain increments, obtain the subelement stress

- (7) If no event has occurred, the state determination is complete. If an event has occurred, recalculate the shape function.
- (8) Apply the remainder of the element deformation increment, and repeat from Step (2).

When the final subelement stresses have been calculated, the slice actions are obtained by summation over the slice cross sections. If the slice actions were to satisfy equilibrium exactly (i.e. linear variation along the element length), the element end actions would be simply the actions on the two end slices. In fact, the slice actions will not exactly satisfy internal element equilibrium, and it is advisable to obtain the element actions using the virtual displacements principle.

In applying the virtual displacements principle, the natural approach would be to impose a virtual displacement defined by the current shape function, \underline{a} . This is not essential, however. It is interesting to note that if the slice actions satisfy equilibrium (linear variation), then any virtual displacement which satisfies compatibility will give the same result (namely that the element end actions equal the actions on the end slices). If the slice actions do not exactly satisfy equilibrium, then the element end actions calculated by the virtual displacements principle will not be the same for all virtual displacements. However, the differences should be small, and one virtual displacement is not necessarily better than any other. For the ANSR-III implementation, the *linear elastic* shape function, \underline{a}_l , has been used to define the virtual displacement, and the element end actions are thus obtained as:

$$\underline{S}_m = \int_0^L \underline{a}_l^T \underline{S}_s dx \quad (C3.36)$$

This equation has the advantage that \underline{a}_l defines a linear variation of deformation along the element length, and the integral is easily evaluated in closed form. If the current shape function, \underline{a} , is used, the deformations vary quadratically, and evaluation of the integral is more difficult. The use of \underline{a}_l is equivalent to assuming that the element is unloaded by an infinitesimal amount, so that it becomes elastic but the slice actions do not change. The "current" shape function thus becomes \underline{a}_l , which is then used to define the virtual displacement.

C3.5.5 Correction Approach

The correction approach allows large steps to be taken and avoids event calculations. However, substantial equilibrium errors may result, which must be corrected in subsequent state determinations. The corrections are made by introducing *internal* degrees of freedom into the element to allow the element to adjust its shape internally, and hence, satisfy internal equilibrium.

One possible approach is to add internal nodes to the element and let the displacements of these nodes be the internal degrees of freedom. This approach, however, is exactly the same as substructuring. It requires that the analyst select appropriate internal nodes and substantially complicates the computational procedure. Hence, this approach was not considered.

An alternative approach is to select one or more generalized internal degrees of freedom (i.e., not necessarily physical displacements) and to let the shape functions associated with these degrees of freedom vary during the analysis. This approach is consistent with the variable shape function concept used for the element end displacements (the external degrees of freedom). It has been explored, as follows, for a *single* internal degree of freedom.

Let the added internal degree of freedom be v_a , and let its shape function at any time be \underline{a}_a . Hence, slice deformation increments are given by:

$$d\underline{v}_s = \underline{a} d\underline{v}_m + \underline{a}_a dv_a \quad (C3.37)$$

If a set of virtual element actions, $\bar{\underline{S}}_m$, is applied, the following virtual work equation must be satisfied:

$$\begin{aligned} \bar{\underline{S}}_m^T d\underline{v}_m &= \int_L \bar{\underline{S}}_s^T d\underline{v}_s dx \\ &= \bar{\underline{S}}_m^T \cdot \int_L \underline{b}^T \underline{a} dx \cdot d\underline{v}_m + \bar{\underline{S}}_m^T \cdot \int_L \underline{b}^T \underline{a}_a dx \cdot dv_a \end{aligned} \quad (C3.38)$$

From this equation it follows that:

$$\int_L \underline{b}^T \underline{a} dx = \underline{I} \quad (C3.39)$$

in which \underline{I} is a unit matrix, and:

in which \underline{I} is a unit matrix, and:

$$\int_L \underline{b}^T \underline{a}_a dx = \underline{O} \quad (C3.40)$$

in which \underline{O} is a null vector.

Equation C3.39 is satisfied automatically. The shape function associated with the internal degree of freedom must satisfy Eqn. C3.40. A convenient choice for \underline{a}_a is $\Delta \underline{a}$, which is the change in \underline{a} when it was last reformed. Because Eqn. C3.39 is satisfied for both \underline{a} (the current shape function) and $\underline{a} - \Delta \underline{a}$ (the preceding shape function), it follows that Eqn. C3.40 is satisfied by $\underline{a}_a = \Delta \underline{a}$. The computational procedure for the state determination is as follows.

- (1) Calculate the element deformation increment from Eqn. C3.32.
- (2) Calculate the slice deformation increment:

$$\Delta \underline{v}_s = \underline{a} \Delta \underline{v}_m + \Delta \underline{v}_{s0} \quad (C3.41)$$

in which $\Delta \underline{v}_{s0}$ is an initial slice deformation increment obtained from the previous state determination, as described later in Step (10).

- (3) Calculate the axial, shear, and hoop strain increments from Eqns. C3.3 and C3.34.
- (4) Obtain the subelement stresses by Mroz material state determination.
- (5) Reform the shape function, \underline{a} , if substantial yielding or unloading has occurred. Hence, also obtain, $\Delta \underline{a}$.
- (6) Obtain the slice forces, \underline{S}_s , by summing the stresses over the cross section.
- (7) Calculate the element end actions, \underline{S}_m , from Eqn. C3.36.
- (8) Calculate the equilibrium error at the slices, $\Delta \underline{S}_e$, as:

$$\Delta \underline{S}_e = \underline{b} \underline{S}_m - \underline{S}_s \quad (C3.42)$$

- (9) Calculate slice force increments associated with a unit increment in the internal degree of freedom, $\Delta v_a = 1$, as:

$$\Delta \underline{S}_a = \underline{k}_s \Delta \underline{v}_s = \underline{k}_s \underline{a}_a \quad (C3.43)$$

(10) Obtain the value of Δv_a which minimizes the slice force errors. That is, select Δv_a so that, say, the RMS value of:

$$\Delta \underline{S}_e - \Delta \underline{S}_a \Delta v_a$$

is a minimum. The slice deformations:

$$\Delta v_{s0} = \underline{a}_a \Delta v_a \quad (C3.44)$$

become *initial* slice deformations to be taken into account in the next state determination (Step 2).

A number of analyses were carried out to explore this procedure. The results were encouraging provided only small element deformation increments were allowed in any load step. If large deformation increments were allowed, however, the initial slice deformations, Δv_{s0} , tended to dominate the response. There was then a tendency for successive yielding and unloading to occur within the element, leading to numerical instability. For this reason it was decided to implement only the "prevention" approach in the ANSR-III element.

C4. REFERENCES

- C1. Suharwardy, M.I.H. and D. A. Pecknold, "Inelastic Response of Reinforced Concrete Columns Subjected to Two-Dimensional Earthquake Motions," Structural Research Series No. 455, Department of Civil Engineering, University of Illinois at Urbana-Champaign, October 1978.
- C2. Mosaddad, B., "Computational Models for Cyclic Plasticity, Rate Dependence and Creep," *Ph.D. Thesis*, Civil Engineering Department, University of California, Berkeley, June 1982.

C5. ANSR-III USER GUIDE

INPUT DATA

INELASTIC MULTI-SLICE TUBE ELEMENT

1. GROUP CONTROL INFORMATION

Columns	Note	Name	Data
1 - 5(I)			Element type number. Input 5.
6 - 10(I)			Number of elements in group.
11 - 15(I)		NFST	Element number of first element in group. Default = 1.
16 - 25(F)			Initial stiffness damping factor, β_o .
26 - 35(F)			Current stiffness damping factor, β_T .
36 - 40			Not used.
41 - 80(A)			Optional group heading.

2. CROSS SECTION AND MATERIAL DATA CONTROL INFORMATION

Columns	Note	Name	Data
1 - 5(I)		NOMAT	Number of different materials (max. 10).
6 - 10(I)		NOSEC	Number of different cross sections (max. 20).

3. MATERIAL PROPERTIES

NOMAT sets of cards, two cards per set.

3(a) FIRST CARD

Columns	Note	Name	Data
1 - 5(I)			Material number.
6 - 10(I)	(1)	NPT	Number of linear segments in stress-strain curve (max. 3).
11 - 20(F)			Poisson's ratio in elastic range.
21 - 30(F)	(2)		Yield overshoot tolerance. Default = .02.

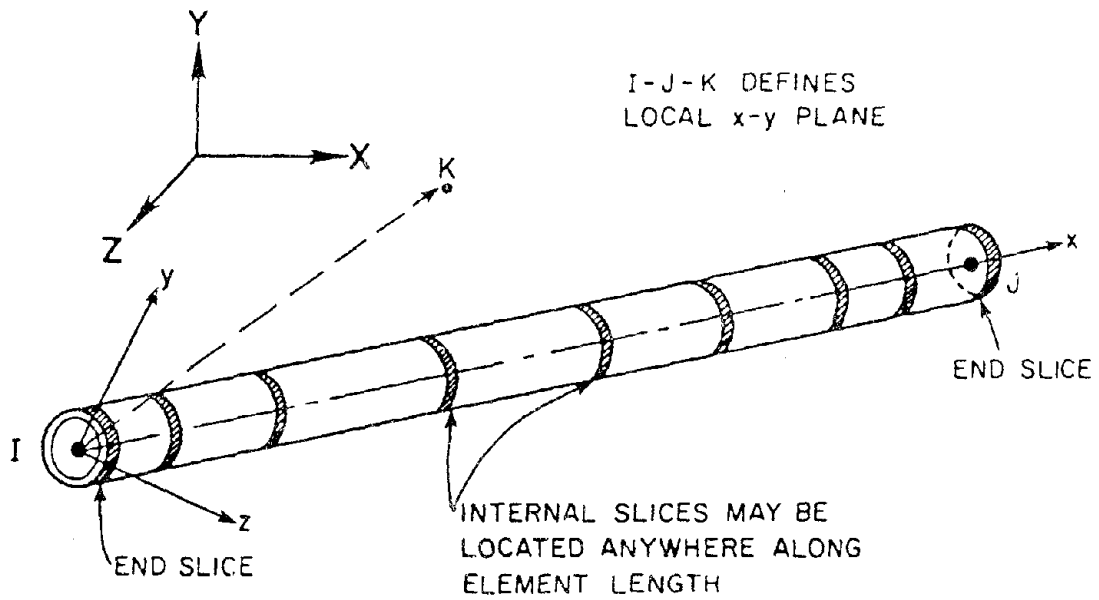
5. ELEMENT SPECIFICATION

As many cards as needed to specify all elements in group. The cards for the first and last element in the group must be input. If cards for intermediate elements are omitted, the data is generated. Elements within the group must be sequentially numbered, starting with NFST.

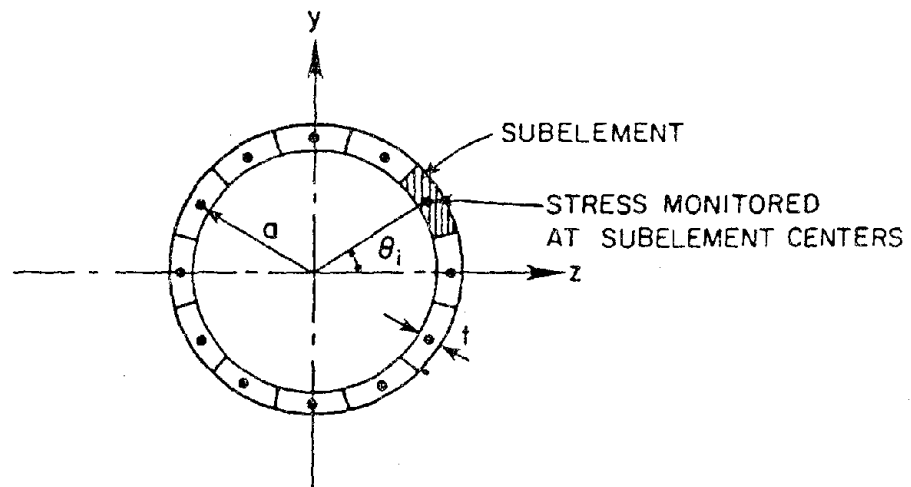
Columns	Note	Name	Data
1 - 5(I)			Element number, or number of first element in a sequentially numbered series of elements to be generated by this card.
6 - 10(I)			Node I.
11 - 15(I)			Node J.
16 - 20(I)			Node K. Default = automatic assignment.
21 - 25(I)			Node number increment for generation. Default = 1.
26 - 35			Blank.
36 - 40(I)			Material number. Default = 1.
41 - 45(I)			Output code: (a) 1 = output actions at nodes only. (b) 2 = also output actions and deformations at end slices. (c) 3 = also output actions and deformations at slices in body of element. Default = 3.
46 - 50(I)			Cross section number. Default = 1.
55(I)			Large displacement code: (a) 0 = small displacement analysis. (b) 1 = large displacement analysis.
60(I)	(7)		Symmetry code: (a) 0 = full 3D motion. (b) 1 = motion in element xy-plane only.
61 - 70(F)			Internal pressure. Default = 0. Negative value = external pressure.

NOTES: INELASTIC MULTI-SLICE TUBE ELEMENTS

- (1) The actual stress-strain curve must be approximated by a number of linear segments. A maximum of 3 segments (trilinear curve) is allowed. The maximum stress in the last segment must be set very high. The default value is 10^{20} .
- (2) In the event-to-event procedure, if zero tolerance were used, a new step would be required each time a subelement yielded, and the number of steps could be excessive. A degree of overshoot of the nominal yield value is permitted. At the end of any substep, all elements which are between their nominal yield stresses and the permissible overshoot values are assumed to yield simultaneously.
- (3) When the element yields, the tangent stress-strain relationship can, in general, change continuously, and hence, the structure stiffness should strictly be modified in every load step. In many cases, however, the stiffness change from one step to the next may be small, and it may be reasonable to retain the same stiffness for several steps. This tolerance enables the user to control the frequency of stiffness reformulation.
- (4) The number of subelements in a cross section must be an even number so that the cross section has symmetry about the two principal axes. If symmetry (motion in element xy-plane) is specified, the maximum number of subelements in the cross section is 24 (i.e. 12 in half section).
- (5) The number of subelements along the element length can be from 1 to 8. A slice is located at each dividing point, in addition to the two slices at the element ends.
- (6) Care must be exercised in specifying the locations of the slices. For example, in a region of large moment gradient, it may be necessary to specify closely-spaced slices.
- (7) In many cases, the structure is symmetrical and motion occurs only in the element xy-plane. In such cases, only one half of the element cross section needs to be considered, and out-of-plane motions can be ignored. The computational effort at the element level is thus substantially reduced. If symmetry is specified, only **one half** of the element is considered. Structure loads and masses must be specified taking this into account.

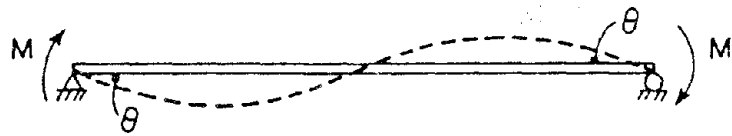


(a) MULTI-SLICE PIPE ELEMENT

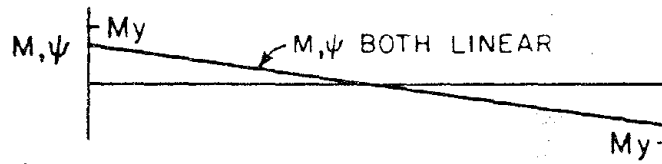


(b) CROSS SECTION SUBDIVISION

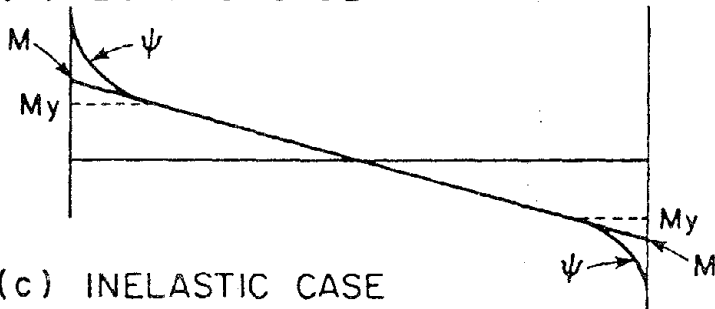
FIG. C2.1 MULTI-SLICE PIPE ELEMENT



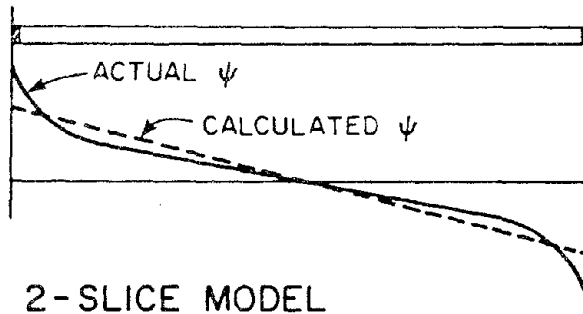
(a) ANTI SYMMETRIC BENDING



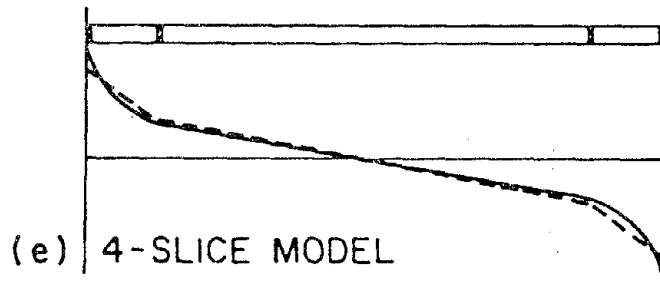
(b) ELASTIC CASE



(c) INELASTIC CASE

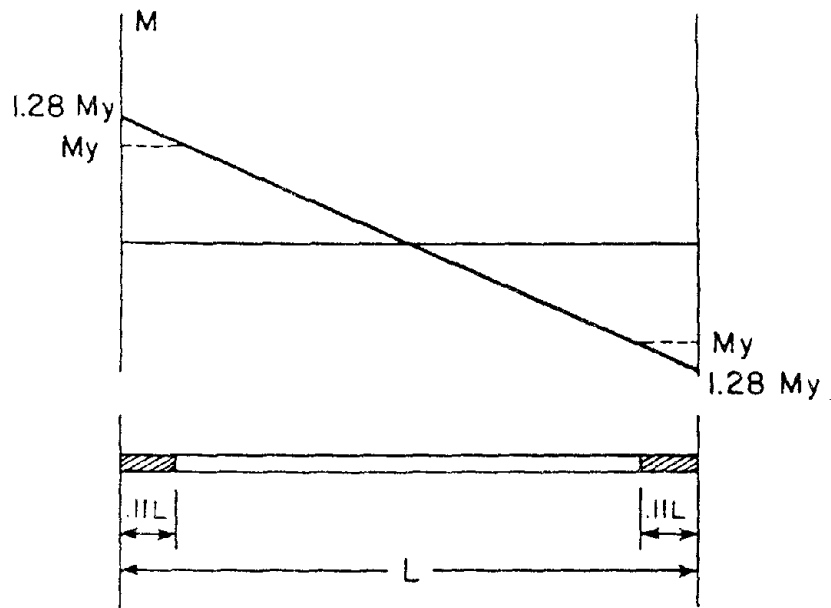


(d) 2-SLICE MODEL

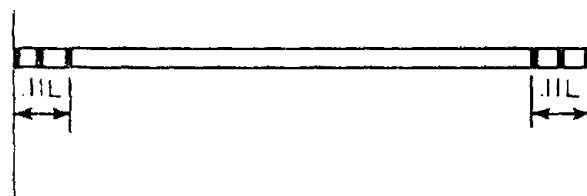


(e) 4-SLICE MODEL

FIG. C2.2 ANTISYMMETRICAL BENDING

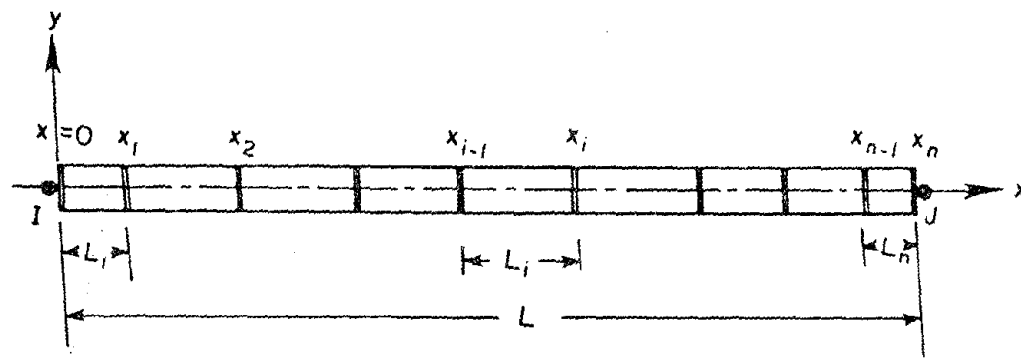


(a) MAXIMUM EXTENT OF YIELD

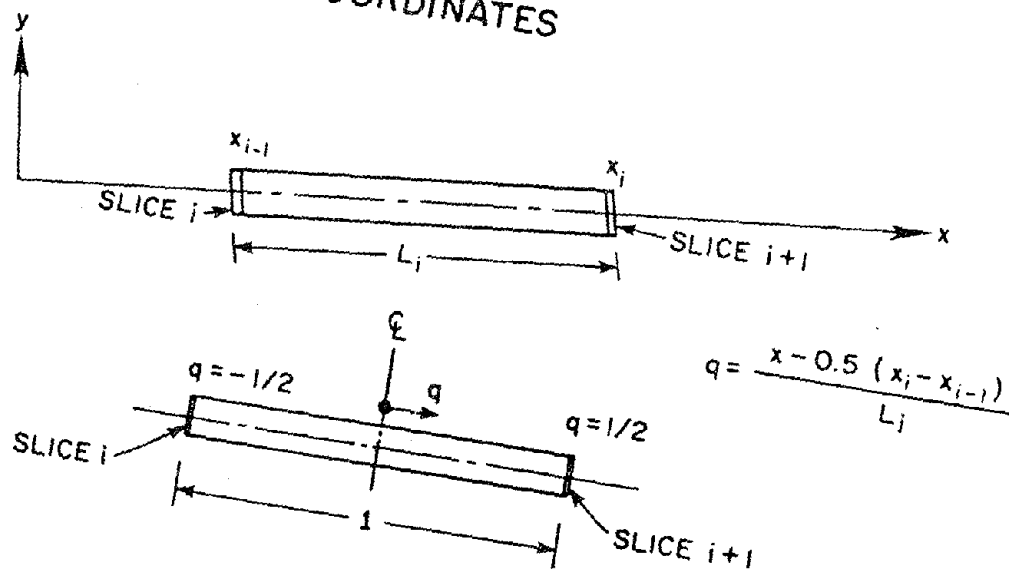


(b) POSSIBLE SLICE LOCATIONS

FIG. C2.3 ELASTIC-PERFECTLY-PLASTIC MATERIAL

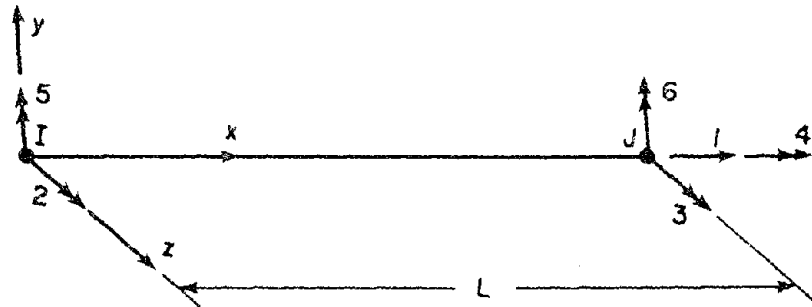


(a) LOCAL COORDINATES

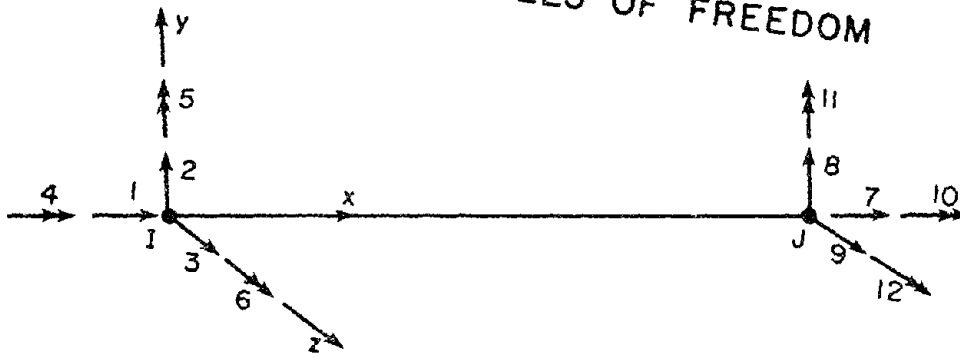


(b) DIMENSIONLESS COORDINATES

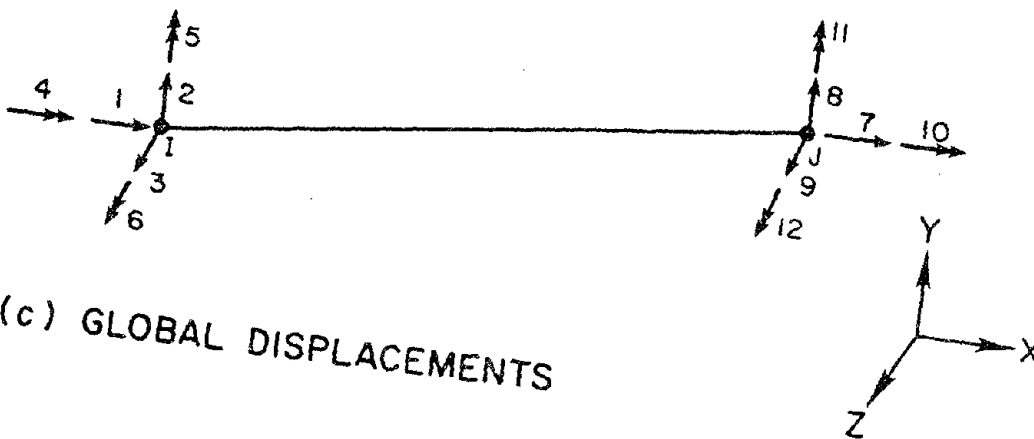
FIG. C3.1 COORDINATES SYSTEM



(a) DEFORMATION DEGREES OF FREEDOM



(b) LOCAL DISPLACEMENTS



(c) GLOBAL DISPLACEMENTS

FIG. C3.2 ELEMENT DEGREES OF FREEDOM

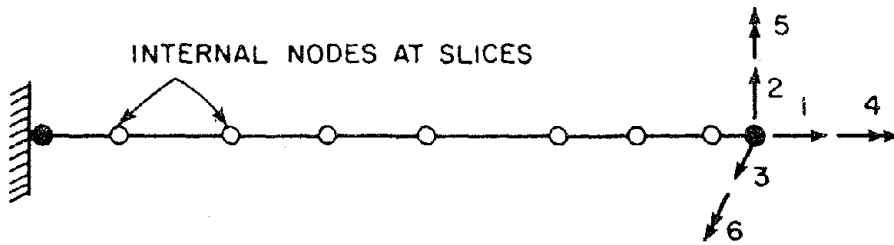


FIG. C3.3 ELEMENT DEFORMATIONS FOR STIFFNESS APPROACH

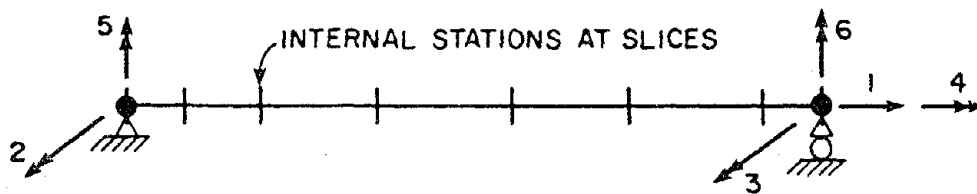


FIG. C3.4 ELEMENT DEFORMATIONS FOR FLEXIBILITY APPROACH

D. EXAMPLES

This section describes a number of examples which have been used to test the straight-curved pipe and multi-slice tube elements.

D1. PIPE WITH AXIAL FORCE AND INTERNAL PRESSURE

D1.1. PURPOSE

The purpose of this example is to check the inelastic behavior of the pipe element under combined axial and hoop stresses and to verify that the Mroz material model has been correctly implemented.

D1.2 CONFIGURATION

A cantilever pipe as shown in Fig. D1.1(a) is considered. The pipe length is 100 feet, with 48-in. outside diameter and 0.6-in. wall thickness. The material stress-strain curve is assumed to be trilinear, as shown in Fig. D1.1(b). Poisson's ratio is 0.3.

D1.3 ANSR ANALYSIS MODEL

D1.3.1 Assumptions for Analysis

The cantilever pipe was modeled by a single straight pipe element, with one end fixed and the other free. The element was specified to have two Gauss points. Because no bending moment exists, the pipe cross section was subdivided into only two subelements (fibers) around the pipe circumference.

D1.3.2 Loadings

A uniform internal pressure of 864 psi was first applied. This pressure produced hoop and axial stresses, with a von Mises effective stress just below yield. An axial tensile load of 2500 kips was then applied at the free end in five equal steps.

D1.3.3 ANSR Input

The ANSR-III input file for the example is listed in Table D1.1.

Preceding page blank

D1.4 RESULTS

The computed von Mises effective stresses and strains in the pipe wall are shown in Fig. D1.1(b). All points lie on the "virgin" uniaxial stress-strain curve. The variation of axial stress with axial strain is shown in Fig. D1.1(c).

These results were compared with the results obtained from the well-established pipeline analysis program PIPLIN [D.1], which uses the Mroz theory but with a significantly different computational scheme. The results from the two analyses were virtually identical.

D1.5 CONCLUSION

This example indicates that the pipe element gives correct results for inelastic behavior under combined axial and hoop stresses and that the Mroz material model has been correctly implemented.

D2. BURIED PIPE BEND WITH TEMPERATURE AND PRESSURE LOADING

D2.1 PURPOSE

This example tests the inelastic behavior of the pipe element under temperature change, internal pressure, and bending.

D2.2 CONFIGURATION

The structural configuration is shown in Fig. D2.1(a). It represents a 12-degree, 120-ft. radius sidebend in a pipeline, with virtual anchors (fixed supports) at both ends. The pipe is modeled using straight and bend elements, with 48-in. outside diameter and 0.6-in. wall thickness. Because of symmetry, only one-half of the structure needs to be modeled, with a roller support at the axis of symmetry. The pipe material stress-strain curve is assumed to be tri-linear, as shown in Fig. D2.1(b). Poisson's ratio is 0.3, and the coefficient of thermal expansion 0.00001 per degree.

D2.3 ANSR ANALYSIS MODEL

D2.3.1 Assumptions of Analysis

The structure was modeled using six pipe elements, three straight elements for the straight segment and three curved elements for the curved segment. Each element was specified to have two Gauss points. The pipe cross section was divided into six subelements (fibers) around one-half of the pipe circumference.

D2.3.2 Loadings

A uniform temperature and internal pressure (equal values at all nodes) were applied to the analysis model as follows.

- (1) Apply internal pressure of 1750 psi in ten steps.
- (2) Decrease internal pressure to zero in ten steps.

- (3) Re-apply internal pressure to 1750 psi in ten steps.
- (4) Apply temperature change of -100 degrees F in ten steps.

D2.3.3 ANSR Input

The ANSR-III input file for this example is listed in Table D1.2.

D2.4 RESULTS

Load sequence (1) causes initial yielding of the pipe and causes outward movement of the side bend (Fig. D2.2). After the pressure is removed in sequence (2), a small inward deflection is present at the midpoint of the model (Fig. D2.2). Re-application of the internal pressure in sequence (3) returns the sidebend segment back to the location at the end of sequence (1). The temperature decrease then causes inward movement of the bend (Fig. D2.2). The computed displacements are shown in Fig. D2.2 and the computed pipe moments in Fig. D2.3. The corresponding results obtained using PIPLIN are also shown in Figs. D2.3 and D2.5. It can be seen that the results are in close agreement.

D2.5 CONCLUSION

The ANSR results are in agreement with those obtained by PIPLIN, which has been widely used and carefully validated. This indicates that the pipe element is applicable for inelastic temperature and internal pressure loading.

D3. PIPE WHIP WITH LARGE DISPLACEMENTS

D3.1 PURPOSE

This example tests the straight-curved pipe element with large displacements and dynamic loading.

D3.2 CONFIGURATION

Analyses of a cantilevered pipe with large displacements and impact have been reported by Hibbitt and Karlsson [D.2]. The dimensions of the pipe are shown in Fig. D3.1.

ANSR-III U-bar elements are located at nodes 16 through 19, with initial gaps specified to represent a flat surface. Each element is arbitrarily assigned a stiffness of 10^4 k/in, which allows a small amount of flexibility after gap closure. In the analysis reported in [D.2], the flat surface was assigned a very large mass, rather than an elastic stiffness. Because impact of an actual pipe would involve substantial local deformation of the pipe, and probably significant deformation of the impacted wall, the assumption of an essentially rigid surface is not realistic, and the computed impact forces are likely to be much larger than those which would occur in actual practice.

The analysis in [D.2] considered a "follower" jet force, acting parallel to line 19-20. Because ANSR-III does not currently include a follower force option for dynamic loads, the analysis was carried out assuming a vertical jet force. The results are thus not directly comparable with those in [D.2], especially after impact. The straight-curved pipe element has also been incorporated into WIPS [D.3], a special purpose computer code for pipe whip analysis. In the verification studies for WIPS, a similar analysis has been carried out with a follower jet force.

The stress-strain relationship for the pipe steel is shown in Table D3.1. The blowdown forcing function is shown in Table D3.2.

D3.3 ANSR ANALYSIS MODEL

D3.3.1 Geometry, Loading, and Pipe Properties

The PIPE element subdivision is shown in Fig. D3.1. This is similar to the subdivision used in [D.2]. It may be noted that only a single element is used in the vertical leg between nodes 19 and 20. This introduces a significant error in the rotational inertia of this leg, and for practical analysis a larger number of nodes is probably desirable.

Motion was permitted in the XY plane only. The default ovaling strengths and stiffnesses were assumed for the curved PIPE elements, with small ovaling assumed. Twelve subelements (the default value) were used in each PIPE element cross section.

The jet force was applied at node 20 in the vertical direction. To allow for the symmetry, the jet forces shown in Table D3.2 were multiplied by 0.5 (because only half of the element strengths and stiffnesses are used in symmetrical segments of the analysis model).

D3.3.2 Analysis Control Parameters

The Newmark scheme with automatic time step selection was used, with the following parameters.

$$\text{Initial time step} = 5 \times 10^{-4} \text{ sec.}$$

$$\text{Minimum time step} = 5 \times 10^{-6} \text{ sec.}$$

$$\text{Maximum time step} = 10^{-3} \text{ sec.}$$

$$\text{Initial } \beta_0 / \Delta t = 0.1$$

$$\text{Lower midstep tolerance} = 50 \text{ k}$$

$$\text{Upper midstep tolerance} = 250 \text{ k}$$

D3.3.3 ANSR Input

The ANSR-III input file for the example is listed in Table D3.3.

D3.4 RESULTS

Deflected shapes at several times are shown in Fig. D3.2. This figure demonstrates that the computational scheme can consider very large displacements. No results are available for confirmation that the analysis is correct. A more detailed comparison with the results from [D.2] is presented in [D.3], using the WIPS version of the element.

The analysis required a total of 228 time steps, 107 up to gap closure at 0.106 seconds, and 121 for the remaining 0.029 seconds. The maximum time step was 0.00100 seconds (in the period before gap closure) and the minimum step was 0.000125 seconds (in the period shortly after gap closure).

D4. INELASTIC MULTI-SLICE BEAM COLUMN

D4.1 PURPOSE

This example tests the multi-slice tube element for its ability to capture the inelastic curvature variation along a single beam-column member. Four different cases have been considered, each with a different number of slices. The load-deflection relationships and the calculated curvature variations are compared, to study how accurately the different cases predict the member behavior. This is only a preliminary test of the multi-slice element. Further work is needed to test the element thoroughly and to study its characteristics in detail.

D4.2 CONFIGURATION

The tubular beam-column shown in Fig. D4.1(a) has its bottom end fixed and its top end restrained by an elastic rotational spring. The spring stiffness of 42,650 k/radian is chosen so that the bending moments at the top and bottom ends are in essentially the ratio 2:1 in the elastic state. The material stress-strain curves for the pipe steel were as shown in Fig. D4.1(b). Two different strain hardening ratios were considered for each model, namely 1% and .01%.

Four different models, each with a different number of slices, have been specified. The numbers of slices and their locations are shown in Table D4.1.

D4.3 ANSR ANALYSIS MODEL

D4.3.1 Assumptions for Analysis

Each slice cross section was subdivided into 8 subelements (fibers) around one-half of the pipe circumference (to account for symmetry only one-half of the beam-column strengths and stiffnesses were used in the analysis model).

For each model, a lateral displacement of 2.2 inches (approximately 4 times the yield displacement) was applied at the top end, in two increments. In the first increment a displacement magnitude of 0.5 inches was applied in one step. This brought the beam-column close to first yield. In the second increment a displacement of 1.7 inch was applied in twenty equal steps.

Constant displacement iteration was specified for all cases.

D4.3.2 ANSR Input

The ANSR-III input data file for the 7-slice model, with strain hardening 0.01%, is listed in Table D4.2. The remaining data files were similar and are not listed.

D4.4 RESULTS

D4.4.1 Expected Behavior

In the elastic range, the bending moment at the bottom of the member is 2.04 times that at the top. Simple hand calculation shows that first yield occurs at a load of 3.33 k and a deflection of 0.53 inches. (This load is on one-half of the member because symmetry is assumed.)

After yield, redistribution of moment occurs, and the top moment increases more rapidly than the bottom moment. For an elastic-perfectly-plastic material, the collapse load is reached when plastic hinges form at both the top and bottom of the member. The plastic moment capacity is 1.28 times the yield moment for a tubular section. Hence, the rigid-plastic collapse load is 5.75 k.

No exact solution is available for the behavior between first yield and collapse. However, a load-deflection relationship can be obtained assuming that ideal plastic hinges develop at the member ends. With this assumption, a hinge forms at the bottom at a load of $(1.28)(3.33) = 4.26$ k. The stiffness then reduces to one-fourth the elastic value, until a hinge forms at the top at the collapse load. The strength then remains constant. The load-deflection curve for this simple "elastic-ideal-hinge" assumption is shown on the figures to provide a reference.

D4.4.2 Load Versus Deflection

The calculated load-deflection curves for a substantial strain hardening ratio (1%) are shown in Fig. D4.2. The results for the seven- and nine-slice models are closely similar, and are believed to be close to the "exact" behavior. The four-slice model gives reasonably accurate

results. However, the two-slice model gives poor results.

The load-deflection curves with negligible strain hardening ratio (0.01%) are shown in Fig. D4.3. Again, the seven- and nine-slice models give closely similar results. In both of these models, a plastic mechanism forms at approximately two inches deflection, with the correct collapse strength. Note that the elastic-ideal-hinge model forms a mechanism at 1.84 inches deflection. The four-slice model again gives fair results, and the two-slice model gives very poor results.

The reason why the two-slice model gives poor results is that the variation of cross section flexibility between slices is obtained by linear interpolation. With only two slices, this provides inaccurate values, and the element is much too flexible. With four slices, the flexibility variation is estimated more accurately, but substantial error still exists. With either seven or nine slices, the linear interpolation appears to give accurate results.

For the seven- and nine-slice models, the ultimate load capacity is some 3% larger than that predicted for the elastic-ideal-hinge model. Approximately 1% of this difference can be attributed to strain hardening. The remaining difference occurs because the slice bending moments in the multi-slice model do not lie exactly on a straight line. This is because the shape function is recalculated only at discrete intervals, so that some error can develop. The result is that the effective end bending moments (obtained by virtual work) are somewhat larger than the bending moments on the end slices. The calculated strength is thus also slightly too large. This aspect of the multi-slice model requires further study.

D4.4.3 Curvature Versus Deflection

The calculated curvatures at the top and bottom of the member are listed in Tables D4.3 and D4.4, for 1% and .01% strain hardening, respectively. For each case the calculated curvatures for the four-, seven-, and nine-slice models are of the same order of magnitude. However, those for the two-slice model are much lower. This again indicates that the two-slice model does not predict the inelastic deformation accurately. The four-slice model is also

significantly inaccurate, whereas the seven- and nine-slice models give closely similar results.

Note that the calculated curvatures with the elastic-plastic material (0.01% strain hardening) are much larger than for the material with significant hardening (1%). This indicates that material properties must be carefully specified if ductility demands based on curvature (or strain) are to be calculated.

D4.5 CONCLUSION

This example, although limited in scope, suggests that the multi-slice element has the ability to calculate accurate curvatures and load-deflection relationships for beam-column members. The example suggests that a seven-slice model should be adequate for practical computation, and shows that calculated curvatures can be sensitive to the material stress-strain curve.

Although the results are not shown here, an analysis was also performed with an extremely low strain hardening ratio ($10^{-10}\%$). For reasons which are not clear, the results were poor for all cases (including seven and nine slices). Hence, it is recommended that if the element is used, a strain hardening ratio of at least 0.01% be specified.

Additional study is needed to test the multi-slice element thoroughly and to develop guidelines for its use. Time and resources have not been available to perform these additional studies under the current project. Nevertheless, it can be concluded that the multi-slice concept is very attractive for modeling beam columns when curvature or strain ductilities are to be calculated.

D5. SUMMARY

D5.1 GENERAL

This section has presented three examples using the straight-curved pipe element and one example using the multi-slice beam-column element.

The examples with the straight-curved pipe element have all been carried out using the ANSR-III computer code and have only exercised the element for two-dimensional behavior. The element has also been incorporated into the WIPS code [D.3]. In the verification studies for WIPS, the element was also exercised for three-dimensional behavior. However, these analyses are not reported here.

The example with the multi-slice element is very limited in scope, exercising the element only in two dimensions and ignoring axial force and torsion.

Elements such as those described in this report are very complex. Developing, testing and documenting them is time-consuming and costly. Time and resources have not permitted thorough testing. If the elements are used in practical applications, the analyst is cautioned to perform additional tests to ensure that the elements are performing correctly.

D6. REFERENCES

- D.1 Structural Software Development, Inc., **PIPLIN**, Proprietary Computer Code and Documentation, Berkeley, California.
- D.2 Hibbitt and Karlsson, Inc., "Analysis of Pipe Whip," *Report EPRI NP-1208*, Providence, Rhode Island, November 1979.
- D.3 Powell, G. H. et al, "WIPS: Computer Code for Whip and Impact Analysis of Piping Systems," Report to Lawrence Livermore National Laboratory, Department of Civil Engineering, University of California, Berkeley, 1982 (to be published as a Nuclear Regulatory Commission NUREG document).

Preceding page blank

TABLE D1.1 - ANSR-III INPUT DATA - CANTILEVER PIPE EXAMPLE

```

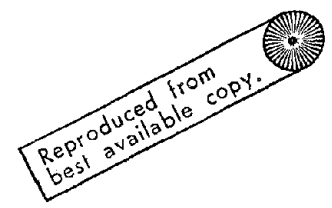
STAR      PIPE UNDER INTERNAL PRESSURE AND AXIAL LOAD

      2      2      2      1
      1 0.0      0.0
      2 1200.
      1      111111
      2      311111
      4      1      1
      1      1
      1      3      0.3
30000.    30.      3000.      39.      300.
      2      2      0 48.      0.6

      1      1      2      1      3      1
      1      1
      1      AXIAL FORCE AT NODE 2
      2 2500.
      1      INTERNAL PRESSURE IN PIPE
      1      2      1      0.864

      1
      2
STAT
      2
      1      1 1.0      1      1      1
      1
      0      0 0.01      1
0.5      2 2.      4.
1.00     1 0.20      5      1      5
      1      1

```



0 0.01

2.2 4.

1.0

0.5

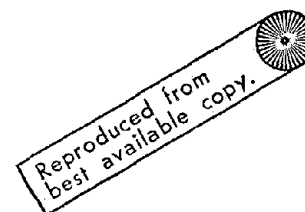
NONE
STOP

TABLE D2.1 - ANSR-III INPUT DATA - PIPE SIDEBEND EXAMPLE

STAR SIDEBEND SEGMENT SUBJECTED TO TEMP. AND PRES.

	0	8		R		1			
1	0.0								
2	99.452								
3	198.904								
4	298.356								
5	348.428								
6	398.622								
7	448.877								
8	448.877								
1	111111								
2	001110								
3	001110								
4	001110								
5	001110								
6	001110								
7	001110								
8	111111								
4	6	1							
1	2								
1	3 .3			.01		.01		1.F-5	
29500.	34.8			11600.		58.0		6666.7	
12	2	0	48.			0.6			
12	2	0	48.			0.6			
			2					0.5	0.1
1	1	2				1	3	1	1
3	3	4				1	3	1	1
4	4	5	8			1	3	2	1
5	5	6	8			1	3	2	1

121



```

      2
      1 INTERNAL PRESSURE IN PIPE
      1 7 1 1.0
      1 TEMPERATURE CHANGES
      1 7 1 1.0
STAT
  4
  1 1 0.10 40 1 5
  1 0 0.1 1
0.5 2 2. 4.
1.75
  1 1 0.10 40 1 5
  1 0 0.1 1
0.5 2 2. 4.
-1.75
  1 1 0.10 40 1 5
  1 0 0.1 1
0.5 2 2. 4.
1.75
  1 1 0.10 40 1 5
  1 0 0.1 1
0.5 2 2. 4.
      -100.
      NONE
      STOP

```

Reproduced from
best available copy. 

TABLE D3.1 - STATIC STRESS-STRAIN RELATIONSHIP FOR PIPE STEEL

Stress (ksi)	Strain	Modulus (ksi)
0	0	26700
26.7	0.001	219
44.0	0.080	2

TABLE D3.2 - BLOWDOWN FORCE RECORD

Time (sec)	Force (k)
0	0
0.0001	650
0.0010	880
0.0020	1000
0.0030	880
0.0050	780
0.0200	430
10.0	430

TABLE D3.3 - ANSR-III INPUT DATA - LARGE DISPLACEMENT PIPE WHIP EXAMPLE

STAR	LARGE DISPLACEMENT PIPE WHIP		
27	27		
1	0.0	0.0	
2	18.0	0.0	
3	36.0	0.0	
4	54.0	-4.823	
5	67.177	-18.0	
6	72.0	-36.0	
7	72.0	-74.0	
8	72.0	-112.0	
9	76.823	-130.0	
10	90.0	-143.177	
11	108.0	-148.0	
12	156.6	-148.0	
13	205.2	-148.0	
14	253.8	-148.0	
15	302.4	-148.0	
16	351.0	-148.0	
17	369.0	-143.177	
18	382.177	-130.00	
19	387.0	-112.0	
20	387.0	-6.0	
21	36.0	-36.0	
22	108.0	-112.0	
23	351.0	-112.0	
24	351.		
25	369.		
26	382.177		
27	387.		
2	001110	20	1

Reproduced from
best available copy.



21	111111	27	1									
1	111111											
1	0.360E-3	0.360E-3										
2	0.719E-3	0.719E-3										
3	0.732E-3	0.732E-3										
4	0.745E-3	0.745E-3										
5	0.745E-3	0.745E-3										
6	0.113E-2	0.113E-2										
7	0.152E-2	0.152E-2										
8	0.113E-2	0.113E-2										
9	0.745E-3	0.745E-3										
10	0.745E-3	0.745E-3										
11	0.134E-2	0.134E-2										
12	0.194E-2	0.194E-2										
13	0.194E-2	0.194E-2										
14	0.194E-2	0.194E-2										
15	0.194E-2	0.194E-2										
16	0.134E-2	0.134E-2										
17	0.745E-3	0.745E-3										
18	0.745E-3	0.745E-3										
19	0.249E-2	0.249E-2										
20	0.212E-2	0.212E-2										
4	19	1	0.0001									
1	2											
1	3	0.3	0.02	0.05								
26700.	26.7	219.0	44.0	2.0								
12	2	0	24.0	1.531								
12	2	0	24.0	1.531								
	3			0.4	0.08							
1	1	2	0	0	0	1	1	1	1	0	1	
2	2	3	0	0	0	1	1	1	1	0	1	
3	3	4	21	1		1	1	2	1	1	1	
5	5	6	21	1		1	1	2	1	1	1	
6	6	7	0	0		1	1	1	1	0	1	
7	7	8	0	0		1	1	1	1	0	1	

8	8	9	22	1	1	1	2	1	1	1
10	10	11	22	1	1	1	2	1	1	1
11	11	12	0	1	1	1	1	1	0	1
15	15	16	0	1	1	1	1	1	0	1
16	16	17	23	1	1	1	2	1	1	1
18	18	19	23	1	1	1	2	1	1	1
19	19	20	0	1	1	1	1	1	0	1
5	4	1								

1	2	124.0	0.1
10000.	10.		
1.E10			
2	2	128.82	0.1
10000.	10.		
1.E10			
3	2	142.0	0.1
10000.	10.		
1.E10			
4	2	160.	0.1
10000.	10.		
1.E10			

1	16	24	1	0	1	1.0	1.0
2	17	25	2	0	1	1.0	1.0
3	18	26	3	0	1	1.0	1.0
4	19	27	4	0	1	1.0	1.0

1	1	16														
JET FORCE																(8F10.0)
0.0	0.0	0.5	0.0001	650.	0.001	88%	0.002	1000.								
0.003	880.	0.005	780.	0.02	43%	10.	430.									

19	19														
2	3	4	5	6	7	8	9	10	11	12	13	14	15	16	17
18	19	20													
2	3	4	5	6	7	8	9	10	11	12	13	14	15	16	17
18	19	20													

```

DYN1 1 1 .0005 1 1 1
0.000005 0.001 0.5 2.0 250. -1 1
1.00 0.135 1.E6 30 50. 0
1 0.0005 20 0.01 20
1 2 -1.0 20
NONE
STOP

```

TABLE D4.1 - SLICE LOCATIONS

SLICE NUMBER	DISTANCE OF SLICE (INCHES) FROM BOTTOM			
	2 SLICES	4 SLICES	7 SLICES	9 SLICES
1	0	0	0	0
2	100	11	10	5
3		89	25	10
4		100	50	20
5			75	50
6			90	80
7			100	90
8				95
9				100

TABLE D4.2 - ANSR-III INPUT DATA - MULTI-SLICE BEAM-COLUMN EXAMPLE

```

STAR      MULTI-SLICE TUBE INPUT DATA

          3          3          3          1

          1 0.0      0.0
          2 0.0      100.
          3 0.0      100.      -10.

          1 111111
          2 011110
          3 011111
          4 2 1
          5 2
          6 2 .3      .01      .01
37000.    30.      3.0      1.56
          7 2 .3
37500.    1.56      150.0      1.510
          8 6 0 10.      0.2
0.05      0.1      0.35      0.35      0.1      0.05
          9 1 1 10.      0.2
1.0
          1 1 2          1 3 1 0 1
          2 2 3          2 2 2

          1
          1 DISPL. AT NODE 2 IN X-DIRECTION
          2 1 1.0

          2
          2 3

STAT
          1 3          1 2 1.0          1 2 3 10 2
          1 0.5
    
```

```

2 1 1.0
1 1 1.0
0.5 2 3
1 1.7
2 1 1.0
1 1 1.0
1.7
NONE
STOP
2 1 2 0.05 20 3 10 2
2
2

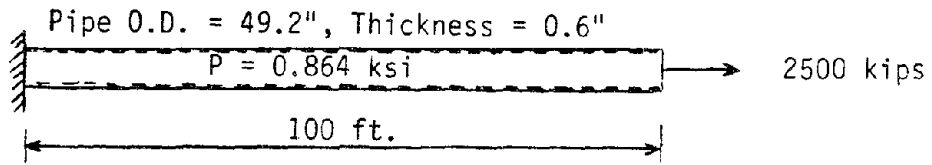
```

**TABLE D4.3 - CALCULATED CURVATURES.
 STRAIN HARDENING = 1%
 RATIO (CALCULATED CURVATURE)/(YIELD CURVATURE)**

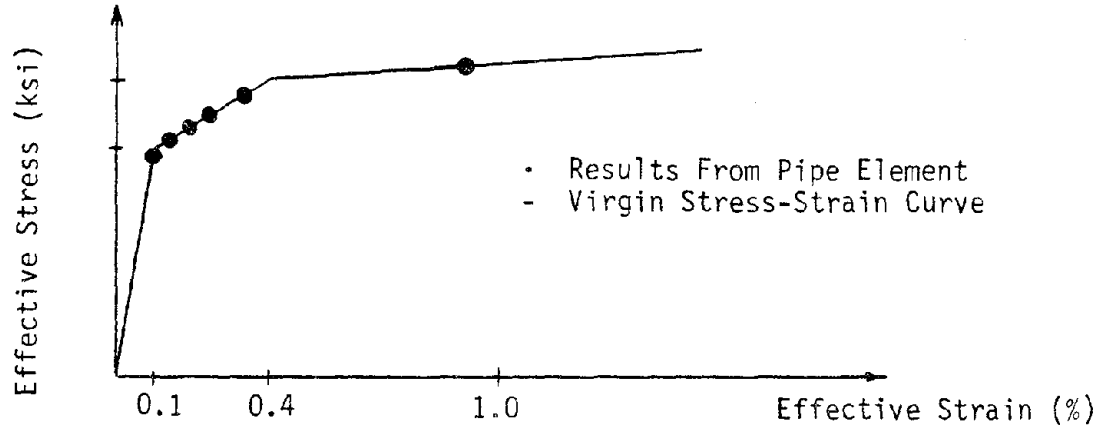
DISL. (in)	2 SLICES		4 SLICES		7 SLICES		9 SLICES	
	Bottom	Top	Bottom	Top	Bottom	Top	Bottom	Top
0.500	0.94	0.46	0.94	0.46	0.94	0.46	0.94	0.46
0.585	1.11	0.54	1.14	0.54	1.14	0.54	1.14	0.54
0.670	1.34	0.60	1.57	0.61	1.56	0.61	1.57	0.61
0.755	1.60	0.66	2.25	0.67	2.24	0.67	2.28	0.66
0.840	1.88	0.71	3.14	0.72	3.51	0.72	3.57	0.72
0.925	2.29	0.73	4.02	0.78	4.77	0.78	4.86	0.78
1.010	2.70	0.75	4.91	0.83	6.35	0.83	7.69	0.89
1.095	3.11	0.77	5.94	0.88	7.58	0.89	7.69	0.89
1.180	3.52	0.79	7.06	0.93	8.80	0.94	8.98	0.94
1.265	3.93	0.81	8.19	0.98	10.03	0.99	10.26	0.99
1.350	4.34	0.83	9.31	1.03	11.26	1.05	11.55	1.05
1.435	4.75	0.85	10.42	1.12	12.48	1.14	12.83	1.15
1.520	5.16	0.87	11.53	1.20	13.69	1.26	14.10	1.27
1.605	5.63	0.88	12.62	1.35	14.88	1.53	15.35	1.52
1.690	6.09	0.89	13.67	1.55	16.05	1.77	16.60	1.78
1.775	6.55	0.90	14.72	1.74	17.12	2.48	17.75	2.54
1.860	7.02	0.91	15.65	2.13	18.14	3.29	18.85	3.39
1.945	7.48	0.92	16.54	2.71	19.16	4.09	19.56	4.20
2.030	7.94	0.93	17.40	3.29	19.78	4.88	20.28	5.02
2.115	8.41	0.94	18.26	3.87	20.37	5.94	20.94	6.17
2.200	8.87	0.95	19.12	4.45	20.91	7.22	21.59	7.45

**TABLE D4.4 - CALCULATED CURVATURES.
 STRAIN HARDENING = 0.01%
 RATIO (CALCULATED CURVATURE)/(YIELD CURVATURE)**

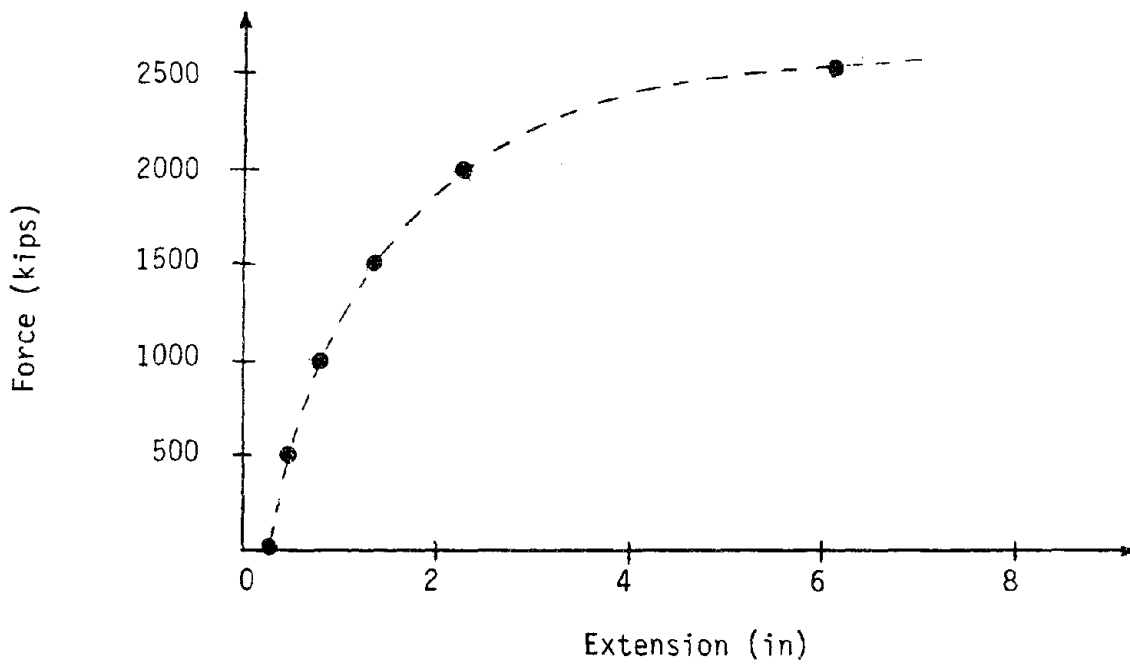
DISPL. (in)	2 SLICES		4 SLICES		7 SLICES		9 SLICES	
	Bottom	Top	Bottom	Top	Bottom	Top	Bottom	Top
0.500	0.94	0.46	0.94	0.46	0.94	0.46	0.94	0.46
0.585	1.11	0.54	1.14	0.54	1.14	0.54	1.14	0.54
0.670	1.34	0.60	1.58	0.61	1.57	0.60	1.59	0.61
0.755	1.61	0.65	2.32	0.67	2.36	0.66	2.46	0.66
0.840	1.90	0.70	3.29	0.72	3.83	0.72	3.95	0.72
0.925	2.33	0.72	4.27	0.77	5.57	0.77	6.39	0.77
1.010	2.76	0.73	5.36	0.82	15.69	0.82	16.69	0.82
1.095	3.20	0.75	19.31	0.86	25.71	0.87	26.71	0.87
1.180	3.63	0.77	33.18	0.89	35.74	0.92	36.74	0.92
1.265	4.07	0.78	47.64	0.93	45.77	0.96	46.77	0.96
1.350	4.50	0.80	60.30	0.96	55.80	1.01	56.80	1.01
1.435	4.94	0.81	74.76	1.00	65.64	1.08	66.63	1.08
1.520	5.39	0.82	88.62	1.03	76.66	1.17	76.66	1.17
1.605	5.89	0.82	102.14	1.09	85.41	1.31	85.97	1.30
1.690	6.39	0.82	115.53	1.16	94.08	1.54	95.13	1.55
1.775	6.89	0.82	128.91	1.22	102.75	1.77	103.92	1.78
1.860	7.39	0.82	140.84	1.39	108.95	2.59	110.05	2.63
1.945	7.89	0.82	152.57	1.56	113.74	3.50	114.95	3.57
2.030	8.39	0.82	164.31	1.73	118.52	4.41	119.85	4.52
2.115	8.89	0.82	173.73	2.05	123.02	5.36	123.99	5.67
2.200	9.39	0.82	178.78	2.64	124.80	7.18	125.77	7.45



(a) PIPE CONFIGURATION

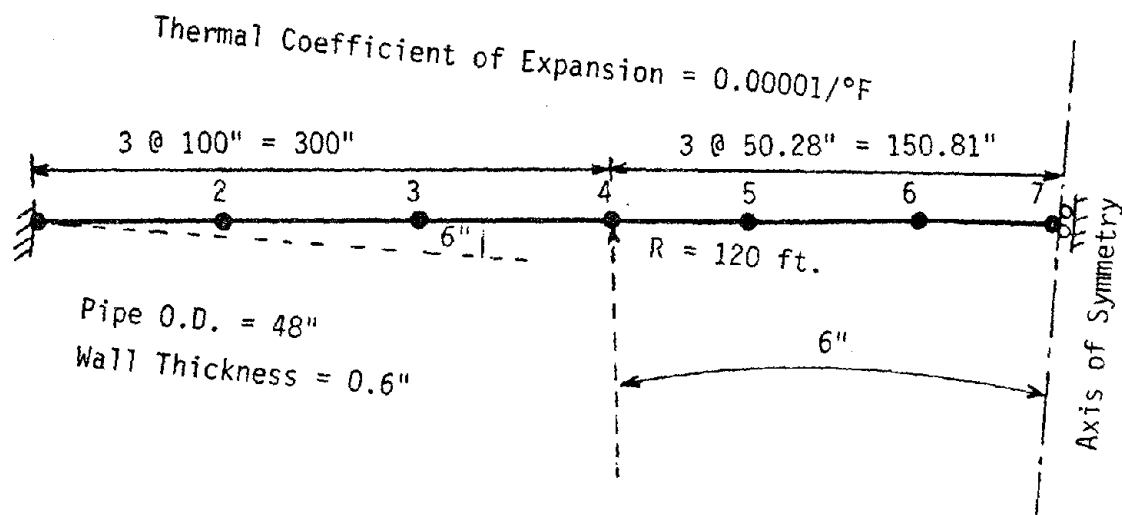


(b) EFFECTIVE STRESS-STRAIN CURVE

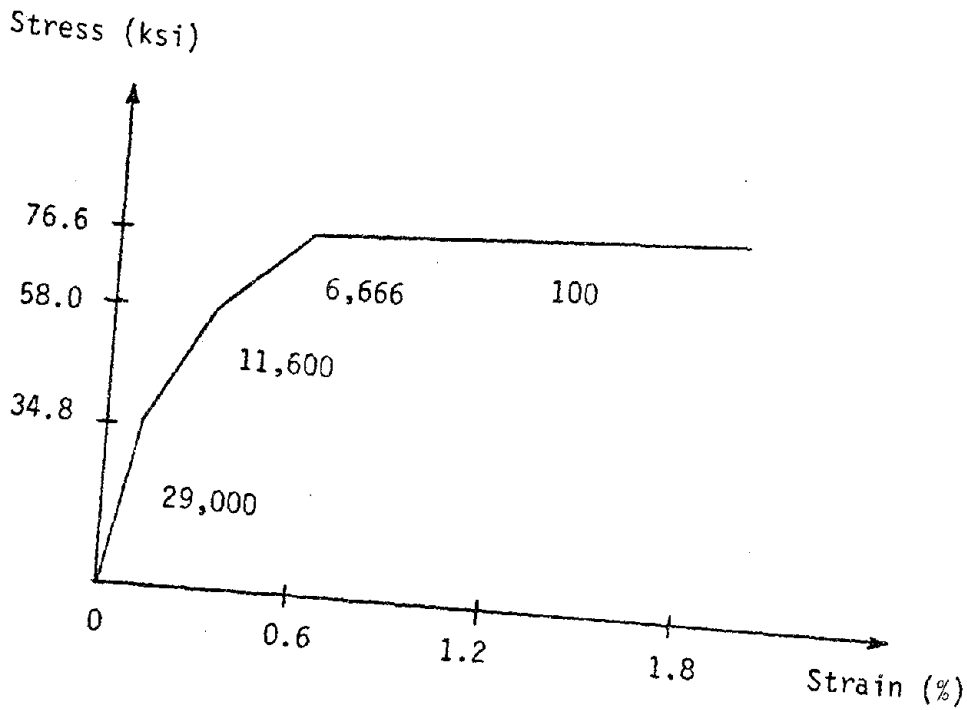


(c) FORCE-EXTENSION CURVE

FIG. D1.1 CANTILEVER PIPE EXAMPLE



(a) ANALYSIS MODEL



(b) MATERIAL STRESS-STRAIN CURVE

FIG. D2.1 PIPE SIDEBEND EXAMPLE

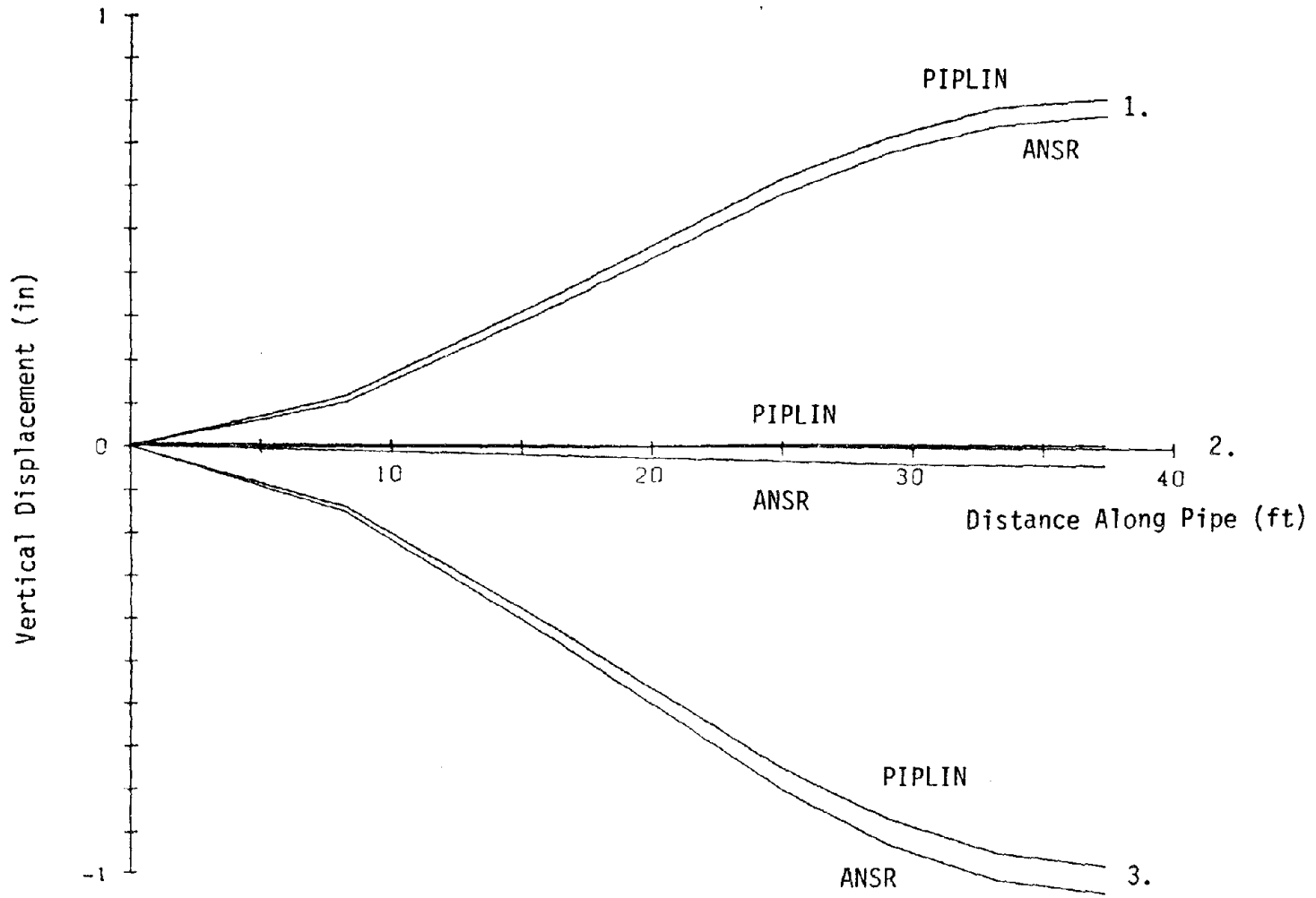


FIG. D2.2 VERTICAL DISPLACEMENT ALONG PIPE

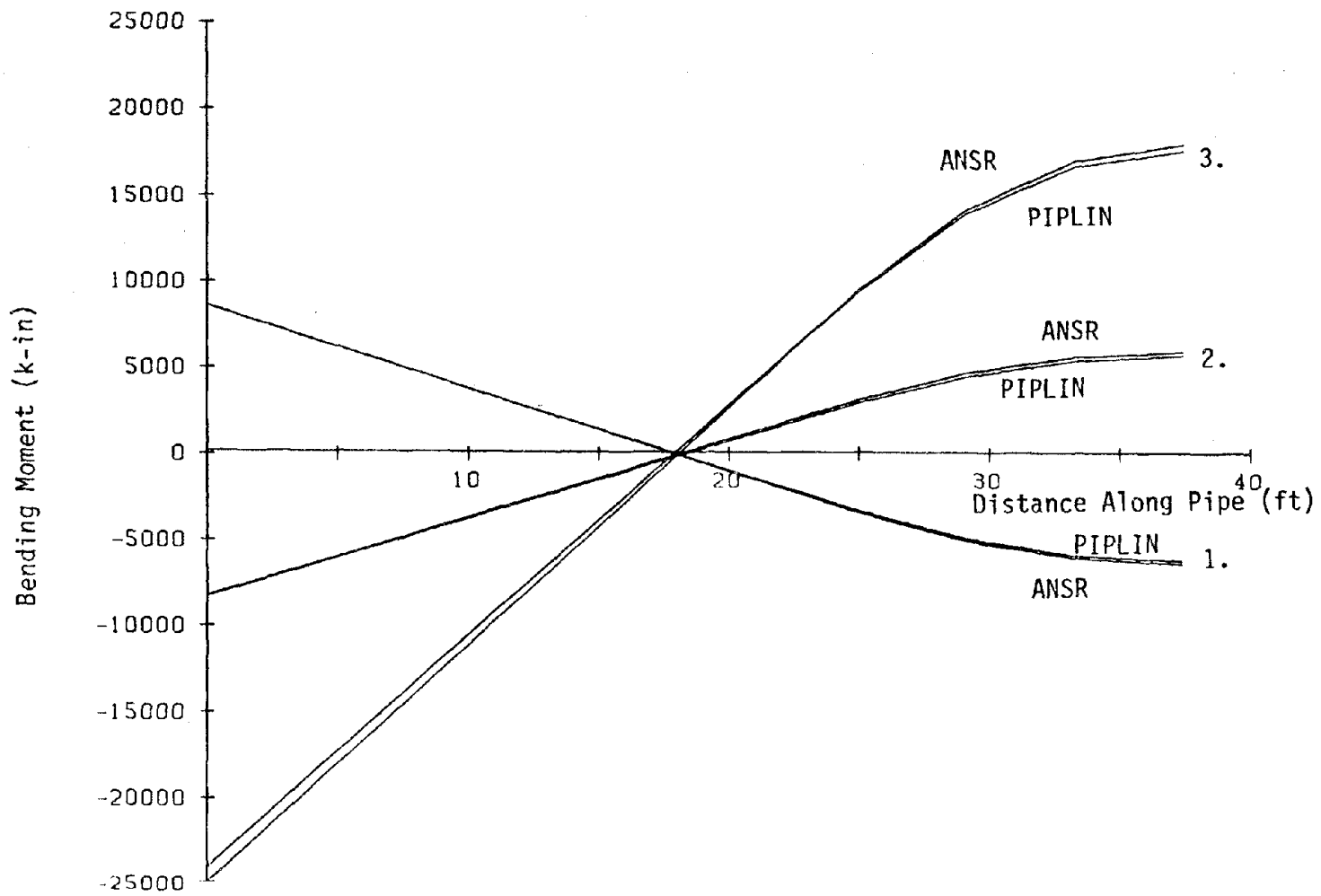


FIG. D2.3 BENDING MOMENT ALONG PIPE

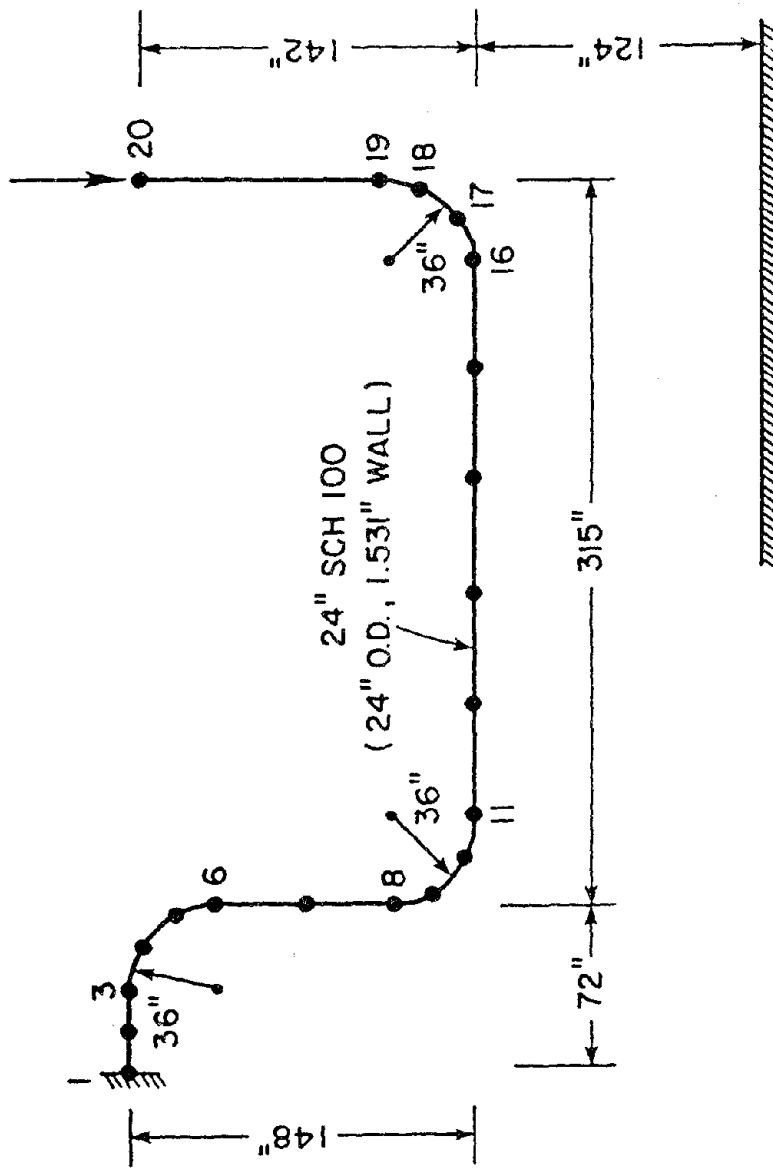


FIG. D3.1 PIPE WHIP WITH LARGE DISPLACEMENTS

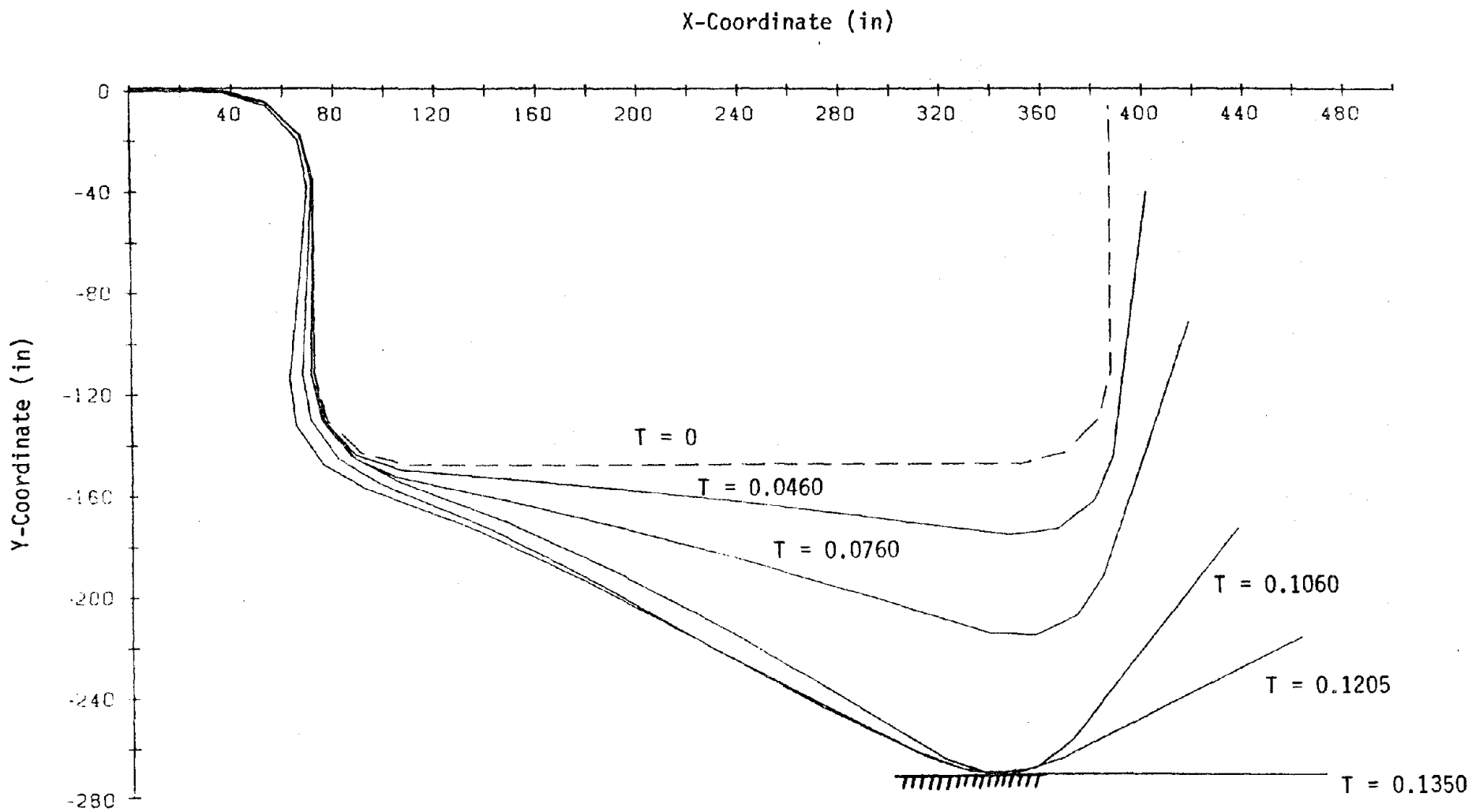
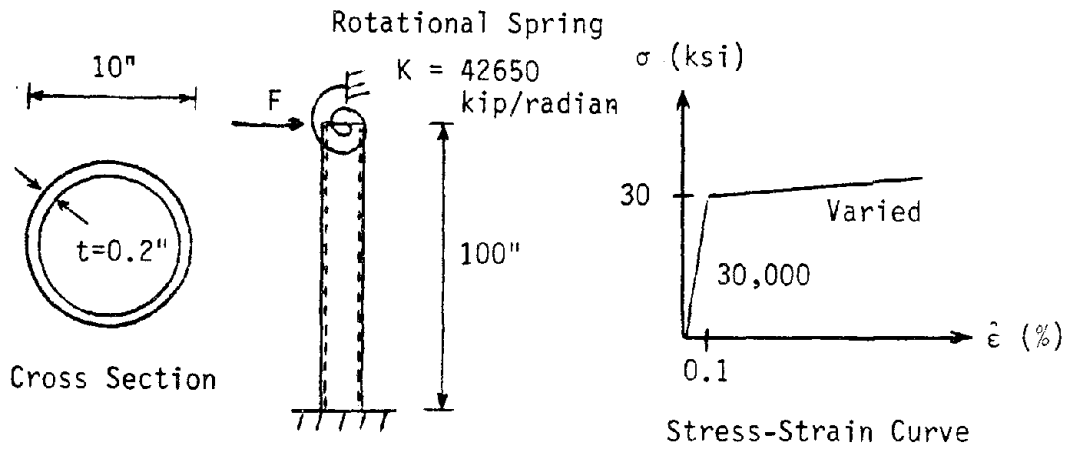
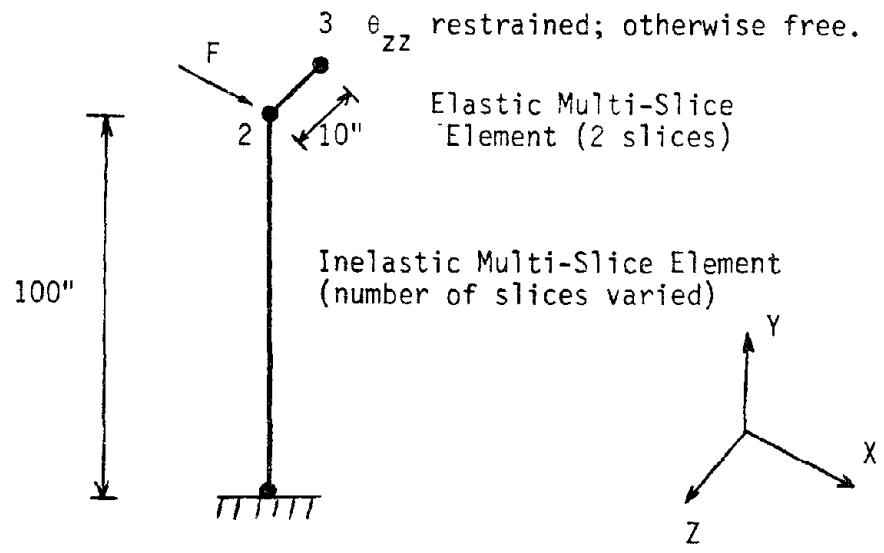


FIG. D3.2 LARGE DISPLACEMENT PIPE WHIP EXAMPLE



(a) STRUCTURAL CONFIGURATION



(b) ANALYSIS MODEL

FIG. D4.1 INELASTIC BEAM-COLUMN EXAMPLE

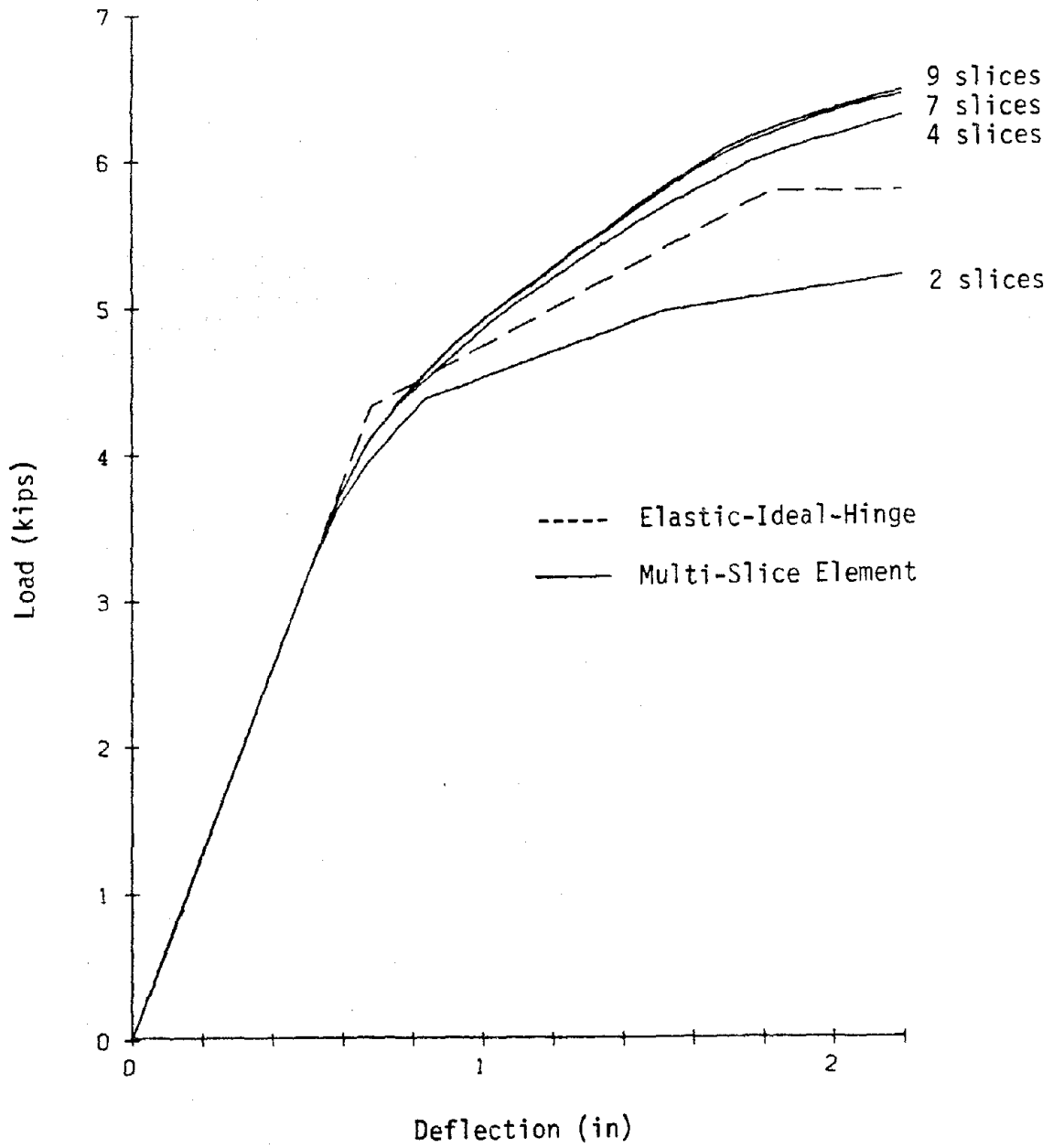


FIG. D4.2 LOAD-DEFLECTION CURVES; 1% STRAIN HARDENING

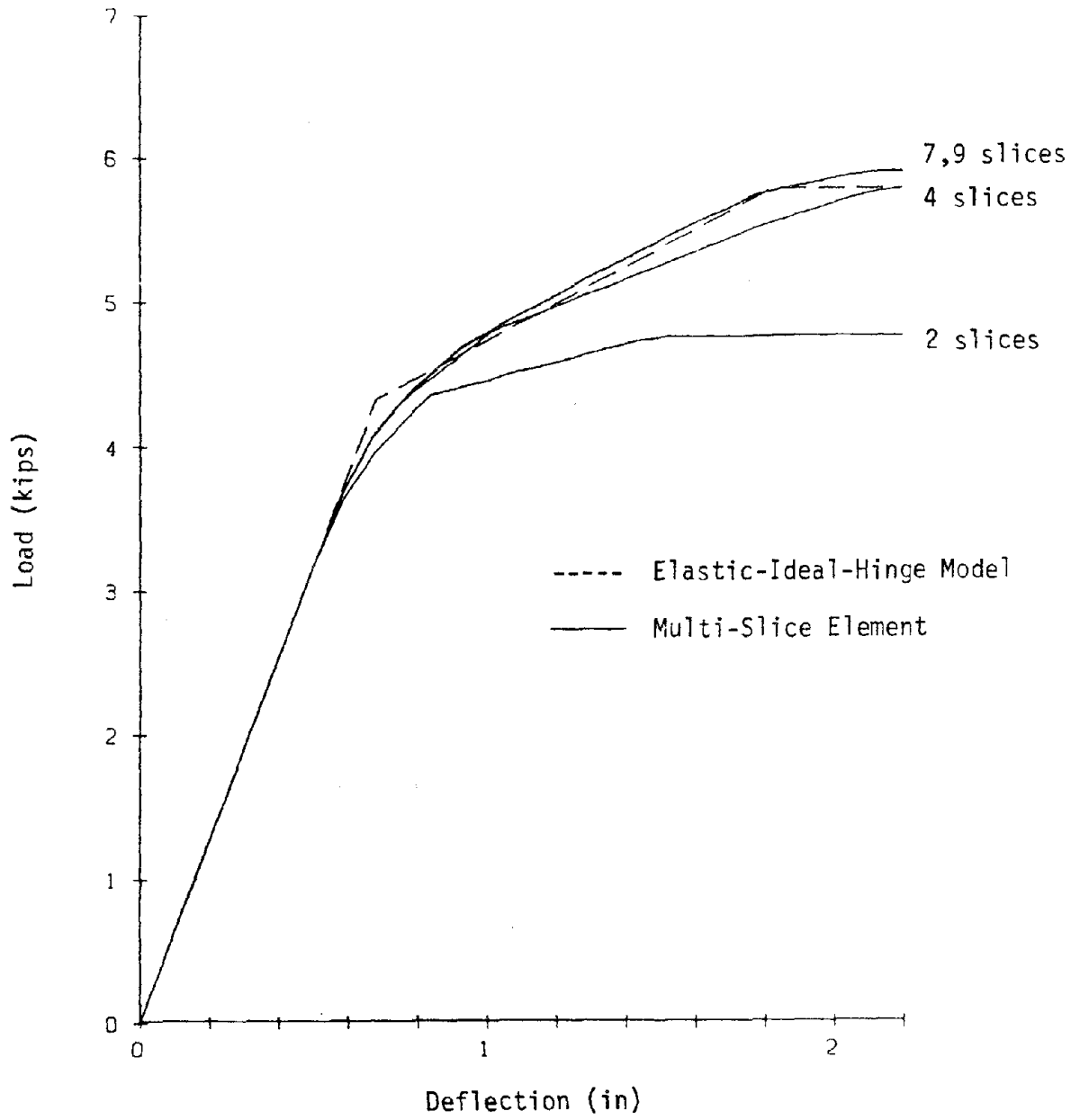


FIG. D4.3 LOAD-DEFLECTION CURVES; 0.01% STRAIN HARDENING



EARTHQUAKE ENGINEERING RESEARCH CENTER REPORTS

NOTE: Numbers in parentheses are Accession Numbers assigned by the National Technical Information Service; these are followed by a price code. Copies of the reports may be ordered from the National Technical Information Service, 5285 Port Royal Road, Springfield, Virginia, 22161. Accession Numbers should be quoted on orders for reports (PB --- ---) and remittance must accompany each order. Reports without this information were not available at time of printing. The complete list of EERC reports (from EERC 67-1) is available upon request from the Earthquake Engineering Research Center, University of California, Berkeley, 47th Street and Hoffman Boulevard, Richmond, California 94804.

- UCB/EERC-77/01 "PLUSH - A Computer Program for Probabilistic Finite Element Analysis of Seismic Soil-Structure Interaction," by M.P. Romo Organista, J. Lysmer and H.B. Seed - 1977 (PB81 177 651)A05
- UCB/EERC-77/02 "Soil-Structure Interaction Effects at the Humboldt Bay Power Plant in the Ferndale Earthquake of June 7, 1975," by J.E. Valera, H.B. Seed, C.F. Tsai and J. Lysmer - 1977 (PB 265 795)A04
- UCB/EERC-77/03 "Influence of Sample Disturbance on Sand Response to Cyclic Loading," by K. Mori, H.B. Seed and C.K. Chan - 1977 (PB 267 352)A04
- UCB/EERC-77/04 "Seismological Studies of Strong Motion Records," by J. Shoja-Taheri - 1977 (PB 269 655)A10
- UCB/EERC-77/05 Unassigned
- UCB/EERC-77/06 "Developing Methodologies for Evaluating the Earthquake Safety of Existing Buildings," by No. 1 - B. Bresler; No. 2 - B. Bresler, T. Okada and D. Zisling; No. 3 - T. Okada and B. Bresler; No. 4 - V.V. Bertero and B. Bresler - 1977 (PB 267 354)A08
- UCB/EERC-77/07 "A Literature Survey - Transverse Strength of Masonry Walls," by Y. Omote, R.L. Mayes, S.W. Chen and R.W. Clough - 1977 (PB 277 933)A07
- UCB/EERC-77/08 "DRAIN-TABS: A Computer Program for Inelastic Earthquake Response of Three Dimensional Buildings," by R. Guendelman-Israel and G.H. Powell - 1977 (PB 270 693)A07
- UCB/EERC-77/09 "SUBWALL: A Special Purpose Finite Element Computer Program for Practical Elastic Analysis and Design of Structural Walls with Substructure Option," by D.Q. Le, H. Peterson and E.P. Popov - 1977 (PB 270 567)A05
- UCB/EERC-77/10 "Experimental Evaluation of Seismic Design Methods for Broad Cylindrical Tanks," by D.P. Clough (PB 272 280)A13
- UCB/EERC-77/11 "Earthquake Engineering Research at Berkeley - 1976," - 1977 (PB 273 507)A09
- UCB/EERC-77/12 "Automated Design of Earthquake Resistant Multistory Steel Building Frames," by N.D. Walker, Jr. - 1977 (PB 276 526)A09
- UCB/EERC-77/13 "Concrete Confined by Rectangular Hoops Subjected to Axial Loads," by J. Vallenias, V.V. Bertero and E.P. Popov - 1977 (PB 275 165)A06
- UCB/EERC-77/14 "Seismic Strain Induced in the Ground During Earthquakes," by Y. Sugimura - 1977 (PB 284 201)A04
- UCB/EERC-77/15 Unassigned
- UCB/EERC-77/16 "Computer Aided Optimum Design of Ductile Reinforced Concrete Moment Resisting Frames," by S.W. Zagajski and V.V. Bertero - 1977 (PB 280 137)A07
- UCB/EERC-77/17 "Earthquake Simulation Testing of a Stepping Frame with Energy-Absorbing Devices," by J.M. Kelly and D.F. Tsztoo - 1977 (PB 273 506)A04
- UCB/EERC-77/18 "Inelastic Behavior of Eccentrically Braced Steel Frames under Cyclic Loadings," by C.W. Roeder and E.P. Popov - 1977 (PB 275 526)A15
- UCB/EERC-77/19 "A Simplified Procedure for Estimating Earthquake-Induced Deformations in Dams and Embankments," by F.I. Makdisi and H.B. Seed - 1977 (PB 276 820)A04
- UCB/EERC-77/20 "The Performance of Earth Dams during Earthquakes," by H.B. Seed, F.I. Makdisi and P. de Alba - 1977 (PB 276 821)A04
- UCB/EERC-77/21 "Dynamic Plastic Analysis Using Stress Resultant Finite Element Formulation," by P. Lukkunapvasit and J.M. Kelly - 1977 (PB 275 453)A04
- UCB/EERC-77/22 "Preliminary Experimental Study of Seismic Uplift of a Steel Frame," by R.W. Clough and A.A. Huckelbridge 1977 (PB 278 769)A08
- UCB/EERC-77/23 "Earthquake Simulator Tests of a Nine-Story Steel Frame with Columns Allowed to Uplift," by A.A. Huckelbridge - 1977 (PB 277 944)A09
- UCB/EERC-77/24 "Nonlinear Soil-Structure Interaction of Skew Highway Bridges," by M.-C. Chen and J. Penzien - 1977 (PB 276 176)A07
- UCB/EERC-77/25 "Seismic Analysis of an Offshore Structure Supported on Pile Foundations," by D.D.-N. Liou and J. Penzien 1977 (PB 283 180)A06
- UCB/EERC-77/26 "Dynamic Stiffness Matrices for Homogeneous Viscoelastic Half-Planes," by G. Dasgupta and A.K. Chopra - 1977 (PB 279 654)A06

UCB/EERC-77/27 "A Practical Soft Story Earthquake Isolation System," by J.M. Kelly, J.M. Eidingger and C.J. Derham - 1977 (PB 276 814)A07

UCB/EERC-77/28 "Seismic Safety of Existing Buildings and Incentives for Hazard Mitigation in San Francisco: An Exploratory Study," by A.J. Meltsner - 1977 (PB 281 970)A05

UCB/EERC-77/29 "Dynamic Analysis of Electrohydraulic Shaking Tables," by D. Rea, S. Abedi-Hayati and Y. Takahashi 1977 (PB 282 569)A04

UCB/EERC-77/30 "An Approach for Improving Seismic - Resistant Behavior of Reinforced Concrete Interior Joints," by B. Galunic, V.V. Bertero and E.P. Popov - 1977 (PB 290 870)A06

UCB/EERC-78/01 "The Development of Energy-Absorbing Devices for Aseismic Base Isolation Systems," by J.M. Kelly and D.F. Tsztoo - 1978 (PB 284 978)A04

UCB/EERC-78/02 "Effect of Tensile Prestrain on the Cyclic Response of Structural Steel Connections," by J.G. Bouwkamp and A. Mukhopadhyay - 1978

UCB/EERC-78/03 "Experimental Results of an Earthquake Isolation System using Natural Rubber Bearings," by J.M. Eidingger and J.M. Kelly - 1978 (PB 281 686)A04

UCB/EERC-78/04 "Seismic Behavior of Tall Liquid Storage Tanks," by A. Niwa - 1978 (PB 284 017)A14

UCB/EERC-78/05 "Hysteretic Behavior of Reinforced Concrete Columns Subjected to High Axial and Cyclic Shear Forces," by S.W. Zagajeski, V.V. Bertero and J.G. Bouwkamp - 1978 (PB 283 858)A13

UCB/EERC-78/06 "Three Dimensional Inelastic Frame Elements for the ANSR-I Program," by A. Riahi, D.G. Row and G.H. Powell - 1978 (PB 295 755)A04

UCB/EERC-78/07 "Studies of Structural Response to Earthquake Ground Motion," by O.A. Lopez and A.K. Chopra - 1978 (PB 282 790)A05

UCB/EERC-78/08 "A Laboratory Study of the Fluid-Structure Interaction of Submerged Tanks and Caissons in Earthquakes," by R.C. Byrd - 1978 (PB 284 957)A08

UCB/EERC-78/09 Unassigned

UCB/EERC-78/10 "Seismic Performance of Nonstructural and Secondary Structural Elements," by I. Sakamoto - 1978 (PB81 154 593)A05

UCB/EERC-78/11 "Mathematical Modelling of Hysteresis Loops for Reinforced Concrete Columns," by S. Nakata, T. Sproul and J. Penzien - 1978 (PB 298 274)A05

UCB/EERC-78/12 "Damageability in Existing Buildings," by T. Blejwas and B. Bresler - 1978 (PB 80 166 978)A05

UCB/EERC-78/13 "Dynamic Behavior of a Pedestal Base Multistory Building," by R.M. Stephen, E.L. Wilson, J.G. Bouwkamp and M. Butten - 1978 (PB 286 650)A08

UCB/EERC-78/14 "Seismic Response of Bridges - Case Studies," by R.A. Imbsen, V. Nutt and J. Penzien - 1978 (PB 286 503)A10

UCB/EERC-78/15 "A Substructure Technique for Nonlinear Static and Dynamic Analysis," by D.G. Row and G.H. Powell - 1978 (PB 288 077)A10

UCB/EERC-78/16 "Seismic Risk Studies for San Francisco and for the Greater San Francisco Bay Area," by C.S. Oliveira - 1978 (PB 81 120 115)A07

UCB/EERC-78/17 "Strength of Timber Roof Connections Subjected to Cyclic Loads," by P. Gülkan, R.L. Mayes and R.W. Clough - 1978 (HUD-000 1491)A07

UCB/EERC-78/18 "Response of K-Braced Steel Frame Models to Lateral Loads," by J.G. Bouwkamp, R.M. Stephen and E.P. Popov - 1978

UCB/EERC-78/19 "Rational Design Methods for Light Equipment in Structures Subjected to Ground Motion," by J.L. Sackman and J.M. Kelly - 1978 (PB 292 357)A04

UCB/EERC-78/20 "Testing of a Wind Restraint for Aseismic Base Isolation," by J.M. Kelly and D.E. Chitty - 1978 (PB 292 833)A03

UCB/EERC-78/21 "APOLLO - A Computer Program for the Analysis of Pore Pressure Generation and Dissipation in Horizontal Sand Layers During Cyclic or Earthquake Loading," by P.P. Martin and H.B. Seed - 1978 (PB 292 835)A04

UCB/EERC-78/22 "Optimal Design of an Earthquake Isolation System," by M.A. Bhatti, K.S. Pister and E. Polak - 1978 (PB 294 735)A06

UCB/EERC-78/23 "MASH - A Computer Program for the Non-Linear Analysis of Vertically Propagating Shear Waves in Horizontally Layered Deposits," by P.P. Martin and H.B. Seed - 1978 (PB 293 101)A05

UCB/EERC-78/24 "Investigation of the Elastic Characteristics of a Three Story Steel Frame Using System Identification," by I. Kaya and H.D. McNiven - 1978 (PB 296 225)A06

UCB/EERC-78/25 "Investigation of the Nonlinear Characteristics of a Three-Story Steel Frame Using System Identification," by I. Kaya and H.D. McNiven - 1978 (PB 301 363)A05

- UCB/EERC-78/26 "Studies of Strong Ground Motion in Taiwan," by Y.M. Hsiung, B.A. Bolt and J. Penzien - 1978 (PB 298 436)A06
- UCB/EERC-78/27 "Cyclic Loading Tests of Masonry Single Piers: Volume 1 - Height to Width Ratio of 2," by P.A. Hidalgo, R.L. Mayes, H.D. McNiven and R.W. Clough - 1978 (PB 296 211)A07
- UCB/EERC-78/28 "Cyclic Loading Tests of Masonry Single Piers: Volume 2 - Height to Width Ratio of 1," by S.-W.J. Chen, P.A. Hidalgo, R.L. Mayes, R.W. Clough and H.D. McNiven - 1978 (PB 296 212)A09
- UCB/EERC-78/29 "Analytical Procedures in Soil Dynamics," by J. Lysmer - 1978 (PB 298 445)A06
- UCB/EERC-79/01 "Hysteretic Behavior of Lightweight Reinforced Concrete Beam-Column Subassemblages," by B. Forzani, E.P. Popov and V.V. Bertero - April 1979(PB 298 267)A06
- UCB/EERC-79/02 "The Development of a Mathematical Model to Predict the Flexural Response of Reinforced Concrete Beams to Cyclic Loads, Using System Identification," by J. Stanton & H. McNiven - Jan. 1979(PB 295 875)A10
- UCB/EERC-79/03 "Linear and Nonlinear Earthquake Response of Simple Torsionally Coupled Systems," by C.L. Kan and A.K. Chopra - Feb. 1979(PB 298 262)A06
- UCB/EERC-79/04 "A Mathematical Model of Masonry for Predicting its Linear Seismic Response Characteristics," by Y. Mengi and H.D. McNiven - Feb. 1979(PB 298 266)A06
- UCB/EERC-79/05 "Mechanical Behavior of Lightweight Concrete Confined by Different Types of Lateral Reinforcement," by M.A. Manrique, V.V. Bertero and E.P. Popov - May 1979(PB 301 114)A06
- UCB/EERC-79/06 "Static Tilt Tests of a Tall Cylindrical Liquid Storage Tank," by R.W. Clough and A. Niwa - Feb. 1979 (PB 301 167)A06
- UCB/EERC-79/07 "The Design of Steel Energy Absorbing Restrainers and Their Incorporation into Nuclear Power Plants for Enhanced Safety: Volume 1 - Summary Report," by P.N. Spencer, V.P. Zackay, and E.R. Parker - Feb. 1979(UCB/EERC-79/07)A09
- UCB/EERC-79/08 "The Design of Steel Energy Absorbing Restrainers and Their Incorporation into Nuclear Power Plants for Enhanced Safety: Volume 2 - The Development of Analyses for Reactor System Piping," "Simple Systems" by M.C. Lee, J. Penzien, A.K. Chopra and K. Suzuki "Complex Systems" by G.H. Powell, E.L. Wilson, R.W. Clough and D.G. Row - Feb. 1979(UCB/EERC-79/08)A10
- UCB/EERC-79/09 "The Design of Steel Energy Absorbing Restrainers and Their Incorporation into Nuclear Power Plants for Enhanced Safety: Volume 3 - Evaluation of Commercial Steels," by W.S. Owen, R.M.N. Pelloux, R.O. Ritchie, M. Faral, T. Ohnashi, J. Toplosky, S.J. Hartman, V.F. Zackay and E.R. Parker - Feb. 1979(UCB/EERC-79/09)A04
- UCB/EERC-79/10 "The Design of Steel Energy Absorbing Restrainers and Their Incorporation into Nuclear Power Plants for Enhanced Safety: Volume 4 - A Review of Energy-Absorbing Devices," by J.M. Kelly and M.S. Skinner - Feb. 1979(UCB/EERC-79/10)A04
- UCB/EERC-79/11 "Conservatism In Summation Rules for Closely Spaced Modes," by J.M. Kelly and J.L. Sackman - May 1979(PB 301 328)A03
- UCB/EERC-79/12 "Cyclic Loading Tests of Masonry Single Piers: Volume 3 - Height to Width Ratio of 0.5," by P.A. Hidalgo, R.L. Mayes, H.D. McNiven and R.W. Clough - May 1979(PB 301 321)A08
- UCB/EERC-79/13 "Cyclic Behavior of Dense Course-Grained Materials in Relation to the Seismic Stability of Dams," by N.G. Banerjee, H.B. Seed and C.K. Chan - June 1979(PB 301 373)A13
- UCB/EERC-79/14 "Seismic Behavior of Reinforced Concrete Interior Beam-Column Subassemblages," by S. Viathanatepa, E.P. Popov and V.V. Bertero - June 1979(PB 301 326)A10
- UCB/EERC-79/15 "Optimal Design of Localized Nonlinear Systems with Dual Performance Criteria Under Earthquake Excitations," by M.A. Bhatti - July 1979(PB 80 167 109)A06
- UCB/EERC-79/16 "OPTDYN - A General Purpose Optimization Program for Problems with or without Dynamic Constraints," by M.A. Bhatti, E. Polak and K.S. Pister - July 1979(PB 80 167 091)A05
- UCB/EERC-79/17 "ANSR-II, Analysis of Nonlinear Structural Response, Users Manual," by D.P. Mondkar and G.H. Powell July 1979(PB 80 113 301)A05
- UCB/EERC-79/18 "Soil Structure Interaction in Different Seismic Environments," A. Gomez-Masso, J. Lysmer, J.-C. Chen and H.B. Seed - August 1979(PB 80 101 520)A04
- UCB/EERC-79/19 "ARMA Models for Earthquake Ground Motions," by M.K. Chang, J.W. Kwiatkowski, R.F. Nau, R.M. Oliver and K.S. Pister - July 1979(PB 301 166)A05
- UCB/EERC-79/20 "Hysteretic Behavior of Reinforced Concrete Structural Walls," by J.M. Vallenias, V.V. Bertero and E.P. Popov - August 1979(PB 80 165 905)A12
- UCB/EERC-79/21 "Studies on High-Frequency Vibrations of Buildings - 1: The Column Effect," by J. Lubliner - August 1979 (PB 80 158 553)A03
- UCB/EERC-79/22 "Effects of Generalized Loadings on Bond Reinforcing Bars Embedded in Confined Concrete Blocks," by S. Viathanatepa, E.P. Popov and V.V. Bertero - August 1979(PB 81 124 018)A14
- UCB/EERC-79/23 "Shaking Table Study of Single-Story Masonry Houses, Volume 1: Test Structures 1 and 2," by P. Gülkan, R.L. Mayes and R.W. Clough - Sept. 1979 (HUD-000 1763)A12
- UCB/EERC-79/24 "Shaking Table Study of Single-Story Masonry Houses, Volume 2: Test Structures 3 and 4," by P. Gülkan, R.L. Mayes and R.W. Clough - Sept. 1979 (HUD-000 1836)A12
- UCB/EERC-79/25 "Shaking Table Study of Single-Story Masonry Houses, Volume 3: Summary, Conclusions and Recommendations," by R.W. Clough, R.L. Mayes and P. Gülkan - Sept. 1979 (HUD-000 1837)A06

- UCB/EERC-79/26 "Recommendations for a U.S.-Japan Cooperative Research Program Utilizing Large-Scale Testing Facilities," by U.S.-Japan Planning Group - Sept. 1979(PB 301 407)A06
- UCB/EERC-79/27 "Earthquake-Induced Liquefaction Near Lake Amatitlan, Guatemala," by H.B. Seed, I. Arango, C.K. Chan, A. Gomez-Masso and R. Grant de Ascoli - Sept. 1979(NUREG-CR1341)A03
- UCB/EERC-79/28 "Infill Panels: Their Influence on Seismic Response of Buildings," by J.W. Axley and V.V. Bertero Sept. 1979(PB 80 163 371)A10
- UCB/EERC-79/29 "3D Truss Bar Element (Type 1) for the ANSR-II Program," by D.P. Mondkar and G.H. Powell - Nov. 1979 (PB 80 169 709)A02
- UCB/EERC-79/30 "2D Beam-Column Element (Type 5 - Parallel Element Theory) for the ANSR-II Program," by D.G. Row, G.R. Powell and D.P. Mondkar - Dec. 1979(PB 80 167 224)A03
- UCB/EERC-79/31 "3D Beam-Column Element (Type 2 - Parallel Element Theory) for the ANSR-II Program," by A. Riahi, G.H. Powell and D.P. Mondkar - Dec. 1979(PB 80 167 216)A03
- UCB/EERC-79/32 "On Response of Structures to Stationary Excitation," by A. Der Kiureghian - Dec. 1979(PB 80166 929)A03
- UCB/EERC-79/33 "Undisturbed Sampling and Cyclic Load Testing of Sands," by S. Singh, H.B. Seed and C.K. Chan Dec. 1979(ADA 087 298)A07
- UCB/EERC-79/34 "Interaction Effects of Simultaneous Torsional and Compressional Cyclic Loading of Sand," by P.M. Griffin and W.N. Houston - Dec. 1979(ADA 092 352)A15
- UCB/EERC-80/01 "Earthquake Response of Concrete Gravity Dams Including Hydrodynamic and Foundation Interaction Effects," by A.K. Chopra, P. Chakrabarti and S. Gupta - Jan. 1980(AD-A087297)A10
- UCB/EERC-80/02 "Rocking Response of Rigid Blocks to Earthquakes," by C.S. Yim, A.K. Chopra and J. Penzien - Jan. 1980 (PB80 166 002)A04
- UCB/EERC-80/03 "Optimum Inelastic Design of Seismic-Resistant Reinforced Concrete Frame Structures," by S.W. Zagajeski and V.V. Bertero - Jan. 1980(PB80 164 635)A06
- UCB/EERC-80/04 "Effects of Amount and Arrangement of Wall-Panel Reinforcement on Hysteretic Behavior of Reinforced Concrete Walls," by R. Iliya and V.V. Bertero - Feb. 1980(PB81 122 525)A09
- UCB/EERC-80/05 "Shaking Table Research on Concrete Dam Models," by A. Niwa and R.W. Clough - Sept. 1980(PB81 122 368)A06
- UCB/EERC-80/06 "The Design of Steel Energy-Absorbing Restrainers and their Incorporation into Nuclear Power Plants for Enhanced Safety (Vol 1A): Piping with Energy Absorbing Restrainers: Parameter Study on Small Systems," by G.H. Powell, C. Goughourlian and J. Simons - June 1980
- UCB/EERC-80/07 "Inelastic Torsional Response of Structures Subjected to Earthquake Ground Motions," by Y. Yamazaki April 1980(PB81 122 327)A08
- UCB/EERC-80/08 "Study of X-Braced Steel Frame Structures Under Earthquake Simulation," by Y. Ghanaat - April 1980 (PB81 122 335)A11
- UCB/EERC-80/09 "Hybrid Modelling of Soil-Structure Interaction," by S. Gupta, T.W. Lin, J. Penzien and C.S. Yeh May 1980(PB81 122 319)A07
- UCB/EERC-80/10 "General Applicability of a Nonlinear Model of a One Story Steel Frame," by B.I. Sveinsson and H.D. McNiven - May 1980(PB81 124 877)A06
- UCB/EERC-80/11 "A Green-Function Method for Wave Interaction with a Submerged Body," by W. Kioka - April 1980 (PB81 122 269)A07
- UCB/EERC-80/12 "Hydrodynamic Pressure and Added Mass for Axisymmetric Bodies," by F. Nilrat - May 1980(PB81 122 343)A08
- UCB/EERC-80/13 "Treatment of Non-Linear Drag Forces Acting on Offshore Platforms," by B.V. Dao and J. Penzien May 1980(PB81 153 413)A07
- UCB/EERC-80/14 "2D Plane/Axisymmetric Solid Element (Type 3 - Elastic or Elastic-Perfectly Plastic) for the ANSR-II Program," by D.P. Mondkar and G.H. Powell - July 1980(PB81 122 350)A03
- UCB/EERC-80/15 "A Response Spectrum Method for Random Vibrations," by A. Der Kiureghian - June 1980(PB81 122 301)A03
- UCB/EERC-80/16 "Cyclic Inelastic Buckling of Tubular Steel Braces," by V.A. Zayas, E.P. Popov and S.A. Mahin June 1980(PB81 124 885)A10
- UCB/EERC-80/17 "Dynamic Response of Simple Arch Dams Including Hydrodynamic Interaction," by C.S. Porter and A.K. Chopra - July 1980(PB81 124 000)A13
- UCB/EERC-80/18 "Experimental Testing of a Friction Damped Aseismic Base Isolation System with Fail-Safe Characteristics," by J.M. Kelly, K.E. Beucke and M.S. Skinner - July 1980(PB81 148 595)A04
- UCB/EERC-80/19 "The Design of Steel Energy-Absorbing Restrainers and their Incorporation into Nuclear Power Plants for Enhanced Safety (Vol 1B): Stochastic Seismic Analyses of Nuclear Power Plant Structures and Piping Systems Subjected to Multiple Support Excitations," by M.C. Lee and J. Penzien - June 1980
- UCB/EERC-80/20 "The Design of Steel Energy-Absorbing Restrainers and their Incorporation into Nuclear Power Plants for Enhanced Safety (Vol 1C): Numerical Method for Dynamic Substructure Analysis," by J.M. Dickens and E.L. Wilson - June 1980
- UCB/EERC-80/21 "The Design of Steel Energy-Absorbing Restrainers and their Incorporation into Nuclear Power Plants for Enhanced Safety (Vol 2): Development and Testing of Restraints for Nuclear Piping Systems," by J.M. Kelly and M.S. Skinner - June 1980
- UCB/EERC-80/22 "3D Solid Element (Type 4-Elastic or Elastic-Perfectly-Plastic) for the ANSR-II Program," by D.P. Mondkar and G.H. Powell - July 1980(PB81 123 242)A03
- UCB/EERC-80/23 "Gap-Friction Element (Type 5) for the ANSR-II Program," by D.P. Mondkar and G.H. Powell - July 1980 (PB81 122 285)A03

UCB/EERC-80/24 "U-Bar Restraint Element (Type 11) for the ANSR-II Program," by C. Oughourlian and G.H. Powell July 1980(PB81 122 293)A03

UCB/EERC-80/25 "Testing of a Natural Rubber Base Isolation System by an Explosively Simulated Earthquake," by J.M. Kelly - August 1980(PB81 201 360)A04

UCB/EERC-80/26 "Input Identification from Structural Vibrational Response," by Y. Hu - August 1980(PB81 152 308)A05

UCB/EERC-80/27 "Cyclic Inelastic Behavior of Steel Offshore Structures," by V.A. Zayas, S.A. Mahin and E.P. Popov August 1980(PB81 196 180)A15

UCB/EERC-80/28 "Shaking Table Testing of a Reinforced Concrete Frame with Biaxial Response," by M.G. Oliva October 1980(PB81 154 304)A10

UCB/EERC-80/29 "Dynamic Properties of a Twelve-Story Prefabricated Panel Building," by J.G. Bouwkamp, J.P. Kollegger and R.M. Stephen - October 1980(PB82 117 128)A06

UCB/EERC-80/30 "Dynamic Properties of an Eight-Story Prefabricated Panel Building," by J.G. Bouwkamp, J.P. Kollegger and R.M. Stephen - October 1980(PB81 200 313)A05

UCB/EERC-80/31 "Predictive Dynamic Response of Panel Type Structures Under Earthquakes," by J.P. Kollegger and J.G. Bouwkamp - October 1980(PB81 152 316)A04

UCB/EERC-80/32 "The Design of Steel Energy-Absorbing Restrainers and their Incorporation into Nuclear Power Plants for Enhanced Safety (Vol 3): Testing of Commercial Steels in Low-Cycle Torsional Fatigue," by P. Spencer, E.R. Parker, E. Jongewaard and M. Drory

UCB/EERC-80/33 "The Design of Steel Energy-Absorbing Restrainers and their Incorporation into Nuclear Power Plants For Enhanced Safety (Vol 4): Shaking Table Tests of Piping Systems with Energy-Absorbing Restrainers," by S.F. Stiemer and W.S. Godden - Sept. 1980

UCB/EERC-80/34 "The Design of Steel Energy-Absorbing Restrainers and their Incorporation into Nuclear Power Plants for Enhanced Safety (Vol 5): Summary Report," by P. Spencer

UCB/EERC-80/35 "Experimental Testing of an Energy-Absorbing Base Isolation System," by J.M. Kelly, M.S. Skinner and K.E. Beucke - October 1980(PB81 154 372)A04

UCB/EERC-80/36 "Simulating and Analyzing Artificial Non-Stationary Earthquake Ground Motions," by R.F. Nau, R.M. Oliver and K.S. Pister - October 1980(PB81 153 397)A04

UCB/EERC-80/37 "Earthquake Engineering at Berkeley - 1980," - Sept. 1980(PB81 205 374)A09

UCB/EERC-80/38 "Inelastic Seismic Analysis of Large Panel Buildings," by V. Schrieker and G.H. Powell - Sept. 1980 (PB81 154 338)A13

UCB/EERC-80/39 "Dynamic Response of Embankment, Concrete-Gravity and Arch Dams Including Hydrodynamic Interaction," by J.F. Hall and A.K. Chopra - October 1980(PB81 152 324)A11

UCB/EERC-80/40 "Inelastic Buckling of Steel Struts Under Cyclic Load Reversal," by R.G. Black, W.A. Wenger and E.P. Popov - October 1980(PB81 154 312)A08

UCB/EERC-80/41 "Influence of Site Characteristics on Building Damage During the October 3, 1974 Lima Earthquake," by P. Repetto, I. Arango and H.B. Seed - Sept. 1980(PB81 161 739)A05

UCB/EERC-80/42 "Evaluation of a Shaking Table Test Program on Response Behavior of a Two Story Reinforced Concrete Frame," by J.M. Blondet, R.W. Clough and S.A. Mahin

UCB/EERC-80/43 "Modelling of Soil-Structure Interaction by Finite and Infinite Elements," by F. Medina - December 1980(PB81 229 270)A04

UCB/EERC-81/01 "Control of Seismic Response of Piping Systems and Other Structures by Base Isolation," edited by J.M. Kelly - January 1981 (PB81 200 735)A05

UCB/EERC-81/02 "OPTNSR - An Interactive Software System for Optimal Design of Statically and Dynamically Loaded Structures with Nonlinear Response," by M.A. Bhatti, V. Ciampi and K.S. Pister - January 1981 (PB81 218 851)A09

UCB/EERC-81/03 "Analysis of Local Variations in Free Field Seismic Ground Motions," by J.-C. Chen, J. Lysmer and H.B. Seed - January 1981 (AD-A099508)A13

UCB/EERC-81/04 "Inelastic Structural Modeling of Braced Offshore Platforms for Seismic Loading," by V.A. Zayas, P.-S.B. Shing, S.A. Mahin and E.P. Popov - January 1981(PB82 138 777)A07

UCB/EERC-81/05 "Dynamic Response of Light Equipment in Structures," by A. Der Kiureghian, J.L. Sackman and B. Nour-Omid - April 1981 (PB81 218 497)A04

UCB/EERC-81/06 "Preliminary Experimental Investigation of a Broad Base Liquid Storage Tank," by J.G. Bouwkamp, J.P. Kollegger and R.M. Stephen - May 1981(PB82 140 385)A03

UCB/EERC-81/07 "The Seismic Resistant Design of Reinforced Concrete Coupled Structural Walls," by A.E. Aktan and V.V. Bertero - June 1981(PB82 113 358)A11

UCB/EERC-81/08 "The Undrained Shearing Resistance of Cohesive Soils at Large Deformations," by M.R. Pyles and H.B. Seed - August 1981

UCB/EERC-81/09 "Experimental Behavior of a Spatial Piping System with Steel Energy Absorbers Subjected to a Simulated Differential Seismic Input," by S.F. Stiemer, W.G. Godden and J.M. Kelly - July 1981

- UCB/EERC-81/10 "Evaluation of Seismic Design Provisions for Masonry in the United States," by B.I. Sveinsson, R.L. Mayes and H.D. McNiven - August 1981
- UCB/EERC-81/11 "Two-Dimensional Hybrid Modelling of Soil-Structure Interaction," by T.-J. Tzong, S. Gupta and J. Penzien - August 1981 (PB82 142 118)A04
- UCB/EERC-81/12 "Studies on Effects of Infills in Seismic Resistant R/C Construction," by S. Brokken and V.V. Bertero - September 1981
- UCB/EERC-81/13 "Linear Models to Predict the Nonlinear Seismic Behavior of a One-Story Steel Frame," by H. Valdimarsson, A.H. Shah and H.D. McNiven - September 1981 (PB82 138 793)A07
- UCB/EERC-81/14 "TLUSH: A Computer Program for the Three-Dimensional Dynamic Analysis of Earth Dams," by T. Kagawa, L.H. Mejia, H.B. Seed and J. Lysmer - September 1981 (PB82 139 940)A06
- UCB/EERC-81/15 "Three Dimensional Dynamic Response Analysis of Earth Dams," by L.H. Mejia and H.B. Seed - September 1981 (PB82 137 274)A12
- UCB/EERC-81/16 "Experimental Study of Lead and Elastomeric Dampers for Base Isolation Systems," by J.M. Kelly and S.B. Hodder - October 1981 (PB82 166 182)A05
- UCB/EERC-81/17 "The Influence of Base Isolation on the Seismic Response of Light Secondary Equipment," by J.M. Kelly - April 1981 (PB82 255 266)A04
- UCB/EERC-81/18 "Studies on Evaluation of Shaking Table Response Analysis Procedures," by J. Marcial Blondet - November 1981 (PB82 197 278)A10
- UCB/EERC-81/19 "DELIGHT.STRUCT: A Computer-Aided Design Environment for Structural Engineering," by R.J. Balling, K.S. Pister and E. Polak - December 1981 (PB82 218 496)A07
- UCB/EERC-81/20 "Optimal Design of Seismic-Resistant Planar Steel Frames," by R.J. Balling, V. Ciampi, K.S. Pister and E. Polak - December 1981 (PB82 220 179)A07
- UCB/EERC-82/01 "Dynamic Behavior of Ground for Seismic Analysis of Lifeline Systems," by T. Sato and A. Der Kiureghian - January 1982 (PB82 218 926)A05
- UCB/EERC-82/02 "Shaking Table Tests of a Tubular Steel Frame Model," by Y. Ghanaat and R. W. Clough - January 1982 (PB82 220 161)A07
- UCB/EERC-82/03 "Experimental Behavior of a Spatial Piping System with Shock Arrestors and Energy Absorbers under Seismic Excitation," by S. Schneider, H.-M. Lee and G. W. Godden - May 1982
- UCB/EERC-82/04 "New Approaches for the Dynamic Analysis of Large Structural Systems," by E. L. Wilson - June 1982 (PB83 148 080)A05
- UCB/EERC-82/05 "Model Study of Effects of Damage on the Vibration Properties of Steel Offshore Platforms," by F. Shahrivar and J. G. Bouwkamp - June 1982
- UCB/EERC-82/06 "States of the Art and Practice in the Optimum Seismic Design and Analytical Response Prediction of R/C Frame-Wall Structures," by A. E. Aktan and V. V. Bertero - July 1982 (PB83 147 736)A05
- UCB/EERC-82/07 "Further Study of the Earthquake Response of a Broad Cylindrical Liquid-Storage Tank Model," by G. C. Manos and R. W. Clough - July 1982 (PB83 147 744)A11
- UCB/EERC-82/08 "An Evaluation of the Design and Analytical Seismic Response of a Seven Story Reinforced Concrete Frame - Wall Structure," by F. A. Charney and V. V. Bertero - July 1982
- UCB/EERC-82/09 "Fluid-Structure Interactions: Added Mass Computations for Incompressible Fluid," by J. S.-H. Kuo - August 1982
- UCB/EERC-82/10 "Joint-Opening Nonlinear Mechanism: Interface Smeared Crack Model," by J. S.-H. Kuo - August 1982 (PB83 149 195)A05
- UCB/EERC-82/11 "Dynamic Response Analysis of Techii Dam," by R. W. Clough, R. M. Stephen and J. S.-H. Kuo - August 1982 (PB83 147 496)A06
- UCB/EERC-82/12 "Prediction of the Seismic Responses of R/C Frame-Coupled Wall Structures," by A. E. Aktan, V. V. Bertero and M. Piazza - August 1982 (PB83 149 203)A09
- UCB/EERC-82/13 "Preliminary Report on the SMART 1 Strong Motion Array in Taiwan," by B. A. Bolt, C. H. Loh, J. Penzien, Y. B. Tsai and Y. T. Yeh - August 1982
- UCB/EERC-82/14 "Shaking-Table Studies of an Eccentrically X-Braced Steel Structure," by M. S. Yang - September 1982
- UCB/EERC-82/15 "The Performance of Stairways in Earthquakes," by C. Roha, J. W. Axley and V. V. Bertero - September 1982

- UCB/EERC-82/16 "The Behavior of Submerged Multiple Bodies in Earthquakes," by W.-G. Liao - September 1982
- UCB/EERC-82/17 "Effects of Concrete Types and Loading Conditions on Local Bond-Slip Relationships," by A. D. Cowell, E. P. Popov and V. V. Bertero - September 1982
- UCB/EERC-82/18 "Mechanical Behavior of Shear Wall Vertical Boundary Members: An Experimental Investigation," by M. T. Wagner and V. V. Bertero - October 1982
- UCB/EERC-82/19 "Experimental Studies of Multi-support Seismic Loading on Piping Systems," by J. M. Kelly and A. D. Cowell - November 1982
- UCB/EERC-82/20 "Generalized Plastic Hinge Concepts for 3D Beam-Column Elements," by P. F.-S. Chen and G. H. Powell - November 1982
- UCB/EERC-82/21 "ANSR-III: General Purpose Computer Program for Nonlinear Structural Analysis," by C. V. Oughourlian and G. H. Powell - November 1982
- UCB/EERC-82/22 "Solution Strategies for Statically Loaded Nonlinear Structures," by J. W. Simons and G. H. Powell - November 1982
- UCB/EERC-82/23 "Analytical Model of Deformed Bar Anchorages under Generalized Excitations," by V. Ciampi, R. Eligehausen, V. V. Bertero and E. P. Popov - November 1982
- UCB/EERC-82/24 "A Mathematical Model for the Response of Masonry Walls to Dynamic Excitations," by H. Sucuoğlu, Y. Mengi and H. D. McNiven - November 1982
- UCB/EERC-82/25 "Earthquake Response Considerations of Broad Liquid Storage Tanks," by F. J. Cambra - November 1982
- UCB/EERC-82/26 "Computational Models for Cyclic Plasticity, Rate Dependence and Creep," by B. Mosaddad and G. H. Powell - November 1982
- UCB/EERC-82/27 "Inelastic Analysis of Piping and Tubular Structures," by M. Mahasuverachai and G. H. Powell - November 1982

